Division of Pharmaceutical Chemistry and Technology
Faculty of Pharmacy
University of Helsinki
Finland

Chemical Surface Modification of Porous Silicon Nanoparticles for Cancer Therapy

Chang-Fang Wang

ACADEMIC DISSERTATION

To be presented, with the permission of the Faculty of Pharmacy of the University of Helsinki, for public examination in lecture room Auditorium 1, Infocenter Korona, (Viikinkaari 11), on 2nd of March 2015, at 12.00 noon.

Helsinki 2015

Supervisors

Docent Dr. Hélder A. Santos
Division of Pharmaceutical Chemistry and Technology
Faculty of Pharmacy
University of Helsinki
Finland

Professor and Dean Dr. Jouni Hirvonen
Division of Pharmaceutical Chemistry and Technology
Faculty of Pharmacy
University of Helsinki
Finland

Reviewers

Assistant Professor Dr. Biana Godin Vilentchouk
Institute of Academic Medicine
Houston Methodist Research Institute
USA

Dr. José das Neves
INEB – Instituto de Engenharia Biomédica
University of Porto
Portugal

Opponent

Dr. Luca De Stefano
Institute for Microelectronics and Microsystems
Unit of Naples-National Research Council
Italy

ISBN 978-951-51-0856-2 (Paperback)
ISBN 978-951-51-0857-9 (PDF)
ISSN 2342-3161

Helsinki University Printing House
Helsinki 2015

To the memory of my grandfather

Abstract

Anticancer drugs inhibit the cancer growth by killing the rapidly dividing cancer cells. However, anticancer drugs also kill the dividing healthy cells and cause severe damage to healthy tissues. More specific delivery of the cancer drugs to the cancer tissue can increase the drug delivery efficiency and reduce the drug's side effects. Nanocarriers can increase the solubility of poorly-water soluble anticancer drugs and be modified for targeted drug delivery and theranostic applications. For efficient drug delivery, the drug loading capacity has been one of the key issues for the development of nanoparticle (NP)-based drug delivery systems. The biocompatible and biodegradable porous silicon (PSi) nanomaterial presents high drug loading capacity and tunable surface chemistry which renders it an ideal candidate as a drug delivery carrier. Chemical surface modification, which is one of the approaches to improve the nanomaterials' properties, can lead to a stable nanosystem for further drug delivery applications. The main aim of this dissertation was to employ chemical approaches and surface modified PSi nanoparticles (NPs) to improve the drug delivery efficiency for potential cancer therapy applications.

Incorporating targeting moieties to the surfaces of the nanocarriers, such as targeting peptides, can increase the nanocarrier's accumulation into the cancer tissue after the intravenous administration. In this thesis, surface modification of amine-terminated PSi NPs was achieved with targeting peptides (RGDS and iRGD) via strain-promoted azide-alkyne cycloaddition click reaction. The functionalization of the PSi NPs with the targeting peptides did not comprise the drug loading capacity, but enhanced the cellular uptake and the drug delivery efficacy of the PSi NPs *in vitro*.

In addition to the targeting NP surface modifications, a multifunctional nanosystem was prepared with simultaneous fluorescence- and radio-labeling, and iRGD surface modification of the carboxylic acid-terminated PSi NPs. Both labelings were accessible for the *in vivo* biodistribution evaluation in mice by single-photon emission computed tomography and X-ray computed tomography, and *ex vivo* by immunofluorescence staining, respectively. The iRGD modification enhanced the tumor uptake of the PSi NPs after the intravenous administration. In order to reduce the plasma protein adsorption onto the PSi NPs, five bioactive molecules (peptides and hydrophilic anti-fouling polymers) were used to modify the surface of alkyne-terminated PSi NPs using copper-catalized click chemistry. Dextran 40 kDa modified PSi NPs presented enhanced cellular uptake and the least protein adsorption of all the tested NPs.

Furthermore, the chemical conjugation of drug molecules was studied. The targeting peptides were successfully conjugated to antisense interleukin-6 via copper-catalyzed [3+2] azide-alkyne cycloaddition for targeted angiogenic anti-inflammation in cancer. Finally, anticancer drug methotrexate (MTX) was chemically conjugated to the cationic PSi NPs and demonstrated to increase the cellular uptake of MTX with up to 96 h sustained drug release. A hydrophobic anti-angiogenic drug, sorafenib, was also loaded to the MTX-conjugated PSi NPs, and the dissolution rate of this drug was considerably increased.

In conclusion, in this thesis different chemical approaches were used to biofunctionalize PSi NPs and to prepare drug-conjugates formulations for potential anti-cancer applications.

Acknowledgements

The laboratory work of this thesis was carried out in the Division of Pharmaceutical Chemistry and Technology, Faculty of Pharmacy, University of Helsinki during 2009–2014. Financial support from the Chinese Scholarship Council, Academy of Finland (decision no. 256394), University of Helsinki Research Funds, Biocentrum Helsinki, and European Research Council (grant no. 310892), are gratefully acknowledged.

I would like to express my deepest gratitude to my supervisor Docent Dr. Hélder A. Santos. Without his trust, excellent supervision and continuous support during this time, this work would have not been possible. His valuable suggestions will also benefit my future academic career.

I own my honest thanks to my second supervisor Prof. Jouni Hirvonen, who has built an outstanding group for both research and education. It was my great honor to join his research group. His positive attitude and encouraging guidance made my PhD study in Finland easier.

Great thanks are given to all my co-authors for their sincere cooperation and productive discussions about the work. Especially thanks to M.Sc. Ermei Mäkilä, Dr. Mirkka Sarparanta, M.Sc. Martti Kaasalainen, Dr. Colin Bonduelle, M.Sc. Jussi Rytkönen, Dr. Anu Airaksinen, Dr. Jarno J. Salonen, Prof. Sébastien Lecommandoux and Dr. Janne Raula for their valuable efforts to this work.

I am greatly thankful to Dr. Biana Godin Vilentchouk, from the Houston Methodist Research Institute (USA), and Dr. José das Neves, from INEB (Portugal), for kindly reviewing my thesis. They have given valuable and important suggestions and comments to improve this dissertation.

I would like to thank all the colleagues at the Division of Pharmaceutical Chemistry and Technology, especially the NAMI Unit and Santos' lab. Thanks for sharing the time with me. I enjoyed a lot the summer and winter activities. It was lucky for me to have the chance to work in this group.

I also wish to take this opportunity to thank all my friends who helped me and shared time with me. When I arrived in Finland, a lot of Chinese and Finnish friends have helped me to settle in Finland. I especially thank Mr. Liming Deng, Dr. Li Tian, Dr. Jing Li, Dr. Xianbao Deng, M.Sc. Lin Chen, and M.Sc. Shuang Wang for their kind help and company.

I own my deepest affection to my beloved Tuomas for his patience, support and encouragement during these years. I also appreciate his lovely family, for spending Christmas and all other important family occasions with me. They have been a great part of my life during these years.

I would like to thank my family for their endless love and support. They are the ones I miss and think about no matter when and where I am.

Helsinki,

Februry 2015

Contents

List of original publications

This thesis is based on the following publications:

I. **Wang CF**, Mäkilä E, Kaasalainen M, Liu D, Sarparanta M, Airaksinen A, Salonen J, Hirvonen J, Santos HA. Copper-free azide-alkyne cycloaddition of targeting peptides to porous silicon nanoparticles for intracellular drug uptake. Biomaterials, 2014, 35:1257-66.

II. **Wang CF**, Sarparanta MP, Mäkilä EM, Hyvönen MLK, Laakkonen PM, Salonen JJ, Hirvonen JT, Airaksinen AJ, Santos HA. Multifunctional porous silicon nanoparticles for cancer theranostics. Biomaterials, 2015, 48:108-18.

III. **Wang CF**, Mäkilä EM, Bonduelle C, Rytkönen J, Raula J, Almeida S, Närvänen A, Salonen JJ, Lecommandoux S, Hirvonen JT, Santos HA. Functionalization of alkyne-terminated thermally hydrocarbonized porous silicon nanoparticles with targeting peptides and antifouling polymers: effect on the human plasma protein adsorption. ACS Appl. Mater. Interfaces, 2015, 7:2006-15.

IV. **Wang CF**, Auriola S, Hirvonen J, Santos HA. Conjugation of peptides to antisense interleukin-6 via click chemistry. Curr. Med. Chem., 2014, 21:1247-54.

V. **Wang CF**, Mäkilä EM, Kaasalainen MH, Hagström MV, Salonen JJ, Hirvonen JT, Santos HA. Dual-drug delivery by porous silicon nanoparticles for improved cellular uptake, sustained release, and combination therapy. Acta Biomaterialia, 2015, doi: 10.1016/j.actbio.2015.01.021.

 In publication **II**, the first two authors share equal contribution. Dr. Sarparanta carried out the work related to ^{111}In-radiolabeling of the modified nanoparticles, and performed the *in vivo* studies together with Wang.

The publications are referred to in the text by their roman numerals.

Abbreviations

APTES	3-aminopropyltriethoxysilane
APS-TCPSi	aminopropylsilane- thermally carbonized porous silicon
BCN	Bicyclononyne
BCS	Biopharmaceutical classification system
CuAAC	Copper-catalyzed [3+2] azide-alkyne cycloaddition
Da	Dalton
DBCO	Dibenzylcyclooctyne
DLS	Dynamic light scattering
DMEM	Dulbecco's modified Eagle's medium
DOTA	1,4,7,10-tetraazacyclododecane-N,N',N'',N'''-tetraacetic acid
EDC	1-Ethyl-3-(3-dimethylaminopropyl)-carbodiimide
FBS	Fetal bovine serum
FDA	Food and Drug Administration
FITC	Fluorescein isothiocyanate isomer I
FTIR	Fourier transform infrared spectroscopy
HBSS	Hank's balanced salt solution
HEPES	4-(2-Hydroxylethyl)-1-piperazineethanesulfonic acid
HPLC	High performance liquid chromatography
IL-6	Interleukin-6
i.t.	Intratumoral
i.v.	Intravenous
MES	2-(N-morpholino)ethanesulfonic acid
MTX	Methotrexate
MW	Molecular weight
NHS	N-hydroxysuccinimide
NP	Nanoparticle
PEG	Poly(ethylene) glycol
PGA	Poly (L-glutamic acid)
PSi	Porous silicon
RES	Reticuloendothelial system
SF	Sorafenib
Si	Silicon
$Si(OH)_4$	Orthosilicic acid
SPAAC	Strain-promoted azide-alkyne cycloaddition
SPECT/CT	Single-photon emission computed tomography and X-ray computed tomography
TCPSi	Thermally carbonized porous silicon
THCPSi	Thermally hydrocarbonized porous silicon
TEM	Transmission electron microscope
TOPSi	Thermally oxidized porous silicon

1 Introduction

Cancer is one of the most life-threatening diseases in humans.[1] The sustained chronic proliferation of mutant cells is the most fundamental characteristic in cancer. Normal tissues carefully produce growth-promoting signals and regulate the cell formation, whereas cancer cells irregularly release the growth-promoting signals resulting in uncontrollable cell proliferation and development.[2] Chemotherapy combined with local therapies, such as surgery or radiotherapy, have been applied as strategies to treat cancer. However, non-specific delivery of chemotherapeutic agents can also harm the normal tissues. In addition, the poor-water solubility and low cellular uptake of various cancer drugs are still the challenges for cancer drug delivery.[3]

Nanotechnology can aid in cancer drug delivery by increasing the aqueous solubility of many drug molecules. The surface properties of the nanocarriers can be modulated to increase the drug delivery efficiency and specificity. For efficient drug delivery, the drug loading capacity has been one of the key parameters for the development of nanoparticle (NP)-based drug delivery systems.[4] Porous silicon (PSi) nanomaterials are a form of the chemical element Si, which have nanoporous holes in the nanostructure, rendering it a large surface area ratio up to 800 m^2/g, which can be used for drug loading.[5] PSi NPs have a number of unique properties that make it a potential drug delivery vector, such as high drug loading capacity, tunable surface chemistry and structure to increase the biocompatibility and other biomedical properties,[6] such as targeted drug delivery.[7] Amine,[8] carboxylic acid,[5] and aldehyde[5] groups have been introduced to the surface of PSi NPs. These chemically reactive moieties can be further functionalized with other biomolecules to manipulate the PSi's properties for biomedical applications, such as cancer therapy and imaging.

In cancer, the various types of cells that comprise the tumor mass all carry molecular biomarkers that are not expressed, or are expressed at much lower levels, in healthy cells.[9] For example, tumor blood vessels express biomarkers that are not present in resting blood vessels of normal tissues, but can be shared by angiogenic vessels in non-malignant conditions.[10] The ligands which can target to the biomarkers can be used to modify the NPs, and thus, increase the interaction of the NPs with the cancer tissue and, consequently, increase the intracellular drug delivery efficiency. The concept of targeted drug delivery is attractive because it can increase the local drug concentration and lower the systemic exposure.[11-12] Small molecules, such as folic acid,[13] various targeting peptides,[10, 14] protein ligands,[15-16] as well nucleic acid-based aptamers,[7, 17] have been widely investigated for the targeted cancer drug delivery of nanocarriers.

Functionalized NPs involve at least one step more to introduce the targeting moieties to the nanosystems by surface modification. Click chemistry has been developed to provide a simple method to couple organic molecules in high yield under mild conditions and high selectivity in the presence of a diverse range of functional groups.[18] One of the most widely used examples of this class of very efficient chemical reactions is the copper-catalyzed [3+2] azide-alkyne cycloaddition (CuAAC) reaction.[19-20] Strain-promoted azide-alkyne cycloaddition (SPAAC) click reaction avoids using copper ion, which might induce cell and biological toxicity, and thus, is becoming an alternative to copper

catalyzed click reaction.[21] There is a great deal of interest in developing biomaterials by introducing biofunctional molecules via the click chemistry. Bioactive molecules, such as proteins, peptides, oligonucleotides and carbohydrates, have several chemical active groups (*e.g.*, amine, carboxyl acid, hydroxyl, and ester). Click reactions are potentially useful in bioactive molecules conjugation applications, because azides and alkynes react to each other without disturbing extensively the molecular or cross reactions with the surrounding components.[18] In addition, the triazoles are extremely stable and not toxic.[18]

As a result of the high surface energy, NPs can associate with plasma proteins in less than one second when the NPs are in contact with the blood stream fluids.[22] This is the first biological barrier the NPs will encounter when administered intravenously. plasma protein adsorption plays an important role in the NPs recognition by the immune system macrophages, which will clear the NPs from the bloodstream and transport them mainly to the liver and spleen, failing to deliver the drug to the desired site(s) in the body. High molecular weight polyethylene glycol (PEG) and dextran have been investigated as hydrophilic polymers to sheath and aid to prevent the protein adsorption in order to increase the blood circulation time of the NPs.[23-24] Biodegradable PSi NPs can also be used as a platform to enhance the cell uptake of low permeability drugs and sustained release of the chemically conjugated drugs, by simultaneously co-loading poorly water-soluble drugs with drug-conjugated PSi NPs.

In this dissertation, different chemical approaches were explored to develop drug delivery systems for targeted cancer therapy potential. In particularly, the studies of this thesis included: (1) development of chemical methods for surface functionalization of PSi NPs and peptide-oligonucleotide conjugation; (2) physicochemical characterization of the developed drug delivery systems; (3) *in vitro* and *in vivo* evaluation of the behavior of the multifunctional PSi NPs; (4) identification of the effect of PSi surface chemistry on plasma protein adsorption; and (5) evaluation of the drug loading and release profiles before and after the surface modification of the PSi NPs.

2 Literature review

2.1 Cancer and cancer therapy

Cancer is a complex disease resulting from genetic mutations.[25] It is the most common cause of death in Europe,[26] and the second leading cause of death in the USA, following the cardiovascular diseases.[27] Lung, prostate, and colorectal cancers are the three leading causes for cancer death among men, and among women the leading causes of cancer death are lung, breast, and colorectal cancers.[26] The possible causes of inducing cancer in individuals include genetic factors, lifestyle factors, such as tobacco, diet and exercise, certain types of infections, and environmental exposures to different types of chemicals and radiation. For most of the cancers, earlier detection and treatment provide substantially longer survival rates.[26-27] Currently, more efficient cancer diagnosis and treatment are still under development.[4]

2.1.1 The features of cancer

Uncontrolled proliferation of mutant cells is the first characteristics of cancer. The cells of normal tissues are regulated by growth-promoting signals and differentiate to tissue forms, while mutated cancer cells irregularly release the growth-promoted signals and continue the cell doubling to form a cancer tissue.[2]

In 2001, Hanahan and Weinberg summarized six "hallmarks of cancer",[1] followed by additional four "hallmarks of cancer" reviewed in 2011.[2] In total, the ten characteristics of cancer are briefly summarized here.

1) Cancer cells can sustain the proliferative signaling. Normal tissues maintain a homeostasis of cell number, and thus, well-functionalized tissue architecture by carefully controlling the production and release of growth-promoting signals that instruct the cell growth and division cycle. Cancer cells can continually produce proliferation signals or elevate the level of receptor proteins and maintain chronic cell growth, typically containing intracellular tyrosine kinase domains.[28]
2) Cancer cells can evade growth suppressors. Similar to the controlled production of growth signals, there is a certain amount of antiproliferative signals operating within the normal tissue. However, in cancer cells dozens of tumor suppressors that control cell growth and proliferation have been discovered undergoing inactivation to tumor growth. Cancer cells can present powerful programs that evade the negative regulation of cell proliferation. The two prototypical tumor suppressors encode the retinoblastoma-associated and TP53 proteins.[29]
3) Cancer cells can resist to cell death. The programmed cell death by apoptosis is a natural barrier for cancer development. However, tumor cells have a variety of strategies to limit or circumvent apoptosis. The most common reason for this is the defunctionalization of TP53 tumor suppressor.[30]

4) Cancer cells enable replicative immortality. The differentiated healthy cells have limited cycles of growth-and-division, while cancer cells have unlimited replicative potential.[31]
5) Cancer cells can induce angiogenesis. Like normal tissues, tumor mass requires supplying of nutrients and oxygen as well as evacuating metabolic wastes and carbon dioxide. During tumor development, neovasculature is activated and sprout new vessels to help sustain the tumor mass increase.[32]
6) Cancer cells can activate invasion and metastasis. During the development of cancer, sooner or later, tumor cells start to move out, invading adjacent tissues to get more nutrients and space. Cancer metastasis is the cause of 90% of human cancer deaths.[33]
7) Genome instability and mutation in cancer. In the case of tumorgenesis, cancer cells often increase the rate of mutation, as well as the genome maintenance/repairing systems lose their functions during the tumor progression.[34]
8) Cancer cells can induce tumor-promoting inflammation. Inflammation can supply bioactive molecules to the tumor microenvironment, such as growth factors that sustain the proliferative signaling, survival factors that limit the cell death, and proangiogenic factors and extracellular matrix-modifying enzymes that facilitate angiogenesis, invasion, and metastasis.[35]
9) Cancer cells can reprogram energy metabolism. Even cancer cells must compensate for the ca. 18-fold lower efficiency of ATP production afforded by glycolysis related to mitochondrial oxidative phosphorylation. In order to fuel cell growth and division, cancer cells up-regulate glucose transporters to substantially increase the glucose import into the cytoplasm.[36]
10) Cancer cells can evade immune destruction. Clinical cases have revealed the existence of anti-tumoral immune responses in some forms of human cancer. However, highly immunogenic cancer cells can evade immune destruction by disabling components of the immune system that have been dispatched to eliminate them.[37]

As a result of the discovery of the cancer characteristics, the mechanism-based targeted cancer therapy of the drug delivery systems are under development. **Figure 1** summarizes the hallmarks of cancer and the possible therapeutic approaches.[2]

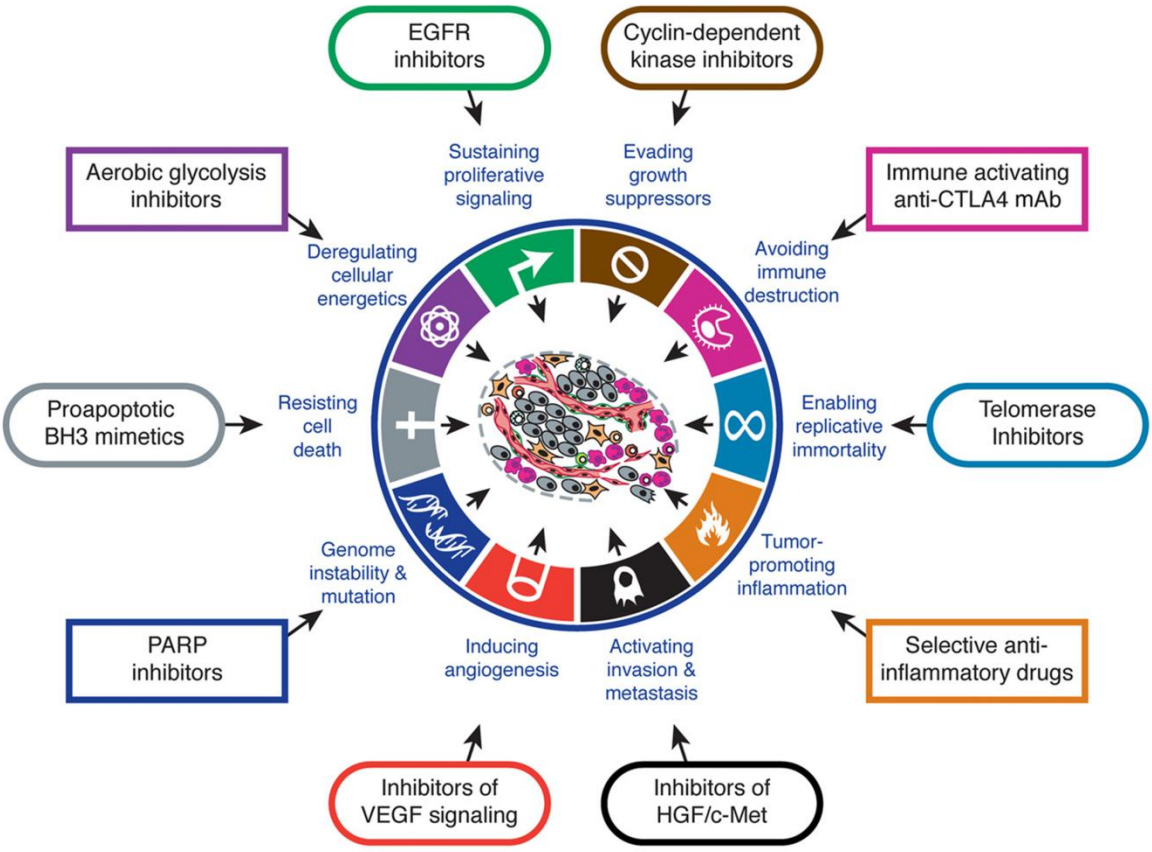

Figure 1. *The hallmarks and therapeutic targeting in cancer treatment. Copyright © (2011) CellPress. Reprinted with permission from ref.* [2].

2.1.2 Clinical cancer treatments

Clinical cancer treatments include surgery, chemotherapy, radiotherapy, targeted therapy and immunotherapy.[25] Surgery is mainly used to remove the solid tumor mass. Chemotherapy is the approach of treating cancer with cytostatic drugs which can kill the rapidly dividing cancer cells, often by disturbing the DNA duplication.[38] Thus, chemotherapeutic reagents need to be delivered into the cancer cells. However, chemotherapy also kills the dividing healthy cells. Radiotherapy is based on the decay of radionuclides to release the x-rays or γ-rays to damage the localized area and to stop the cancer cells from growing or dividing. The radiation can be delivered by external beam radiation, or local implantation or system administration of radioactive agents.[39] Radiotherapy can be used to treat almost all types of cancer. Radiotherapy induces side effects to the nearby tissues and organs. Different from chemotherapy and radiotherapy, targeted therapies generally involve the pharmaceutically active agents to specifically interact with the proteins related to cancer development and inhibit the tumor growth.[2] Targeted therapies aim to achieve more specific tumor treatment and reduce the side-effects. For example, antiangiogenic drugs specifically inhibit the tumor neovasculature and inhibit tumor growth.[40] Targeted therapies also include the targeting cargos mediated specific delivery of radionuclides or chemotherapeutical agents to the cancer site and

minimize the exposure to the healthy tissue.[10] Cancer immunotherapy is another set of therapeutic strategies designed to fight against the cancer by stimulating the patient's own immune system.[41] In practice, one patient can be treated with a combination of several treatments to increase effectiveness, precision, survivability, and the quality of the patient's life. Surgery is often combined with chemotherapy and/or radiotherapy. Chemotherapeutical and targeted therapeutic agents can be co-delivered in a form of combination therapy.

Figure 1 lists the cancer treatment targets that the drugs can interfere with each of the acquired hallmarks necessary for the tumor growth and progression.[2] Understanding the principle of cancer and mechanism-based targeted therapies can direct the cancer drug development. Commonly drug molecules are targeted to one or several specific receptors to inhibit signaling pathways, which may not be enough to completely stop the whole hallmark capability or the tumor growth. An unstable gene mutation in the cancer cells induces signaling pathway remodeling that can reset the tumor growth capability.[42] For example, antiangiogenic therapies have been expected to starve the tumor growth leading to tumor dissolution.[43-44] However, the clinical results showed that antiangiogenic agents treatment did not achieve the fantastic effect as they were expected.[45] Another concern is the tumor resistance due to overcompensation from the parallel signaling pathways and side effects to the normal vasculature.[46] Multidrug resistance has been rising as a problem resulting from the chemotherapy.[47] The mechanisms for multidrug resistance include increasing the expression of drug efflux or elevated anti-apoptotic pathways due to the mutations and metastases of tumor cells.[47] Delivering simultaneously more than one cancer drug molecule to inhibit several cancer hallmarks at the same time can increase the chance to inhibit the tumor growth. Chemotherapeutic agents have been co-delivered with small interference RNA (siRNA) against multidrug resistance proteins for cancer treatment.[48] Chemotherapeutic agents can be delivered at the same time as the antiangiogenic drugs for combination therapy.[49]

2.1.3 Nanomedicines for cancer treatment in clinics

Highly effective chemotherapeutic agents often present poor water solubility or low permeability across biological barriers.[4] Nanomedicines have been intensively investigated to increase the solubility of antineoplastic drugs in the past decades. The definition of a nanomedicine is the application of nanotechnology in the medical field.[3] There are several advantages of nanomaterials used for biomedical applications,[50] such as: (1) the nanostructure can increase the solubility and stability of the chemotherapeutic agents in physiological conditions; (2) the NPs can carry a group of nanosized drugs composed of thousands of molecules as a unit in a small location, and thus, high therapeutic effect; (3) nanomaterials can be functionalized with biomolecules to enable them for targeting into specific organelles or certain tissues to increase the drug delivery efficacy and to reduce the side effects; (4) nanocarriers can be co-loaded with more than one drug into one single nanocarrier for combination therapy; (5) the NPs can be loaded with both drugs and imaging agents for simultaneous therapy and diagnosis or imaging to follow-up the biofate of the NPs. Systemic chemotherapeutic drug administration is one of

the few treatments for metastase stages of cancer. Among the various treatments for cancer therapy, eight nanomedicine-based formulations have been approved for clinical use (**Table 1**) and many other formulations are under clinical trials.[3]

Doxil® is a PEGylated liposome formulation loaded with doxorubicin in the aqueous core and has long blood circulation time (half-life of 2–3 days).[51-52] The mean size of Doxil is in the range of 80–90 nm. Doxil® has substantially higher efficacy and significant lower cardiotoxicity than the free drug. However, the two most severe side effects of Doxil are mucositis and palmar plantar erythrodysesthesia.[53] Myocet® is a liposomal doxorubicin formulation, the same as Doxil® except the PEGylation, with a particle size of ca. 190 nm.[54] The blood circulation half-life of Myocet® is ca. 2.5 h. Compared to Doxil®, Myocet® is not associated with palmar plantar erythrodysesthesia and significantly reduced incidence of mucositis. Myocet® has similar efficacy and lower cardiac-related toxicity than free doxorubicin.[55] Daunoxome® is a liposome formulation encapsulated with daunorubicin, which lacks a hydroxyl group at the 14-position of doxorubicin, but has better aqueous stability compared to doxorubicin.[56] The particle size is ca. 50 nm and the circulation half-life is 2 to 4 h.[57] The clinical results have showed higher drug accumulation in the tumor for the Daunoxome® than for the free daunorubicin. The clinical efficacy for various forms of leukemia is active.[57] Abraxane® is a nanoscale albumin-bound formulation of paclitaxel with size ca. 100 nm.[58] Abraxane® has dramatically decreased the toxicity of the traditional paclitaxel formulations and increased the efficacy of the drug in clinical trials involving patients with an advanced breast cancer. Albumin can actively bind to endothelial glycoprotein receptor gp60 and secrete the protein acid and rich in cysteine, which is overexpressed in the extracellular space for a variety of cancers.[59] Rexin-G® is a cancer collagen matrix targeted liposome platform loaded with microRNA targeting retrovector encoding an N-terminal deletion mutant of the cyclin G1 gene for antineoplastic activity.[60] Rexin-G® is the first gene therapy nanomedicine for cancer treatment on the market. Oncaspar® is a formulation of asparaginase covalently conjugated by PEG to prolong its circulation and retention time, decreasing proteolysis and renal excretion.[61] PEGylation also shields antigenic determinants from immune detections, and thus, reduce the side effects of the native asparaginase, such as hypersensitivity.[62] Oncaspar® was approved as the first-line treatment for acute lymphoblastic leukemia as a component of a multiagent thermotherapy regimen by the Food and Drug Administration (FDA) in 2006.[63]

Beyond the nanomedicines for cancer therapy, there are two nanotechnology-based systems for diagnostics approved for clinical applications (**Table 1**).[3] Both two formulations are superparamagnetic iron oxide NPs (SPIONs) coated with dextran, acting as magnetic resonance imaging agents for the diagnostic of liver lesions.[64]

Table 1: *Nanomedicines approved by one or more regulatory bodies. Copyright © (2013) Hindawi. Adapted with permission from ref.* [3].

Product/ Company	Nanoplatform/API	Indication	Status
Doxil / Ortho Biotech	PEGylate liposome/doxorubicin	Ovarian cancer	Approved by FDA in 1995
Myocet / Sopherion Therapeutics (North American) and Cephalon Inc. (Europe)	Non-PEGylated liposomal/doxorubici	Metastatic breast cancer	Approved in Europe in 2000 and in Canada in 2001
DaunoXome/ Galen Ltd.	Lipid encapsulation/dauno rubicin	Advanced HIV-associated Kaposi's sarcoma	Approved by FDA in 1996
Abraxane/ Abraxis Bioscience	Nanoparticulate albumin/paclitaxel	Breast, lung, and pancreatic cancers	Approved by FDA in 2013
Rexin-G/ Epeius Biotecnologies	Targeting protein tagged phospholipid/ microRNA-122	Sarcoma, osteo-sarcoma, pancreatic cancer, and other solid tumor	Approved in Philippine in 2007, and approved by FDA for clinical trials phase III in 2011
Oncaspar/ Enzon Phar-maceuticals	PEGylated asparaginase	Acute lympho-blastic leukemia	Approved by FDA in 2006
Resovist/ Bayer Schering Pharma AG	Iron oxide NPs coated with carboxydextran	Liver lesion imaging	Approved in Europe in 2001
Feridex/ Berlex Laboratories (USA) and Endorem/ Guerbet (Europe)	Iron oxide NPs coated with dextran	Liver lesion imaging	Approved by FDA and in Europe in 1996

2.1.4 Nanomaterials in pre-clinical studies for cancer therapy

In addition to the nanomedicine formulations used in the market, there are diverse types of nanotechnology-based drug delivery systems under pre-clinical and clinical research for cancer diagnosis and therapy. The nanosystems under pre-clinical research include organic and inorganic nanomaterials, as well as organic–inorganic hybrid nanomaterials.[50, 65-66] Based on the composition used to prepare the nanosystems, the commonly investigated nanomaterials can be divided into lipid-based nanosystems, polymeric NP platforms, protein-based drug delivery systems, and inorganic nanosystems (e.g., gold NPs, mesoporous silica and silicon NPs, magnetic NPs, quantum dots, and single/multiwall carbon nanotubes) (**Figure 2**). The composition of the nanomaterials, as well as the size, charge, and shape are the key parameters determining the *in vivo* fate of the nanovectors, the drug delivery potential, and the therapeutical efficacy.[67]

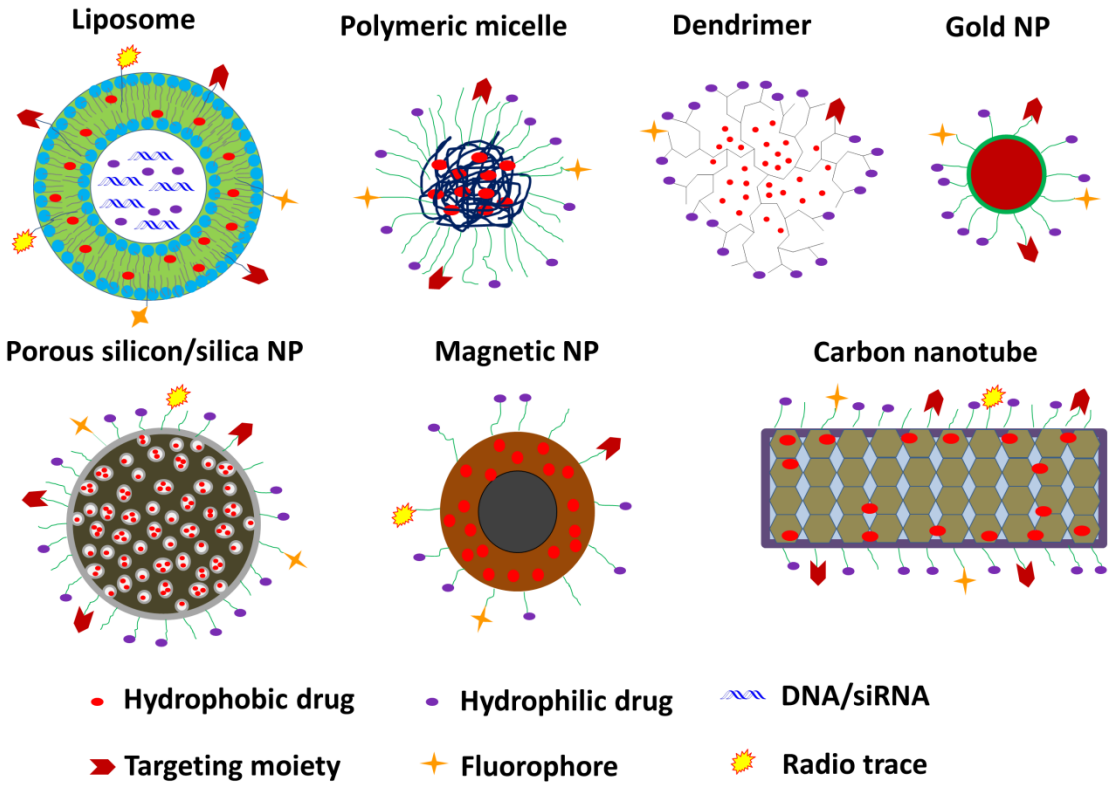

Figure 2. *Schematic illustration of the representative NP platforms that have been synthesized for drug delivery purposes in cancer therapy. Copyright © (2013) Elsevier B.V. Adapted with permission from ref.* [65].

Lipid-based nanomaterials have contributed with the highest amount of formulations in pre-clinical studies, which have also led to many products entering the clinics.[3] Liposomes, which are bilayered structures made of phospholipids, are the most widely studied nanomaterials for drug delivery due to their benign biological behavior, such as good biocompatibility, biodegradability, low immunogenicity, and the capacity to deliver both hydrophobic and hydrophilic drugs.[68] Hydrophobic drugs can be loaded in the lipid bilayers to increase the water solubility, while hydrophilic drugs can be loaded in the aqueous core to increase the blood circulation and reduce the drug's side effects.[69] PEGylation of liposomes can further prevent the recognition by the reticuloendothelial system (RES) and increase the blood circulation, for example, Doxil®.[51, 68] Liposomes can also be formulated with targeting moieties on the surface of the nanocarriers for active targeting and drug delivery.[70] Controlling the drug release at certain site/tissue *in vivo* can achieve more precise drug delivery. Triggered drug release from liposomes by pH, temperature, light, and enzymes has been investigated.[71] Liposomes have further been investigated as theranostic nanovectors by combining chemotherapeutic agents with diagnostic tracers for magnetic resonance imaging (MRI) and single-photon emission computed tomography/computed tomography (SPECT/CT) imaging.[72]

Polymeric nanosystems are another large family of nanomaterials that have been investigated intensively in the past decades, such as dendrimers, micelles, and polymersomes. Different polymer building blocks such as homopolymers, copolymers and

triblock polymers at different chain lengths make the polymeric nanostructures very flexible and the properties can be tailored to meet the medical requirements. Due to the tunable chemical structures, the polymeric nanosystems can be easily surface modified and reach high drug loadings, which are very important parameters to translate them into clinical trials.[73] The polymer-drug conjugates also increase the flexibility of the drug administration routes. For example, poly(L-glutamic acid)-paclitaxel (CT-2103, Xyotax®), developed by CTI BioPharma, is a formulation of polymer-drug conjugate that increases the solubility of the hydrophobic drug paclitaxel.[74] This formulation has also increased the anticancer drug efficacy and reduced its side effects, as well as increased the patient compliance compared to standard taxanes in clinical trials.[75] Doxorubicin and methotrexate as well as some other cancer drugs have been conjugated to different polymers to increase the therapeutic index.[76-77] It is worth to mention here that the polymer-drug conjugates are prodrug-like formulations and their efficacy depends on the chemical structure and pharmaceutical active site of the drug. The release of the drug from the conjugation is critical for some drugs.[78] Amphiphilic polymeric micelle formulations have a hydrophobic core, where hydrophobic drugs can be complexed. The pH, temperature, ionic strength and amphiphilic surfactants can affect the micelle formation, which in turn can be utilized for triggered drug release.[79] Nanogel is another polymeric structure, which is a nanosized polymeric structure and crosslinked to increase the stability of the nanostructure and to obtain a sustained drug release.[80] Depending on the crosslinker or the composite of the nanogel, thermal,[81] pH,[82] or photo-triggered[83] drug release profiles can be obtained. Polymersomes, also called polymeric vesicles, are another type of self-assembled nanostructures of amphiphilic copolymers, which have similar hydrophobic bilayer and hydrophilic core structures like liposomes.[84] Polymersomes provide higher drug loading degrees and are more stable as compared to liposomes.[85] Other structural carriers include, for example, dendrimers, which are repetitively branched molecules, with sizes in a range between 1 and 15 nm and near monodispersibility in a 3D structure.[86] The "hole" between dendrimer units can be used for physical drug loading. Another feature of dendrimers is the abundant terminal groups, which can be used to conjugate drug molecules for sustained drug release.[77, 87] These terminal groups can also be labeled with targeting moieties,[88-89] radiotracers,[90] or fluorescence dyes,[91] for biomedical imaging. Polyamidoamine (PAMAM) dendrimer is one of the most studied dendrimers for anticancer drug delivery. Anticancer methotrexate (MTX) conjugated to PAMAM increased the cellular uptake and the binding affinity of MTX to the folate binding protein.[92]

Protein molecules as drug delivery carriers have presented decent outcomes as nanoplatforms for drug delivery due to their biocompatibility and biodegradability.[93] Abraxane is the formulation of paclitaxel loaded into albumin NPs, which has been approved by the FDA in 2005 for the treatment of breast cancer.[94] Protein NPs consist of natural protein subunits or combination of natural protein with further chemical modification. Albumin,[95] gelatin,[96] elastin,[97] gliadin and legumin,[98] have been studied to form protein-based NPs and further applied for drug delivery.

DNA-based nanotechnology, especially DNA origami, provides another platform which can be used for drug and gene delivery for cancer therapy and diagnosis.[99-101] DNA origami is the type of nanomaterials formed by self-assembling of DNA sequence with

precisely defined shapes and uniform sizes.[102-104] Aptamer-based DNA self-assembling nanocomposite has been built for targeted cancer therapy.[17] Both doxorubicin and therapeutic antisense oligonucleotides were co-loaded to the DNA nanostructure to decrease the drug resistance *in vitro*. A DNA microsponge containing extremely high ratio of repeating oligonucleotide copies was stabilized by the layer-by-layer assembly technique.[105] The formulation significantly improved the nucleic acid stability *in vitro* against the DNase and during the *in vivo* biodistribution. A hybrid nanocomposite containing gold NP functionalized with double-stranded DNA and temperature-responsive polymer has been formed as well.[101] Chemotherapeutic drug doxorubicin was loaded in the nanocomposite and a temperature controlled release profile was achieved.[101]

Inorganic NPs, such gold NPs (AuNPs), single-wall/multiwall carbon nanotubes (SWCNT/MWCNT), mesoporous silica NPs, quantum dots (QDs), magnetic NPs as well as porous silicon (PSi) NPs are another family of investigated nanovectors for biomedical diagnostics and drug delivery.[50, 106-111] In particular, most of the inorganic NPs present photosensitivity and can be used for photothermal therapy combined with chemotherapy.[106]

AuNPs have gained great attention for biomedical applications due to the controllable size and superior optical properties in the near-infrared at 700 to 900 nm.[107] AuNPs can be surface stabilized/modified through gold-thiolate bonds (Au-S) by disulfide (S-S) or thiol (-SH) bonds reacting with fresh gold surface.[112] AuNPs have been surface functionalized by targeting ligands/drugs for photothermal/radiation therapy and drug delivery.[113-115] External light triggering of liposome/AuNPs complexed nanocomposites or polymer-modified AuNPs by glutathione can be applied for triggered drug release and phototherapy.[114, 116]

SWCNTs (0.4–2.0 nm in diameter and 20–1000 nm in length) are more suitable for imaging after surface functionalization.[108] In addition, SWCNTs can also be chemically conjugated with drug molecules to achieve sustained drug release.[110, 117] MWCNTs with sizes of 1.4–100 nm in diameter, and not less than 1 μm in length, can be used for large biomolecules delivery, such as plasmids.[109]

Mesoporous silica NPs have a size range from 50 to 300 nm and pore size between 2 and 6 nm, which can be used for both drug loading, and internal and external functionalization.[118-119] 'Cornell Dots', which are made of silica NPs, have been approved for clinical phase I trials by the FDA in 2011.[120] Mesoporous silica NPs can be synthesized and surface modified by co-condensation, grafting, and imprint coating methods.[121-122] The surface chemistry can determine the cellular uptake mechanism of the mesoporous silica NPs.[123-125] Recently, a luminescent mesoporous silica/Europium-based nanocomposite was prepared, which incorporated drug delivery and an ideal time-gated luminescence imaging without labeling.[126]

Magnetic nanoparticles, such as SPIONs, have been used in clinic for hepatic imaging [111]. SPIONs were synthesized by electrodeposition with controllable size range from nanometers to micrometers.[127-128] SPIONs with high magnetic flux density have been prepared with optimal drug targeting, magnetic to heat, non-toxicity, biocompatibility, injectability, and surface tunability properties.[129] NPs with sizes of 5 to 100 nm have been attractive for biomedical applications and widely studied in the pre-clinical stages.[130-131]

PSi NPs are another group of NPs with high potential for biomedical applications. The properties of these NPs will be discussed in more detail in section **2.2**.

The physical parameters and chemical composition of the NPs can dramatically determine the drug delivery efficacy. The surface modification is an important approach to improve the bio-properties of the NPs, which can affect the NPs' interactions with the biological systems, and thus, modulate the biofate of the NPs *in vivo*, as well as the success of the drug delivery. The various tunable structures for surface modification are the advantages of these nanoplatforms in drug delivery applications.

2.2 Porous silicon (PSi) NPs

2.2.1 Preparation and surface chemistry

Porous silicon (PSi) based materials are in the form of crystalline Si with nanosized pores in the bulk structure. The PSi structure was first fabricated accidentally by Arthur Uhlir Jr. and Ingeborg Uhlir at the Bell Labs in 1956.[132] However, it was not until later in 1980s, that PSi started to draw attention by others due to the discovery by Leigh Canham of the photoluminescence property of the quantum sized highly porous crystalline Si.[133] Following this discovery, Canham also demonstrated that PSi can be used for biomedical applications by testing the cell hydroxyapatite growth on microporous Si-film.[134]

The most common method to produce PSi nanomaterials is anodization.[6] Briefly, Si wafers are immersed in an electrochemical cell containing a hydrofluoric acid (HF)/ethanol solution to create a porous structure. The Si wafer is placed as the anode and the cathode is conventionally made of platinum. Specific electric current is applied to etch the Si wafers. The surface area, porosity and pore size distribution (2–50 nm) depend on the fabrication parameters, such as current density, anodization time, temperature and HF concentration, as well as the Si substrate type.[6, 135]

Freshly prepared PSi contains crystalline Si with Si hydrides ($SiSi_xH_y$; $x + y = 4$) terminals, which is highly reactive by hydrolysis and oxidation (**Eqs. 1–3**).[136] In addition, the Si hydride end can react slowly with ambient air and affect the porous structure and its optoelectronic properties.[137] The surface stabilization freshly after preparation of the PSi films has been widely applied to prevent native oxidation.

$$SiH_4 + 2H_2O \rightarrow SiO_2 + 4H_2 \quad (1)$$

$$Si + O_2 \rightarrow SiO_2 \quad (2)$$

$$SiO_2 + 2H_2O \rightarrow Si(OH)_4 \quad (3)$$

Thermal oxidation is one of the methods used to stabilize the fresh Si surface by inducing the Si hydride to O_ySiOH at 300–400 °C.[138] With increasing temperature, the Si backbone becomes oxidized by incorporating one oxygen atom within the backbone of Si.[139] At 600 °C and above, all the Si-H_x residues on the surface are oxidized to O_ySiOH and Si-O-Si species.[140] This thermal oxidation creates a hydrophilic PSi surface. Aqueous

oxidation is another approach to form O_ySiOH and Si-OH species on the fresh surface of PSi materials.[141]

Thermal carbonization and thermal hydrocarbonization are two alternative surface stabilization methods developed by Salonen in 2002 and 2004.[142-144] These methods consist of treating the freshly prepared Si surfaces with acetylene at elevated temperatures. Thermal hydrocarbonization is performed by flushing the Si surface with acetylene at 650 °C to create a Si-C and C-H surface. Thermal carbonization obtained by heating the PSi materials above 700 °C after the absorbance of acetylene leads to the formation of Si-C bonds on the surface of PSi. Thermal carbonization produces a more hydrophilic surface, which is more stable than after thermal hydrocarbonization. Chemically reactive groups, such as carboxylic acids (-COOH) and amines ($-NH_2$), can be introduced to the above stabilized PSi materials by continuing the liquid phase hydrosilylation with undecylenic acid or (3-aminopropyl)triethoxysilane (APTES).[8, 145]

Hydrosilylation is another approach for the surface stabilization of PSi, including Si-H reacting with an unsaturated compound bearing C=C, C≡C and C=O, forming Si-C-C, Si-C=C and Si-C-O bonds, respectively, originated after the catalysis induced by heat, light, metal and Lewis acid reactions.[146-149] Thermal hydrosilylation is obtained by immersing the hydride terminated PSi into diluted solutions of alkenes, alkynes, or aldehydes and refluxing for certain times.[149] Further functional moieties can be introduced by using the link molecules containing chemical reactive groups at the opposite end. Light hydrosilylation involves illuminating the PSi in a neat alkene or alkyne with tungsten or mercury lamp at room temperature.[150-151] Light hydrosilylation can prevent oxidation and form photopatterns by controlling the light illumination.[151] For example, 1,6-heptadiyne and 1,8-nonadiyne have been introduced onto the PSi surface by thermal or light hydrosilylation to obtain alkyne-terminated surfaces and further attached to PEG, methyl, alcohol, amine, and bromine via click chemistry.[152-154]

Metal ions (rhodium and platinum) can catalyze the hydrosilylation, enabling to achieve some functionalization onto the PSi surface, which are not possible by other functionalization routes.[6] However, in the case of biomedical applications, the risk of metal ions contamination is not optimal. Lewis acids ($EtAlCl_2$) catalyzing the hydrosilylation can introduce alkenes and alkynes to the surface of PSi in a solution at room temperature, although this is a rather slow process.[155]

Anodization is one of the top-down approaches to prepare PSi nanomaterials. It is carried out by etching the Si wafer in HF solution to generate porosity, which causes high Si mass loss. Recently, bottom-up approaches to prepare PSi have been under investigation. One of the methods is magnesiothermic reduction of silica to produce PSi.[156] Sodiothermic reduction of zeolite NaY can achieve higher surface area than the magnesiothermic method. Both of the methods need pre-formed porous materials as the precursor.[157] Porous Si/C composite materials use a chemical vapour deposition method. It is an effective bottom-up approach, but the produced Si unit is not porous.[158] Wet chemical synthesis is used to produce mesoporous crystalline Si materials by reduction of Si halogenide precursor ($SiCl_4$) and the production of salts precipitated for self-templating in order to synthesize PSi materials without chemical corrosion of Si.[159]

2.2.2 Biomedical applications

2.2.2.1 Biocompatability of PSi

The biocompatibility is the first characteristic of the biomaterials that needs to be assessed before applying it in healthcare. The biocompatibility of PSi has been investigated extensively both *in vitro* and *in vivo.*[160-165] Thermally-oxidized, aminosilanised PSi membranes were planted under the rat conjunctiva and underwent slow dissolution to silicic acid by colorimetric assay, but remained visible at the operating microscope for more than 8 weeks.[166] At the end-stage, histological assessment displayed that there was a thin fibrous capsule surrounding the implant, but little evidence of any local accumulation of acute inflammatory cells or vascularization were observed. In another study, three types of PSi particles (freshly etched particles, thermally hydrosilylated, and thermally oxidized particles) were injected into the rabbit vitreous to evaluate the stability and toxicity of each type of particles by ophthalmoscopy, biomicroscopy, tonometry, electroretinography and histology.[167] The results showed that no toxicity was observed with all three types of the particles during the more than 4 months study period. The surface alkylation led to significant increase in the intravitreal stability and slower degradation ($t_{1/2}$ 1 week *vs*. 5 weeks *vs*. 16 weeks). Further elimination of the Si element from the vitreal was investigated for fresh PSi and oxidized PSi by quantifying the Si from the samples of aqueous, vitreous and retina compartments by inductively coupled plasma-optical emission spectroscopy.[168]

Thermally hydrocarbonized PSi (THCPSi) and thermally oxidized PSi (TOPSi) particles have been reported to induce non-significant toxicity, oxidative stress, or inflammatory response *in vitro* to colon cancer cells Caco-2 and mouse leukemic monocyte macrophages RAW 264.7. However, *in vivo* the ^{18}F-labeled THCPSi NPs passed intact through the gastrointestinal track after oral administration and there was no absorption observed from the subcutaneous deposit.[160] The surface chemistry of PSi NPs also affects the biocompatibility of PSi NPs. Negatively charged hydrophilic (TCPSi and TOPSi) and hydrophobic (THCPSi) NPs induced less ATP depletion and genotoxicity than positively charged PSi NPs on immune cells and human red blood cells (RBCs).[161] **Figure 3** shows the effect of the PSi NPs with different surface chemistries on the cell morphology in RBCs. In another study, the myocardial infarction injection of THCPSi microparticles (7 and 19 μm) induced higher activation of inflammatory cytokine and fibrosis promoting genes compared to TOPSi microparticles (7 and 19 μm) and NPs (110 nm), but none of the particles affected the cardiac function or the hematological parameters.[162]

In another recent report, the acute immunotoxicity and subacute toxicity of PSi-based multistage siRNA delivery composite was addressed *in vitro* and *in vivo.*[163] The siRNA loaded composites did not increase the level of TNF-α or IL-6 in RAW 264.7 cells, nor triggering secretion of proinflammatory cytokines and chemokines, such as IL-1β, interferon-γ, and MCP-1, was observed *in vivo* after the intravenous administration. The subacute toxicity was studied by administration of this composite once a week for four

weeks and the mice were sacrificed 24 h after the final treatment. The results showed that the repeated treatments did not cause damages to major organs in the wild-type mice.

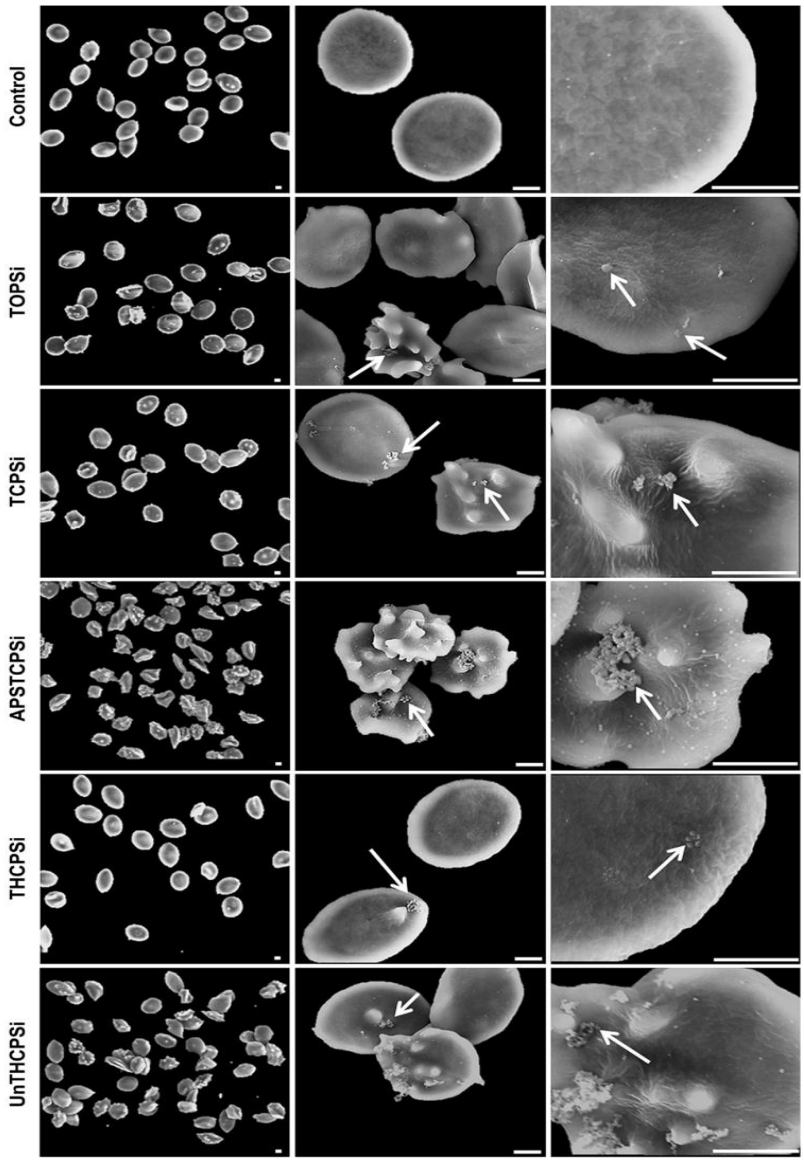

Figure 3. *Effect of different PSi NPs on the morphology of RBCs. Few TOPSi and THCPSi NPs were associated on the surface of erythrocytes with low morphological alterations, while higher amounts of (3-aminopropyl)triethoxysilane functionalized TCPSi (APS-TCPSi) and undecylenic acid functionalized (UnTHCPSi) NPs were associated with the erythrocytes and induced cell membrane wrapping and shrinking around the PSi NPs. Copyright © (2013) Elsevier B.V. Reprinted with permission from ref.* [161].

Besides the biocompatibility, the degradation of the NPs is also an important parameter for biomedical applications. The product obtained from the degradation of PSi is orthosilicic acid [$Si(OH)_4$], which is a common trace element in humans and is naturally found in numerous tissues.[169-170] But the degradation profiles of PSi depend, for example, on the fabrication method, surface properties, porous size, and porous volume.[167-168, 171-172]

Park *et al*. reported the *in vivo* degradation of luminescent PSi NPs administered subcutaneously, intramuscularly, and intravenously to mice, monitored by near-infrared photoluminescence.[173] The intravenously administered PSi NPs were eliminated in 4 weeks and the dextran-coating decreased the degradation rate of the NPs. There was no significant histopathological toxicity observed in the liver, spleen, and kidney. The studies indicated that the aqueous vitreous humor was a significant pathway for Si elimination from the eye following the intravitreal injection of PSi particles.

2.2.2.2 PSi for drug delivery applications

The nanoporous structure and the high surface area-to-volume ratio of PSi render it a potential carrier for drug delivery purposes. The most common method of loading payloads to PSi is physical adsorption.[174] In addition, chemical conjugation of drugs to the surface of PSi is an alternative to obtain sustained release of the payloads from PSi [175-176]. Small conventional drugs, peptides, proteins as well as nucleotides have been loaded into PSi materials for drug delivery applications.[163, 174, 176-182]

Surface stabilized PSi has been more commonly used for drug delivery applications. Freshly etched PSi NPs with Si-H_x (x = 1, 2 or 3) can react with redox active drugs and destroy the bioactivity of the drugs.[175] To avoid this, the anthracycline drug daunorubicin was conjugated to undecylenic acid terminated PSi particles for long-term drug delivery.[175] The three different methods used to stabilize the PSi particles were hydrosilylation in the presence of neat undecylenic acid, hydrosilylated PSi by air oxidation at 150 °C, and high temperature oxidation at 800 °C in air for 1 h. None or minor amounts of daunorubicin were detected in the release buffer from the first and second type of PSi particles due to the redox reaction of the residue Si-H species with daunorubicin. For daunorubicin conjugated PSi particles at high temperature oxidization, the major compound from the release media was daunorubicin. The results indicated that all the S-H or elemental Si species on the PSi particles used for drug delivery should be removed to avoid the reaction with redox-active drugs.[175]

In 2005, Salonen *et al*. studied five model drugs belonging to different biopharmaceutics classification system (BCS) categories (antipyrine, BCS class I; ibuprofen and griseofulvin, BCS class II; ranitidine, BCS class III; and furosemide, BCS class IV) loaded into TCPSi and TOPSi microparticles for oral drug delivery applications.[174] The results showed that the surface chemistry of PSi affected the drug affinity to the PSi particles, and thus, the drug loading degree. The nature of the drug and the loading solutions played critical roles in the drug loading efficiencies. PSi particles enhanced the dissolution rate of the poorly-water soluble drugs due to the disordered (amorphous) drug molecules adsorbed onto the surface of the inner wall of the nanosized PSi structure.

In another study, the physical state of the small drug molecule, ibuprofen, loaded into THCPSi particles with a loading concentration of 350 mg/mL of ibuprofen in ethanol was studied using three experimental methods (nitrogen sorption, thermogravimetry, and differential scanning calorimetry).[183] Three thermodynamically different states of ibuprofen were found: (1) a crystalline state outside the pores; (2) a crystalline state inside

the pores; and (3) a disordered state adjacent to the inner wall of the pores. Other studies have shown that TOPSi and THCPSi particles increased the permeability of poorly-water soluble drugs, griseofulvin and indomethacin, across the Caco-2 monolayer, which is an *in vitro* model used to mimic the intestinal epithelial cell barrier.[180, 184] Tablet formulations made from 25 weight-% of indomethacin (IMC)-loaded TOPSi microparticles were shown to increase the dissolution rate and drug permeability across Caco-2 monolayers of IMC.[185] *In vivo* orally administered IMC-loaded in TOPSi particles achieved enhanced oral delivery performance in comparison with crystalline IMC and Indocid®, showing a 4-time reduction on T_{max}, a 200% increase on C_{max}, as well as a significant increase in the IMC bioavailability.[186] **Figure 4** shows the plasma concentration profiles of IMC-loaded TOPSi microparticles, the commercially available formulation Indocid®, and free IMC on a fasted rat model after oral administration.

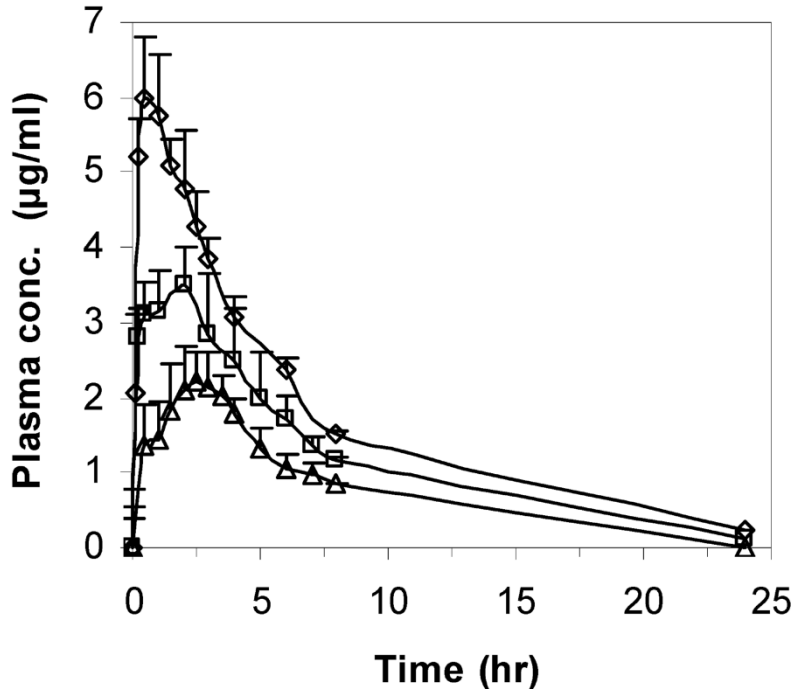

Figure 4. *Plasma concentration profiles of IMC-loaded TOPSi (◊), Indocid® (□) and free IMC (Δ) in a fasted rat model after oral administration. Copyright © (2010) the American Chemical Society. Reprinted with permission from ref.* [186].

Peptides have also been loaded into PSi for biomedical applications. For example, D-lys-GHRP6 (ghrelin antagonist) was used as a model peptide to study the loading, release and biological activity both *in vitro* and *in vivo*.[177] The pharmacological activity of the peptide was remained after the adsorption loading procedure. *In vivo* the peptide loaded in THCPSi microparticles presented a prolonged release effect compared with the peptide in solution after subcutaneous administration. Kovalainen *et al*. studied the effect of PSi particles with various surface chemistries on endogenous peptide YY3-36 (PYY3-36) delivery both *in vitro* and *in vivo*.[178, 187] *In vitro* and *in vivo* sustained release of PYY3-36 was in the same order and the release rate followed the order: TOPSi > THCPSi > UnTHCPSi. *In vitro*, the highest release from TOPSi was 27% after 14 days, which was

still not the completed release of PYY3-36. However, the *in vivo* sustained release of PYY3-36 for all the PSi particles lasted for more than 4 days. The bioavailability of PYY3-36 reached 98% for the loaded TOPSi particles and only 38% for the PYY3-36 solution when administered subcutaneously, with a half-life increase of 21 h *vs.* 25 min. In another study, co-loading of PYY3-36 and IMC into PSi enhanced the dissolution rate of both drugs.[181] On the other hand, glucagon-like peptide 1 (GLP-1) loaded into TOPSi, TCPSi, and amine-modified TOPSi and TCPSi particles did not achieve sustained release *in vitro* or *in vivo* after subcutaneous injection, however, the amine-terminated particles increased the adsorption of GLP-1 onto PSi microparticles.[179] Furthermore, chitosan coating increased the permeation of GLP-1 loaded in PSi NPs across an intestinal *in vitro* model.[188] The surface chemistry of the particles affects the peptide loading and release, and each peptide interaction with the PSi particles also depends on the properties of the peptides.

Protein drug delivery has been an increasing area for pharmaceutical research. The tailorable porosity of PSi can be used for encapsulation and delivery of proteins. For example, lysozyme, papain and human serum albumin (HSA) were loaded into the unoxidized and thermally oxidized PSi particles.[189] For all the three proteins, the unoxidized PSi particles presented higher loading degrees compared to the oxidized PSi particles, but a change in the proteins' structure occurred. This might be due to the highly reactive Si-H species on the surface of the PSi particles. Thermally oxidized PSi heated at 800 °C retained the protein structures of lysozyme and papain, but not HSA. Due to the hydrophobicity/hydrophilicity interactions, electrostatic attraction and the high surface area inside the pores of the particles, the protein interacts with the PSi particle and is oriented in a different way from the protein in physiological conditions. The pharmacological activity of the loaded protein should be studied individually case by case. Insulin has also been loaded to PSi particles and nearly 10-fold higher permeability across intestinal Caco-2 cell monolayer was achieved compared to the insulin solution alone.[190] In another report, chitosan-conjugated UnTHCPSi microparticles also enhanced extensively the permeability of insulin across the Caco-2/HT-29 cell monolayers.[191]

Gene therapy has been one of the novel model approaches to treat genetic defects and cancer, particularly the traditionally considered "non-druggable" genetic diseases.[192] For example, siRNA has been involved to knock-down the drug resistant gene when co-delivered with chemotherapeutic agents for multidrug resistant cancer therapy [193]. PSi-based nanomaterials have also been studied for gene delivery. However, different from conventional small drug molecules or peptides/proteins, negatively charged plasmid DNA and siRNA have not been directly loaded to the stabilized PSi nanomaterials for gene delivery. Multistage stage PSi-based vectors encapsulating siRNA for cancer therapy have been reported both *in vitro* and *in vivo.*[194-195] The developed multistage vectors, siRNA targeted proteins and the *in vitro* and *in vivo* effects are listed in **Table 2**. The representative *in vivo* success of siRNA delivery and biocompatibility at the therapeutic dose of PSi-based multistage complex systems give the dawn of the PSi materials for clinical applications. ^{32}P BioSilicon, which is made of PSi materials loaded with ^{32}P isotope, is currently used in brachytherapy for pancreatic cancer treatment in clinical trials phase III.[196-197]

Table 2. *Summary of the PSi-based multistage siRNA delivery systems.*

Multistage PSi-siRNA system	siRNA targeting	Results	Ref
APTES stabilized PSi microparticles loaded with neutral siRNA-DOPC[1] nanoliposome	EphA2 oncoprotein	Sustained EphA2 gene silencing for at least 3 weeks in ovarian cancer model following a single intravenous administration and reduced tumor burden, angiogenesis and cell proliferation	194
	EphA2 oncoprotein	Combination treatment with paclitaxel completely inhibited SKOV3ip2 tumor. Combination with docetaxel inhibited tumor growth of HeyA8-MDR tumor	195
APTES stabilized PSi microparticles modified with arginine-PEI[2] inside the nanopores	STAT3 siRNA or GRP78 siRNA	91% (STAT3)[3] or 83% (GRP78)[4] reduction of gene expression in MDA-MB-231 cells. In murine model of MDA-MB-231 breast cancer reduced STAT3 expression in cancer cells, and significant reduced cancer stem cells in the residual tumor tissue, with no triggered acute immune response	163
APTES stabilized PSi microparticles loaded with siRNA-DOPC nanoliposomes	ATM siRNA	Biweeky treatment, suppressed ATM[5] expression in tumor tissues, inhibited growth of MDA-MB-231 orthotopic tumor. No acute immune response was observed	198
APTES stabilized PSi microparticles modified by ESTA[6], loaded with siRNA/PEG-PEI	siRNA targeting to the human STAT3 gene	Knock-down of STAT3 expression in 48.7% of cancer cells inside the bone marrow. Weekly systemic administration significantly extended survival of mice with MDA-MB-231 bone metastasis	199
TEIC[7] stabilized PSi microparticles loaded with siRNA/PEI complex	siRNA against ATM	siRNA/PEI complexes induced dramatic gene silencing *in vitro* and enhanced biocompatibility	200

*[1]DOPC: 1,2-dioleoyl-*sn*-glycero-3-phosphocholine; [2]PEI: polyethyleneimine; [3]STAT3: essential gene for breast cancer stem cells; [4]GRP78: gene encodes a 78-kDa glucose-regulated protein; [5]ATM: ataxia-telangiectasia mutated; [6]ESTA: E-selectin thioaptamer. [7]TEIC: 3-(triethoxysilyl)propyl isocyanate.*

2.2.2.3 PSi for imaging applications

In addition to the drug loading capacity, PSi nanomaterials have been employed as a potential imaging tool for biomedical application, such as cancer imaging.[201] The imaging properties of the materials give the possibility to assess and monitor the biofate of the developed drug nanocarriers *in vivo*.

Fluorescent-labeled PSi NPs have been used for *in vivo* cancer imaging.[202] After targeting peptides functionalization, accumulation of the fluorescent PSi NPs was followed in the tumor tissue. In another study, both Quantum-dots and SWCNTs have been loaded into PSi to form multistage fluorescent vectors.[203] This study also showed that the surface chemical properties of both the nanocomposites affected the loading efficiency and stability of the assembled multistage carrier systems.

Sarparanta *et al*. developed a direct one-step ^{18}F-radiolabeling reaction suitable for three types of PSi particles (THCPSi, TCPSi, and TOPSi).[204] All the three radiolabeled

particles presented excellent radiolabeling stability in simulated gastric and intestinal fluids and in plasma. Furthermore, the ^{18}F-labeled THCPSi NPs was used to monitor the *in vivo* fate of THCPSi NPs after oral administration (**Figure 5**),[160] and intravenous administration.[205]

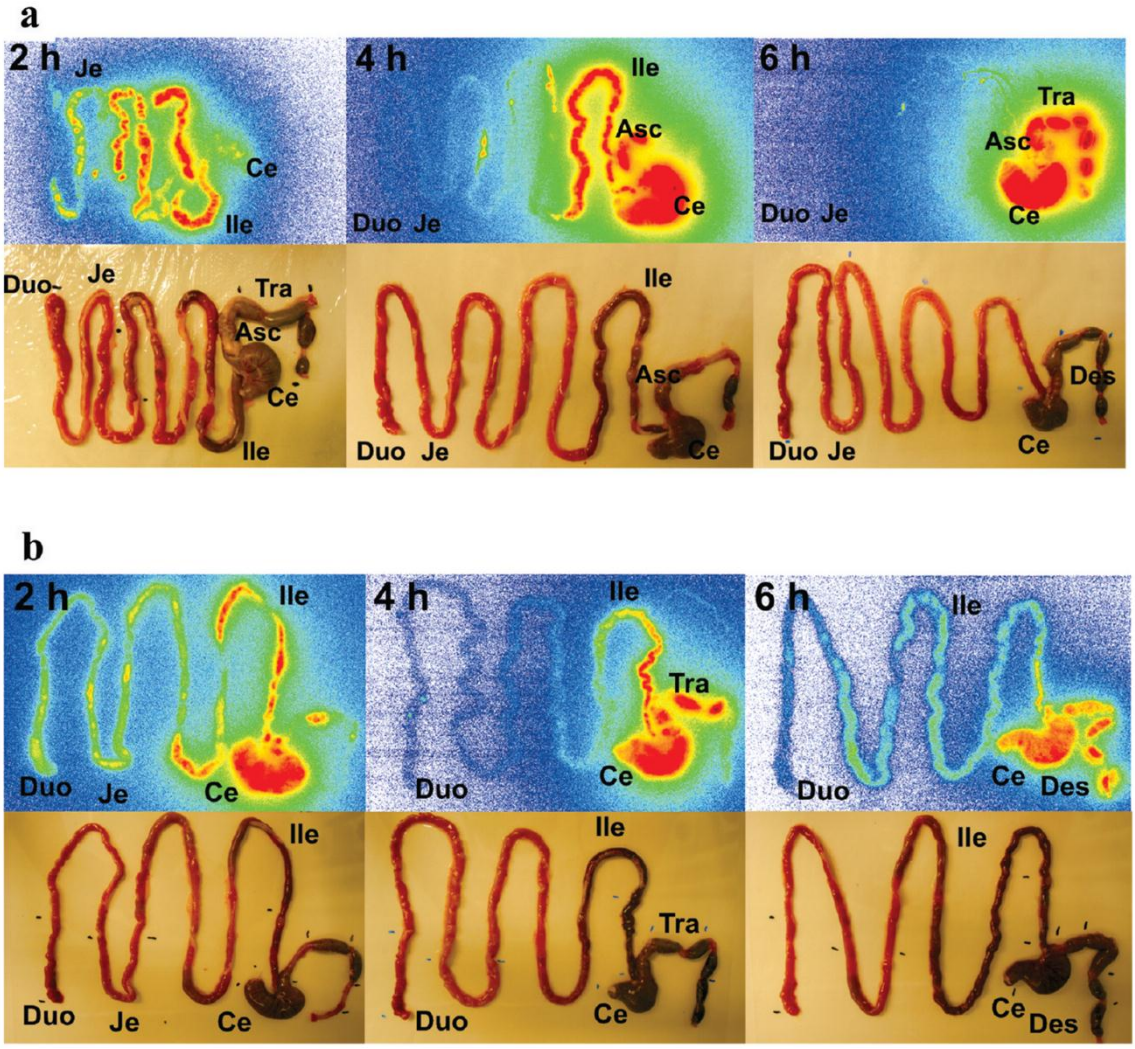

Figure 5. *Macroautoradiographs and respective photographs of the gastrointestinal tracts of rats at 2, 4, and 6 h after oral administration of ^{18}F-labeled THCPSi NPs (a) and free ^{18}F-NaF (b). Abbreviations denote: Duo, duodenum; Je, jejunum; Ile, ileum; Ce, cecum; Asc, ascendens; Tra, transversum; and Des, descendens. Copyright © (2010) the American Chemical Society. Reprinted with permission from ref.* [160].

Luminescent colloidal Si suspension was reported in 1992.[206] Following the high quantum yield, Si nanocrystals were fabricated.[207-208] The luminescence of PSi NPs displayed radiation lifetimes in the order of 100 ns to several microseconds, which can be used for late time-gating (capturing the signal at a delayed time after excitation) to reduce the tissue autofluorescence.[209] In 2009, Park *et al*. developed biodegradable luminescent PSi NPs used for *in vivo* imaging.[173] *In vitro*, the PSi NPs degraded into silicic acid and lost the luminescence very fast (80% loss of luminescence in 1 h) after incubation in

buffer solution (pH 7.4, 37 °C). The *in vivo* biodistribution and degradation of this luminescent PSi NPs can be monitored non-invasively in live animals by microscopy. The *in vivo* administered luminescent PSi NPs did not present any toxicity. Gu *et al*. reported luminescent PSi NPs displaying sufficiently long lifetimes (5-13 μs) to permit late time-gate imaging.[201] This PSi-based luminescent probe presented the improvement of signal to background contrast ratio by more than 50-fold and 20-fold *in vitro* and *in vivo*, respectively.

PSi NPs have been utilized as cargos to encapsulate the magnetic resonance imaging (MRI) contrast which were further investigated for MRI.[210-211] In 2010, Ananta and Godin reported three gadolium-based contrast agents – magnevist, gadofullerenes and gadonanotubes were loaded inside the porous structure of PSi particles.[210] By loading to the PSi particles, the relaxivity values were about 4- to 50-fold higher than those of the gadolinium-based agents in clinical use. The mechanism of enhancing the relaxivity was due to the geometrical confinement of the agents which further affect the paramagnetic movement of the Gd^{3+} ions. Magnetic NPs (Fe_3O_4) has been trapped into the PSi NPs.[211] The MRI contrast was significantly enhanced by controlling over the clustering of iron oxide NPs in the pores of the PSi NPs.

2.3 Biological barriers and surface modification of drug carriers

2.3.1 Biological barriers and targeting drug delivery

2.3.1.1 Intestinal barriers

After a drug is administered in the body, there are several biological barriers before the drug reaches the targeting site and generates the pharmacological effect.[212] The most common drug delivery route is oral drug administration. Some cancer drugs can be applied for oral administration in clinics, such as methotrexate and sorafenib.[213-214] For oral drug delivery, the first obstacle is the acidic conditions in the stomach. Coating or encapsulation with acidic insoluble polymers has been one of the approaches to help the drugs to overcome the acidic conditions and safely pass from the stomach to the intestine. The major adsorption of the orally administered drug occurs at the small intestine due to the large surface area with the presenting of villi and microvilli.[215] For many small drugs, as well as peptides and proteins with low permeability across the intestinal wall, modification of the drug formulation with intestinal mucus adhesive materials, for example chitosan, could increase the drug adsorption.[216]

2.3.1.2 Plasma Protein barrier

The plasma barrier is the first biological barrier for the intravenously delivered NPs. Due to the physicochemical properties, NPs can be surrounded by protein corona in less than one second after intravenous administration.[22] In plasma, the most abundant protein is serum albumin, followed by the more hydrophobic protein, fibrinogen. The immunoglobulins, complement proteins, and fibrinogen proteins are the major proteins related to the immune system, which can stimulate the phagocytosis by the mononuclear phagocyte system (MPS).[217] Complement C3 associated to the NPs triggered the recognition and elimination by macrophages when the complement C3 protein is converted to the C3a/b form.[24] For many low water-solubility anticancer drugs, NP-based drug delivery systems are used to increase the aqueous solubility of drugs, and this has been a hot field for anticancer drug delivery.[65] Nanoparticulated chemotherapeutic drug formulations for intravenous administration can achieve 100% bioavailability, with reduced incidence of serious side effects in the intestine.[218] However, the protein corona can dramatically determine the biofate of the NPs. When NPs are recognized by the immune system macrophages, the NPs will be mainly transported to the liver and spleen and fail to deliver the drug to the desired site.[219] High molecular weight polyethylene glycol (PEG) and dextran have been investigated as hydrophilic polymers to sheath the surface of the NPs and aid to prevent the plasma protein association.[24, 220]

2.3.1.3 Cancer tissue/cell uptake and endosomal escape

For chemotherapy, only the anticancer drugs reaching the cancer tissue will function and inhibit the cancer growth.[221] Directing the anticancer drugs or drug loaded carriers to the cancer tissue is one of the major steps for chemotherapy. Due to the rapid dividing of cancer cells and formation of neovasculature, the blood vessels in the cancer tissue are leakier than the established blood vessels in healthy tissues.[222] NPs circulating in the bloodstream can penetrate the leaky blood vessels into the tumor tissue,[223-224] which is a passive targeting drug delivery approach. In addition, numerous molecular biomarkers at the surface of the neovascular endothelial cells and cancer cells have been identified, as well as the targeting ligands which have specific high affinity to the biomarkers.[225] Surface modification of the NPs with the specific ligands can increase the interaction of the NPs with the cancer tissue, and thus, increase the drug delivery efficiency.[10, 226]

Some cancer drugs work by intercalating DNA synthesis, such as doxorubicin, paclitaxel, cisplatin,[227-229] or inhibiting the enzyme involved in DNA synthesis during cell proliferation, such as methotrexate.[230] These kinds of anticancer drugs have to be delivered into the cytoplasm or nuclei. The negatively charged cell membrane is another barrier for the delivery of anticancer drugs into the cytosol. Enhancing the cellular uptake of the drugs or NPs is one of the approaches for chemotherapeutical drug delivery development. It has been reported that cationic charged nanocarriers can increase the interaction with the cell membrane and induce endocytic cellular uptake.[231-232] Thus, for low cellular uptake of drug molecules or to overcome multidrug resistance, researchers have investigated the use of cationic nanovector-based drug delivery approaches.[233]

Cell membrane receptor-mediated uptake of NPs is another approach to increase the cellular uptake of the nanocarriers.[92, 234] Integrins, vascular endothelial growth factor (VEGF) or transforming growth factor α (TGF-α) are the common biomarkers of the neovascular endothelial cells.[235] Targeting ligands, such as peptide arginine-glycine-aspartic acid (RGD), VEGF receptors, TGF receptors, can be incorporated onto the surface of nanocarriers and increase the cellular uptake of the nanocarriers for anticancer drug delivery.[236-238]

The endocytic cellular uptake pathway is the major mechanism for the nanocarriers by the cells.[239] Following the endocytosis, endosome escape to the cytoplasmic compartment is an important step for certain drugs, especially the biological drugs, such as peptides, proteins, and genes. The mechanisms of endosome escape include: (1) pore formation in the endosomal membrane; (2) the proton sponge effect; (3) fusion in the endosomal membrane; and (4) external photochemical disruption of the endosomal membrane.[239]

2.3.1.4 Targeting drug delivery

The concept of actively targeted drug delivery is attractive, because it recapitulates some of the advantages of typical application of drugs, such as increasing the local concentration and lowering the systemic exposure.[11-12] Tumor blood vessels express biomarkers that are not present in resting blood vessels of normal tissues, but can be shared by angiogenic vessels in non-malignant conditions.[11] Among these biomarkers, a number of cell-specific epitopes have been explored to show specific binding to certain antibodies, peptides or small molecules.[12, 238, 240] These differentially expressed biomarkers can be used as docking sites accumulating drug molecules and/or drug carriers at the tumor tissue, which is described as targeting drug delivery.

Targeting peptides, aptamers, antibodies, as well as small molecules have been used to increase the specific targeting delivery of nanocarriers.[7, 13, 241-242] The three-amino acid peptide RGD was identified as a ligand for integrins, such as αvβ3, αvβ5, and α5β1.[243-244] Intravenously administrated RGD-targeted nanovectors are capable to deliver a payload of antiangiogenic or antitumor agents to tumor sprouting tissue while sparing healthy tissues. RGD-modified NPs superiorly accumulated within the tumor-associated blood vessels, but showed little binding to other vascular beds.[241, 245] iRGD is a disulfide-based 9-amino acid cyclized peptide, identified by phage display as a tumor targeting and tissue penetrating peptide.[244] It can first associate with tumor cells by specific affinity to αvβ3/5 integrins on the tumor endothelium. On the cell membrane, iRGD is cleaved between lysine (K)/arginine (R) and glycine (G) by proteolysis to produce a C-terminal motif, which can form neuropilin-1 mediated cell internalization. The iRGD surface modified nanovector incorporates both tumor targeting and tissue penetrating properties to the drug delivery vectors.[241]

2.3.2 Pre- and post-surface modification of nanovectors

Surface functionalization is an important approach to modulate the properties of nanomaterials for biomedical applications, such as to introduce fluorophores for fluorescent imaging,[202] and chelators for radiolabeling,[246] hydrophilic targeting moieties for targeted drug delivery,[236] or antifouling polymers to prevent plasma protein association.[247]

Biofunctionalized nanocarriers can be prepared by pre- or post-functionalization approaches.[248-249] Both approaches have their advantages and disadvantages. Pre-functionalization needs to synthesize the functionalized building blocks prior the formation of the NPs. With this method, the ratio of the functional moiety on the nanocomposite's surface can be controlled accurately.[72] On the other hand, this approach demands that the building blocks and reaction reagents need to be dissolved well in the same solution. The functionalized moiety might disturb the self-assembling formation process.[250] Post-functionalization is the way that the nanostructural carrier is prepared before the functionalization. The post-modification ensures the functional moiety on the surface of the nanocarrier. However, the functionalization ratio is usually limited by the crowdedness on the surface of the NPs. In addition, it might be problematic to remove the unreacted species in some cases.[250] Post-surface functionalization has been more commonly used for inorganic nanosystems modification, such as carbon nanotubes,[246] quantum dots,[251] SPIONs,[252] mesoporous silica,[16] or the more rigid polymer-based nanosystems.[250] Various chemical reaction linkages that can be used for surface modification of NPs are listed in **Figure 6**.[253] Among these reactions, click chemistry has gained abundant attention during the past decade due to the efficiency and high selectivity to conjugate biomolecules.[254]

2.3.3 Click chemistry reactions

Click chemistry was reported by Sharplees in 2001 as a simple method to couple organic molecules in high yields under mild conditions and high selectivity in the presence of a diverse range of functional groups.[255] One of the most widely used examples of this class of extremely efficient chemical reactions is the copper catalyzed azide-alkyne cycloaddition (CuAAC) reaction. Due to its high thermodynamic driving force, usually greater than 20 kcal/mol, the click reaction normally proceeds rapidly to completion and also tends to be highly selective.[19] Both reaction active groups (azide and alkyne) are almost entirely inert to the functional groups, such as amines, carboxylic acids, thiols etc., which widely exist in many molecules. CuAAC is interesting for NPs' surface biofunctionalization, because of the high specificity, efficiency and mild reaction conditions to preserve the bioactivity of some biomolecules.[19] Strain promoted azide-alkyne cycloaddition (SPAAC) click reaction, which is also called copper-free click reaction, becomes an alternative for the copper catalyzed click reaction.[256-257] SPAAC avoids using copper ion as a catalyst, which could induce cell and further *in vivo* biological toxicity. SPAAC has become an interesting tool for surface modification of biomaterials and coupling functional molecules to the NPs' surface for drug delivery

and/or *in vivo* imaging applications. Bicyclononyne (BCN) and dibenzylcyclooctyne (DBCO) are two of the most commonly used moieties containing the strain-promoted alkyne components.[257]

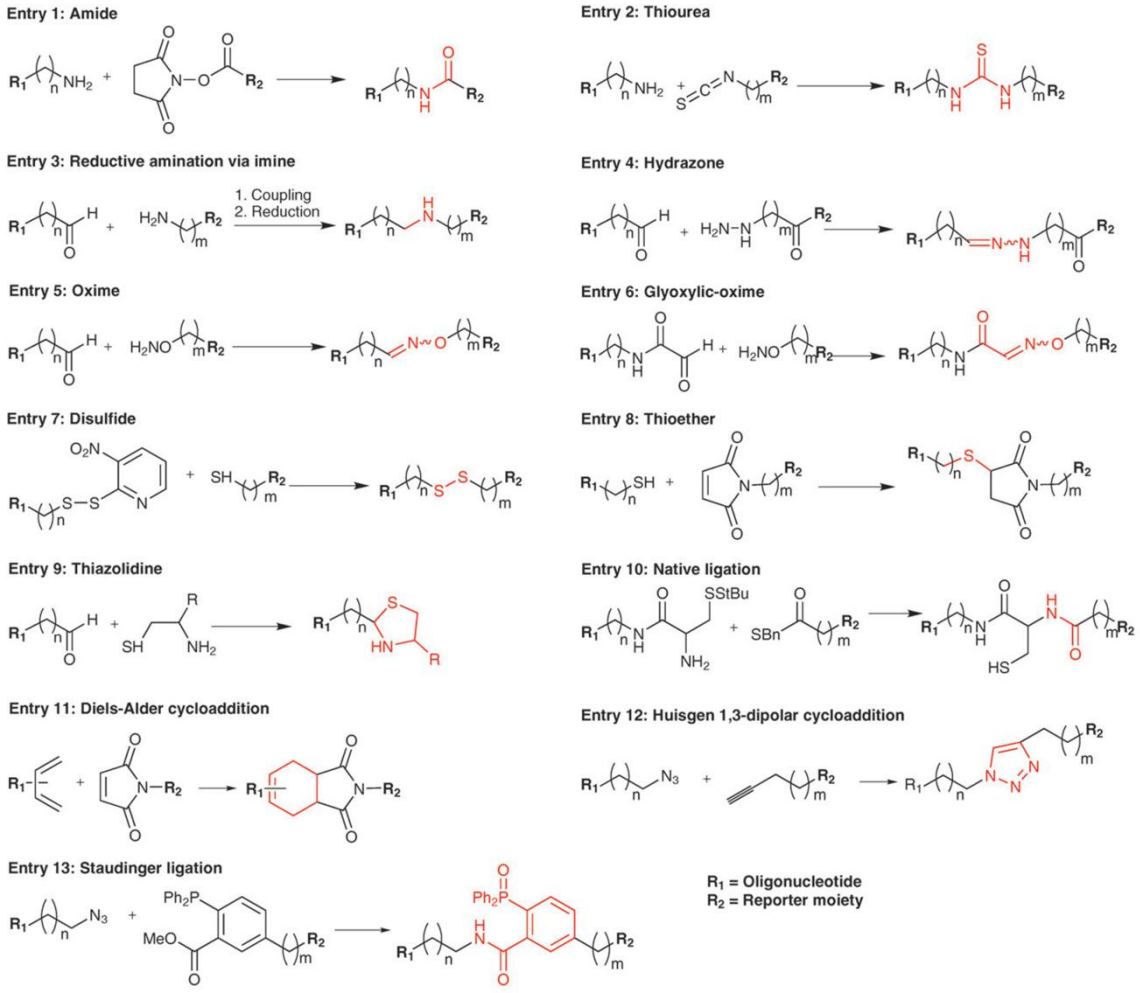

Figure 6. *Common chemical reactions used for molecular conjugation. Copyright © (2011) Elsevier B.V. Reprinted with permission from ref.* [253].

2.3.4 Surface modification of PSi materials

During primary stabilization of the freshly prepared PSi materials, chemically reactive moieties can be introduced to the surface of PSi as discussed in section **2.2.1**. These functional end-groups can be further chemically reacted with various molecules for different purposes. Ciampi *et al*. reported surface modification of acetylene-terminated PSi films by CuAAC.[152] The two-step hydrosilylation/cycloaddition procedure has achieved growing interest in chemical functionalization where the modified surface displayed lowered nonspecific bovine serum albumin adsorption. In one study published in 2008, different functionalization of the internal and external surfaces of the PSi films was achieved.[258] The fresh PSi surface was stabilized by alkyne monolayer to achieve hydrophobic surface which can completely prevent the access of water. The external

surface of the PSi was modified in aqueous solution. Next, the internal surface was pre-wetted with ethanol, and thus, was accessed for modification. The external surface grafted RGD peptide increased the cell adhesion to the PSi films. Furthermore, a route to differently surface modifying the external and internal surfaces of PSi material was achieved by CuAAC.[153] A highly parallel PSi biosensor platform was prepared by α.ω-diyne adsorption to the photonic PSi monolayer and modified by click chemistry in the presence of titanium mask.[259] Chemical conjugation of PEG onto the PSi's surface can prevent albumin adsorption, whereas the smaller protein lysozyme adsorption was of very low extent.[154] The anionic porphyrin-grafted to hydrosilylation stabilized PSi NPs were delivered inside breast cancer cells for more efficient photodynamic therapy.[176] In this study, the PSi NPs were stabilized by hydrosilylation with allyl isocyanate. The antibody was conjugated to 1,8-nonadiyne stabilized PSi microparticles for selective binding to the targeted cell type over the others.[242] In another study, three antibodies have been used to functionalize PSi NPs for targeted delivery of hydrophobic drug camptothecin.[260] These three antibodies MLR2 (monoclonal antibody to p75NTR), mAb528 (monoclonal antibody to EGFR) and Rituximab (monoclonal antibody to CD20) were used to target neuroblastoma, glioblastoma and B lymphoma cells, respectively. E-selectin thioaptamer ligand, which can target to E-selectin, was conjugated to the APTES modified PSi particles for bone marrow targeted drug delivery.[7] Hyaluronic acid, which can target the CD44 over-expressed cancer cells, were amine modified and conjugated to carboxylic acid terminated PSi NPs for breast cancer targeting.[261] The developed NPs showed enhanced cellular interaction and internalization in breast cancer cells.

Physical coating is another important method to improve the targeting properties of PSi. Hydrophobin II protein coating increased the biocompatibility and wettability of PSi particles, as well as the mucus adhesion of the NPs *in vivo*.[262-264] In addition, the hydrophobin protein coating did not affect the drug loading and the drug release profiles of the bare PSi particles.[262] In order to evade the immune system, cellular membranes purified from leukocytes were used to coat PSi particles.[265] These hybrid particles (called leukolike vectors) showed enhanced circulation time and improved accumulation in the tumor.

In summary, surface modification of the NPs can modulate the surface properties of the NPs, which can intensively affect the biofate and the function of the nanocarriers *in vivo*. By considering the functional mechanism of the biological system, drug delivery systems can be chemically surface modified to introduce desired bioactive properties for more specific cancer drug delivery applications.

3 Aims of the study

The main aim of this dissertation was to employ different chemical approaches to improve the drug delivery efficiency, particularly by using the PSi platform for both cancer therapy and imaging and targeting peptides conjugated to oligonucleotide via click chemistry. The conjugation routes for PSi NPs and oligonucleotides were investigated, including the versatile SPAAC and CuAAC click conjugation methods. The developed PSi NPs were prepared and characterized, and the proof-of-concept demonstrated both *in vitro* and *in vivo*.

The specific objectives of this study were:

1. To conjugate targeting peptides to cationic PSi (amine terminated) via SPAAC for enhanced intracellular drug uptake of the NPs (**I**).
2. To prepare multifunctional anionic PSi NPs (carboxylic acid terminated) for theranostic studies by SPECT/CT *in vivo* and fluorescence microscopy *ex vivo* (**II**).
3. To surface functionalize alkyne terminated PSi NPs by targeting peptides and anti-fouling polymers *via* CuAAC, and to study the effect of the NPs on the cellular uptake and human plasma protein adsorption (**III**).
4. To conjugate targeting peptides to oligonucleotide via CuAAC for targeting angiogenic anti-inflammation (**IV**).
5. To sustain the release and enhance the cellular uptake of MTX by chemical conjugation of MTX to PSi, as well as to co-load hydrophobic antiangiogenic drug, sorafenib, to the MTX-PSi NPs for combination cancer therapy (**V**).

4 Experimental

This experimental section summarizes the experimental methods used in this dissertation. More detailed information on the materials and methods used in this work can be found in the respective original publications (**I–V**). The primary surface stabilized PSi NPs (**I–III and V**) were fabricated at the Laboratory of Industrial Physics, Department of Physics and Astronomy, University of Turku. The Radiolabeling of the PSi NPs was performed at the Laboratory of Radiochemistry, Department of Chemistry, University of Helsinki.

4.1 Preparation of primary surface stabilized PSi NPs (I–III, and V)

PSi films were fabricated prior to the NPs' preparation. Monocrystalline p+-type Si ⟨100⟩ wafers with the resistivity of 0.01–0.02 Ωcm were electrochemically etched to multilayer Si-H terminated PSi films, as reported elsewhere.[8] The electrolyte used was 1:1 (v/v) hydrofluoric acid (HF, 40%)-ethanol. Thermally hydrocarbonized PSi (THCPSi) films were obtained by heating at 500 °C under 1:1 N_2-acetylene flow for 15 min. Thermally carbonized PSi (TCPSi) films were obtained by heating the THCPSi films absorbed with acetylene at 820 °C for 10 min.

TCPSi films were immersed in HF to generate the silanol terminals. Next, the TCPSi films were placed in 10 v-% APTES-toluene solution to obtain aminopropylsilane-TCPSi (APS-TCPSi) films. The NPs were obtained by wet-milling of the APS-TCPSi films using a 5 v-% APTES-toluene solution as the milling liquid. The final size selection of the NPs was done by centrifugation.

THCPSi films were activated to silanol terminals by immersing in HF. Carboxilyc acid-terminated THCPSi (UnTHCPSi) films were obtained by treating the activated THCPSi films in undecylenic acid at 120 °C for 16 h to obtain terminated carboxylic acid films, adapting the thermal addition process described elsewhere.[178] Next, the UnTHCPSi NPs were prepared by wet-milling in undecylenic acid and then centrifuged to obtain the required PSi NP size.

Alkyne-terminated THCPSi films were fabricated in such a way that the activated THCPSi films were immerged in 10 v-% 1,7-octadiyne–mesitylene solution at 150 °C for 16 h, adapting the thermal addition process described elsewhere.[187] The THCPSi-alkyne NPs were obtained by wet-milling of THCPSi-alkyne film in a fresh 10 v-% octadiyne–mesitylene solution and then centrifuged to obtain the required NP size.

4.2 Chemical modification

4.2.1 Targeting peptides surface modification of APS-TCPSi NPs (I)

The functionalization of targeting peptides onto the TCPSi NPs's surface via SPAAC was achieved in two steps. Firstly, APS-TCPSi NPs were reacted with (1R,8S,9s)-bicyclo[6.1.0]non-4-yn-9-ylmethyl succinimidyl carbonate (BCN-NHS) in 200 µL of 4-(2-hydroxyethyl)-1-piperazineethanesulfonic acid (HEPES) buffer (0.1 M, pH 7.8) at room temperature to obtain click moiety decorated TCPSi-BCN NPs. Secondly, azide-functionalized Arg-Gly-Asp-Ser (RGDS) and iRGD were reacted with TCPSi-BCN NPs via SPAAC in Milli-Q water at 37 °C for 30 min. The TCPSi NPs were then harvested from the reaction mixture by centrifugation and washed with 1 mL ethanol/water three times to remove the unreacted peptides.

For confocal fluorescence imaging and flow cytometry analyses, the APS-TCPSi NPs were first covalently labeled with fluorescein isothiocyanate isomer I (FITC). Briefly, 2 mg of APS-TCPSi NPs were mixed with 0.1 mg of FITC in 400 µL ethanol and 100 µL 0.1 M HEPES (pH 7.4). The FITC-labeled TCPSi NPs were continually reacted with BCN-NHS and the peptides as described above to obtain peptide-functionalized FITC-labeled NPs.

4.2.2 Multifunctional PSi NPs preparation (II)

DBCO-PEG4-amine and Alexa Fluor® 488 (Life Technologies, USA) were conjugated to UnTHCPSi NPs via N-hydroxysuccinimide (NHS) and 1-ethyl-3-(3-dimethylaminopropyl)-carbodiimide (EDC) coupling reaction to obtain UnTHCPSi-Alexa488-DBCO NPs. 1,4,7,10-tetraazacyclododecane-N,N',N'',N'''-tetraacetic acid (DOTA) and iRGD with azide moiety were sequentially conjugated to UnTHCPSi-Alexa488-DBCO by the SPAAC reaction.

For ^{111}In-labeling of the multifunctional NPs, 1.25–1.5 mg UnTHCPSi-Alexa488-DBCO-DOTA NPs were incubated with 178–309 MBq of $^{111}InCl_3$ at 85 °C in 1.0 mL of 0.1 M ammonium acetate buffer (pH 6.0) for 20 min. The peptide was conjugated to the NPs after ^{111}In-labeling to achieve a multifunctional nanocarrier system. The NPs were formulated in sterile 0.9% NaCl solution to a concentration of 83 MBq/mL before injection.

4.2.3 Surface modification of THCPSi-alkyne the NPs by CuAAC (III)

The azide-functionalized compounds (RGDS, iRGD, and dextran of MW 6 kDa and 40 kDa) were dissolved in anhydrous dimethyl sulfoxide (DMSO) and poly(glutamic acid) (PGA) was dissolved in Milli-Q water. The azide-functionalized reagents were added to the THCPSi-alkyne NPs, with copper (II) sulfate pentahydrate and sodium ascorbate, and all stirred at room temperature protected from the light for 24 h. After reaction, the NPs

were collected from the reaction mixture by centrifugation, washed with DMSO/ethanol/water, and re-suspended in ethanol for further use.

4.2.4 Peptide-oligonucletide conjugation (IV)

Linear iRGD and other peptides (H-RN, C16Y, and ATW) targeting to neovasculature were prepared through the standard Fmoc-chemistry solid support peptide synthesis (SPPA) by an automated peptide synthesizer. iRGD was prepared by cyclization through a disulfide bond presented in cysteine of linear iRGD. The amino acid containing azide functional group was induced to the N-terminal of iRGD in order to keep the CendR property of iRGD,[266] and to the C-terminal for all the other peptides during the SPPS synthesis. Alkyne terminated oligonucleotide antisense interleukin-6 (ASIL-6-Alkyne) and fluorescent labeled ASIL-6 were synthesized by an automated DNA synthesizer on a 400 nM scale.

Azide functionalized targeting peptides and ASIL-6-alkyne were conjugated in water/formamide solution by CuAAC. Briefly, ASIL-6-Alkyne (10 nmol) in Milli-Q water was added to the peptide (100 nmol) in 250 μL formamide, following the "click solution" (1 μmol $CuSO_4$, 1 μL sodium ascorbate, and 2 μmol μmol tris(benzyltriazolyl-methyl)amine (TBTA) in 40 μL DMSO/tert-butyl alcohol 3:1) added. The reaction mixture was mixed at room temperature overnight and the conjugated products were purified by HPLC and confirmed by mass spectrometer (MS). More detailed information about the techniques used in this work is presented in the publication (**IV**).

4.2.5 Conjugation of MTX to the APS-TCPSi NPs (V)

MTX was conjugated to the amine-terminated PSi (APS-TCPSi) NPs using NHS/EDC coupling reaction. The conjugated PSi NPs was separated from the reaction mixture and washed by 1 mL of DMSO/water/ethanol three times to obtain the MTX conjugated PSi NPs (MTX–PSi), which were then re-suspended in ethanol for further use.

4.3 Physicochemical characterization (I–V)

The surface area, pore volume, and pore diameter of the prepared PSi NPs were determined by N_2 sorption at 77 K using TriStar 3000. The specific surface area of the PSi NPs was calculated using the Brunauer-Emmett-Teller theory.[267] The total pore volume was obtained as the total adsorbed amount at a relative pressure p/p0 = 0.97. The average pore diameter was calculated from the obtained surface area and pore volume by assuming the pores as cylindrical (**I**–**III**, and **V**).

The chemical surface modification of the PSi was characterized by Fourier transform infrared spectroscopy (FTIR) (**I–III**, and **V**), elemental analysis (EA) (**I** and **V**) and thermal gravimetric (TG) analysis (**III**). The size and zeta-potential of the NPs prepared

were measured by dynamic light scanning (DLS) (**I–III**, and **V**). The morphology of the NPs was determined by a transmission electron microscopy (TEM), JEM-1400, using a voltage of 80 kV and magnifications between 250× and 50000× (**III** and **V**). The peptide-oligonucleotide (including fluorescent labeled ASIL-6) conjugates were confirmed by MS (**IV**).

4.4 Drug loading and release

4.4.1 Sorafenib loading and release studies (I, II, and V)

The poorly water-soluble antiangiogenic drug, sorafenib, was used as model compound to test the physical adsorption of the loaded drug and its release profiles from the surface of the modified NPs. The chemotherapeutic drug, MTX, was chemically conjugated to APS-TCPSi NPs (see section **4.1.4**). Sorafenib was loaded to the NPs using an immersion method. Sorafenib was dissolved in acetone (15 mg/mL, **I** and **V**) or dimethylformamide (DMF) (50 mg/ml,), and the drug/NP ratio used was 15:1 (w/w) (**II**).

The drug loading degrees of the drugs were determined by immersing 200 μg of the drug-loaded NPs to 1 mL of acetonitrile/water mixture (42:58%, v/v) under vigorous stirring for 1 h and the supernatant was analyzed by high pressure liquid chromatography (HPLC) with the mobile phase of 0.2% trifluoroacetic acid (pH 2) and acetonitrile at a ratio of 42:58% (v/v) with a 1.0 mL/min flow rate and UV detector set at the wavelength of 254 nm.

The drug release tests were performed in sink conditions using a shaking method.[262] The release media used were cell culture medium with/without FBS (**I**), 10 mM of 2-(N-morpholino)ethanesulfonic acid (MES, pH 5.5) with/without 10% FBS (**I**, **II**, and **V**) and 10 mM HEPES (pH 7.4) with/without 10% FBS (**I**, **II**, and **V**).

4.4.2 MTX release analysis (V)

The MTX release was determined in sink conditions using a shaking method. The release media used were 10 mM MES (pH 5.5) and 10 mM HEPES (pH 7.4) with/without 10% FBS. The released MTX fragment from the MTX–PSi NPs was confirmed by mass spectrometer. The amount of the released MTX vs. time was quantified by HPLC. The chromatographic separation was achieved using a Zorbax C_{18} (4.6 × 100 mm, 5 μm) column with the mobile phase consisting of 90% of aqueous phase (0.1 M of citric acid and 0.2 M of Na_2HPO_4 mixed at a ratio of 2:1, pH 6.0) and 10% of acetonitrile with flow rate of 1 mL/min with a UV detector set at the wavelength of 302 nm.

4.5 Plasma interaction and identification

4.5.1 Human plasma–NP interaction studies (I)

The size and zeta-potential of the PSi NPs during exposure to human plasma were studied by incubation of the NPs with human plasma at 37 °C during 2 h. Anonymous donor plasma was supplied by the Finnish Red Cross Blood Service under the permission from the respective institutional ethical committee.

4.5.2 Identification of plasma proteins associated with the PSi NPs (III)

In paper **III**, the plasma proteins associated to the NPs with different surface modifications were identified. After the NPs incubation with human plasma at 37 °C for 2 h, the proteins associated with the NP samples were separated by sodium dodecyl sulphate polyacrylamide gel electrophoresis (SDS-PAGE). The whole set of protein bands from the THCPSi-RGDS NPs were excised, alongside with the possible protein bands from all the other samples to verify the presence of complement C3 and its derivatives. The excised bands were digested and the peptides obtained by digestion were analyzed by MS. The proteins were identified from peptide mass fingerprint data with MASCOT search engine (v1.6b25 http://www.matrixscience.com).

4.6 *In vitro* assays (I–III, and V)

Endothelial EA.hy926 (ATCC, USA), U87 MG and PC3-MM2 cells were cultured according to the standard protocols described in the publications.

4.6.1 Cell viability studies (I–III, and V)

The *in vitro* cytotoxicity of the NPs was determined by an ATP-based cell viability kit following the manufacturer's protocol, as described elsewhere.[160] Briefly, cells were seeded in 96-well plates at the density of (1.0–1.5) $\times 10^4$ cells/well and allowed to attach overnight. Then, the cell culture medium was replaced by 100 µL of medium (with or without 10% FBS) containing different concentrations of NPs. After predetermined incubation times, the number of living cells was determined based on the amount of ATP produced by the cells. Each experiment was performed at least in triplicate. Cells cultured in growth medium without NPs or with 1% of Triton X-100 served as positive and negative controls, respectively. The luminescence was measured with a Varioskan Flash fluorometer. The *in vitro* inhibition of cancer cell growth by the drug loaded into the NPs was also evaluated using the same cell viability assay and conditions, as described above.

4.6.2 Cellular uptake studies (I, III, and V)

Confocal fluorescence microscopy (**I**), flow cutometry analysis (**I**), and TEM experiments (**I**, **III** and **V**) were used to evaluate the cellular uptake of the NPs. In confocal fluorescence microscopy assay, about 200 µL of 8×10^4 cells/well were seeded in Lab-Tek® chamber slides (Thermo Fisher Scientific, USA) one day before the experiment. The NPs were incubated with cells for 3 h. The NPs suspension was removed and the cells were rinsed three times with HBSS (pH 7.4). The cell membranes were stained with CellMask™ Orange according to the manufacturer's protocol, followed by cell fixation with 2.5% glutaraldehyde. Confocal images were taken with a Leica SP5 inverted confocal microscope, equipped with argon (488 nm) and DPSS (561 nm) lasers and HCX Plan Apochromate 63/1.2-0.6 water immersion objective.

For flow cytometry, 1 mL of 2×10^5 cells/well was seeded in 12-well plates. After reaching 80% confluency, the culture medium was replaced with a medium containing different concentrations of each NP and incubated with the cells for 3 h. After removing the NP solutions and washing the cells three times with HBSS (pH 7.4), to remove non-adherent NPs, the cells were harvested by trypsin-ethylenediaminetetraacetic acid (EDTA) and treated with trypan blue (0.04% v/v) to quench the fluorescence of possible surface adherent NPs. Flow cytometry was performed with an LSR II flow cytometer with laser excitation wavelength of 488 nm using a FACSDiva software. About 10,000 events were collected for each sample and the data was analyzed using the Flowjo 7.6 software.

The cell–NP interactions of non-fluorescence labeled NPs were studied *in vitro* by TEM. About 2 mL/well of 5–6 × 10^5 cells/well were seeded in 6-well plates containing 18×18 mm cover slip in each well. After overnight attachment, the medium was replaced by new medium containing each NP. After 2 to 3 h of incubation, the NPs' suspensions were removed and the cells were washed three times with HBSS (pH 7.4) and fixed by 2.5% glutaraldehyde. Ultrathin sections of both control and exposed cells to the NPs were prepared, as described in detail in each publication. The TEM images were examined as described in section 4.3.

4.6.3 Cell apoptosis (V)

MTX causes cell death by inhibiting the activity of DHFR, and thus, inhibiting the DNA biosynthesis. In order to confirm the bioactivity of the released MTX fragments from the MTX-conjugated PSi NPs, 7-amino-actinomycin D (7-AAD) labeling DNA fragmentation programmed cell death experiments were performed by flow cytometry analysis. Briefly, 2×10^5 cells/mL/well of each cell was seeded in 12-well plates separately. After overnight incubation, the medium was replaced by new medium containing certain concentrations of the NPs for 24 h incubation. After removing the NPs' solutions and washing the cells three times with HBSS (pH 7.4) to remove non-adherent NPs, the cells were harvested by trypsin-EDTA and kept on ice. Cells were then re-suspended in 100 µL BioLegand's cell staining buffer and 5 µL of 7-AAD (50 µg/mL) was added to each sample and incubated for 15 min at room temperature in the dark. After that, 400 µL of HBSS buffer was added and the samples were analyzed by flow cytometry as descripted in section 4.5.4.

4.7 *In vivo* assays (II)

4.7.1 Animal model

Animal experiments were carried out in accordance to the European Union and Finnish national legislation and guidelines for animal experimentation. Subcutaneous xenograft tumor model was established by injections of 5×10^6 prostate cancer cells PC3-MM2 in 50 μL DMEM into each of the bilateral flanks of male Hsd:NMRI-Foxnlnu/nu nude mice (6–8 weeks of age from Harlan) under isoflurane anesthesia. Tumors were allowed to develop for 8 days prior the studies and the mice were randomized into the imaging and therapy study groups (n = 3–4/group). The NPs and drug administration were performed under the isoflurane anesthesia. Intravenous injections were given in a volume of 120 μL via a temporary catheter followed by a flush of the catheter with 0.1 mL of sterile 0.9% NaCl. Intratumoral administration was performed with a U100 insulin syringe and a 30G needle in a volume of 50 μL/tumor.

4.7.2 SPECT/CT imag

ing and biodistribution

The *in vivo* biodistribution of the tested ^{111}In-radiolabeled multifunctional nanocarriers was assayed by using the small animal nanoSPECT/CT system. The whole-body SPECT/CT images were acquired under isoflurane anesthesia at 5 min after intravenous or intratumoral injections for 60 min (in dynamic scanning mode with 20 min frames and 16 projections at 90 s per projection), and again at 26 h after administration (16 projections and 225 s per projection). The CT images were taken using 45 or 55 kV X-ray source, 500 ms exposure time in 180 projections, pitch 0.5 with an acquisition time of 5 min after the respective SPECT scan. All images were reconstructed with HiSPECT NG software and analyzed using InVivo Scope software.

After the last scan (27 h after administration), the mice were sacrificed and the samples of blood, urine, liver, spleen, lung, heart, kidney, skeletal muscle, lymph node (inguinal), bone, and tumor were collected for independent radioactivity measurements using an automated γ-counter. In addition, a 3-μL blood sample for radioactivity measurement was obtained after the first SPECT/CT scan (at 65 min post-administration) by venipuncture of the saphenous vein.

4.7.3 Anti-tumor effect

The drug delivery efficiency to inhibit the tumor growth of the developed NPs was evaluated. Sorafenib was used as the model therapeutic agent in this study. The animals received two repeated doses of sorafenib-loaded NPs (3 mg/kg of sorafenib) 24 h apart, on

days 9 and 10 after the tumor inoculation. Tumor growth was monitored every other day after the tumor inoculation throughout the study by digital caliper measurements and the approximate tumor volume was calculated using the formula, V (mm^3) = $[(\pi/6)\times(a\times b)^{3/2}]$, where a and b are the values of the two perpendicular measurements of the tumor, length and width, respectively. The detailed information about size of the tumor at the initiation of therapy was provided in publication (II). The animals were euthanized when any of the diameters reached the maximum upper limit of 1.0 cm.

4.8 *Ex vivo* assays (II)

Immunofluorescence staining was used to determine the long-term biodistribution of the prepared multifunctional nanocarriers. The liver, spleen, lung, kidney, heart, and tumors were collected and snap-frozen in liquid N_2 for *ex vivo* assays. The tissues were sectioned to 5 and 10-μm thickness and the sections were thaw-mounted on SuperFrost™ Plus microscope slides. For visualizing the blood vasculature, the tumor samples were stained with rat anti-mouse CD31 antibody followed by Alexa Fluor® 594-labeled anti-rat secondary antibody. The tumor cell surface expression of integrin αvβ3 was visualized using a hamster anti-mouse CD61 antibody followed by Texas Red-labeled anti-hamster secondary antibody. The nuclei were counterstained with 4',6-diamidino-2-phenylindole (DAPI). The stained sections of the tumors were imaged using a Leica SP5 inverted confocal microscope and the data was collected and analyzed by Leica LAS AF Lite software.

Hematoxylin and eosin (H&E) staining was performed to analyze the biocompatibility of the multifunctional PSi and PSi-iRGD NPs and the tumor pathology after treatment. The slides were observed and photographed by an optical microscope (Leica DM LB research microscope). Histopathological assessment of the tissue samples was also performed for the H&E stained sections by a veterinary pathologist.

4.9 Statistical analysis (I–V)

Results of the assays were presented as mean ± standard deviation (s.d.) of at least three independent experiments. Student's *t*-test (**I–V**) and a non-parametric Kruskall-Wallis test (**II**) were used to evaluate the statistical significance when applicable and set at probabilities of $*p < 0.05$, $**p < 0.01$ and $***p < 0.001$ using Origin 8.6 and GraphPad Prism 6 softwares, respectively.

5. Results and discussion

Chemical approaches can be employed to modify the surface of nanocarriers in order to improve the bioactivity of the drug delivery carriers for biomedical applications, as well as to prepare drug conjugates to overcome the limitations of certain drugs. Nanocarriers for targeting cancer drug delivery aim at increasing the drug delivery efficiency into the cancer tissue by the introduction of the targeting moieties onto the nanocarriers' surface, which can specifically increase the nanocarrier–cancer tissue interactions.

In this context, the effect of the surface modification of PSi NPs with targeting peptides was studied on the cellular uptake, drug delivery and the *in vitro* and *in vivo* behavior of these NPs. For intravenous drug administration, the plasma protein association to the nanocarrier can dramatically affect the biofate of the nanocarriers. Therefore, the protein adsorption onto the PSi NPs modified with targeting peptides and anti-fouling polymers was also studied. Furthermore, targeting peptides conjugated to oligonucleotides and drug-conjugated PSi NPs for combination cancer therapy were studied.

5.1 Enhancing the cellular uptake by targeting peptide-functionalized PSi NPs (I)

RGD has been identified to have high affinity to integrins expressed by the nonvascular endothelial cells and tumor cells.[243, 268] RGDS and iRGD are two derivatives of the targeting peptide RGD. In this study, RGDS and iRGD were conjugated to BCN-modified PSi NPs via SPAAC click chemistry. The cellular internalization efficiency, together with drug loading and drug dissolution profiles of the modified PSi NPs were evaluated.

5.1.1 Surface functionalization of the PSi NPs by targeting peptides

RGDS is a linear peptide, while iRGD is a cyclized peptide, which also presents tumor tissue penetrating properties.[266] In this study, both the linear and cyclized peptides were chosen to study the surface conjugation ratio of the peptides to the PSi NPs, as well as to further evaluate the cellular interaction effect of the modified NPs with cancer cells. SPAAC click moiety BCN was introduced to the amine-terminated PSi NPs prior to the peptide biofunctionalization. Azide-functionalized RGDS and iRGD were conjugated to the BCN-modified PSi (APS-TCPSi) NPs via SPAAC click reaction (**Scheme 1**). The conjugation ratios to the amine functional group were 15.2% and 3.4% (molar ratios to the amine functional groups of APS-TCPSi) for RGDS and iRGD, respectively. The conjugated ratio was calculated based on the elemental analysis, which determines the percentage of each element in the samples. The increasing weight on hydrogen, nitrogen and carbon in the samples before and after conjugation were used for calculation. The lower conjugation ratio of TCPSi-iRGD was probably due to the ring structure of iRGD, which presented higher "steric hindrance" on the surface of the NPs. In the confocal imaging and flow cytometry experiments, the APS-TCPSi NPs were first covalently labeled with FITC before the peptides conjugation. Covalent labeling and peptides modifications produced a robust nanosystem for further drug loading and delivery studies. The size and zeta-potential of the modified NPs are presented in **Table 3**.

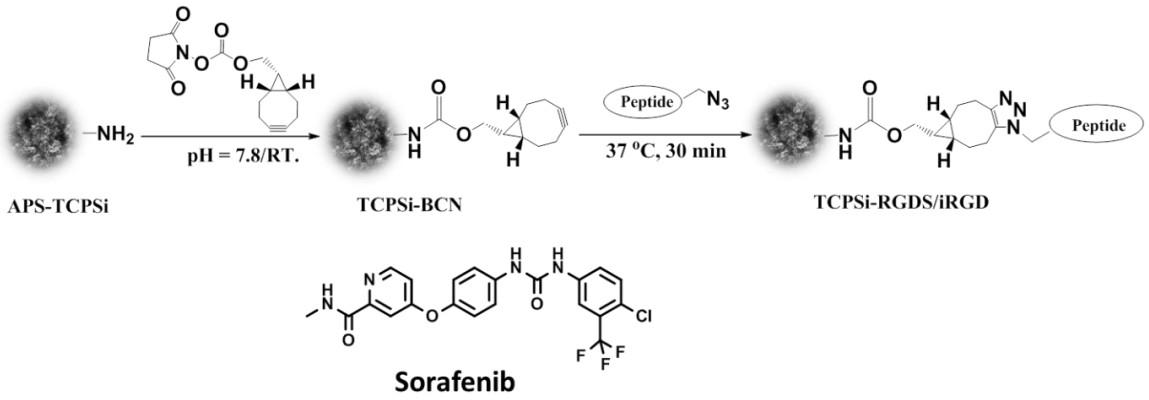

Scheme 1. *Chemical conjugation of the peptides RGDS and iRGD to APS-TCPSi. BCN-NHS was reacted with the amine groups of APS-TCPSi NPs at pH 7.8 in order to obtain a SPAAC click moiety decorated TCPSi-BCN NP. Next, RGDS and iRGD were conjugated to the NPs via SPAAC in order to obtain TCPSi-RGDS and TCPSi-iRGD NPs. The chemical structure of the model drug sorafenib is also presented. Copyright © (2014) ElsevierB.V. Reprinted with permission from publication (**I**).*

Table 3. *The size, polydispersity index (PDI),* zeta-*potential and drug loading degree of sorafenib by APS-TCPSi, TCPSi-RGDS and TCPSi-iRGD NPs. Copyright © (2014) Elsevier B.V. Reprinted with permission from publication (**I**).*

NP	Size (nm)	PDI	Zeta-potential (mV)	Drug loading degree (w-%)
APS-TCPSi	165.6 ± 1.1	0.08 ± 0.02	35.1 ± 0.8	6.06 ± 0.65
TCPSi-RGDS	179.6 ± 1.2	0.08 ± 0.01	11.3 ± 0.4	6.12 ± 0.87
TCPSi-iRGD	188.8 ± 6.9	0.13 ± 0.04	11.2 ± 0.8	5.64 ± 0.56

5.1.2 Cellular uptake of the NPs

The cellular uptake of the peptide-modified NPs was evaluated in hybrid endothelial EA.hy926 cells using confocal and flow cytometry measurements (**Figure 7**). Both the RGDS and iRGD surface modifications of the PSi NPs enhanced the cellular uptake of the NPs compared to the unmodified APS-TCPSi. Furthermore, there were more TCPSi-RGDS NPs located in the cytoplasm than TCPSi-iRGD, as observed in confocal and flow cytometry analyses. Both the peptide-modified PSi NPs showed similar size and zeta-potential. The difference on the cellular uptake was probably due to the surface modification ratio (15.2% *vs*. 3.4%). A higher content of the peptide on the surface of the PSi NPs resulted in a better cell–NP interaction, and thus, improved the cell internalization *in vitro*.

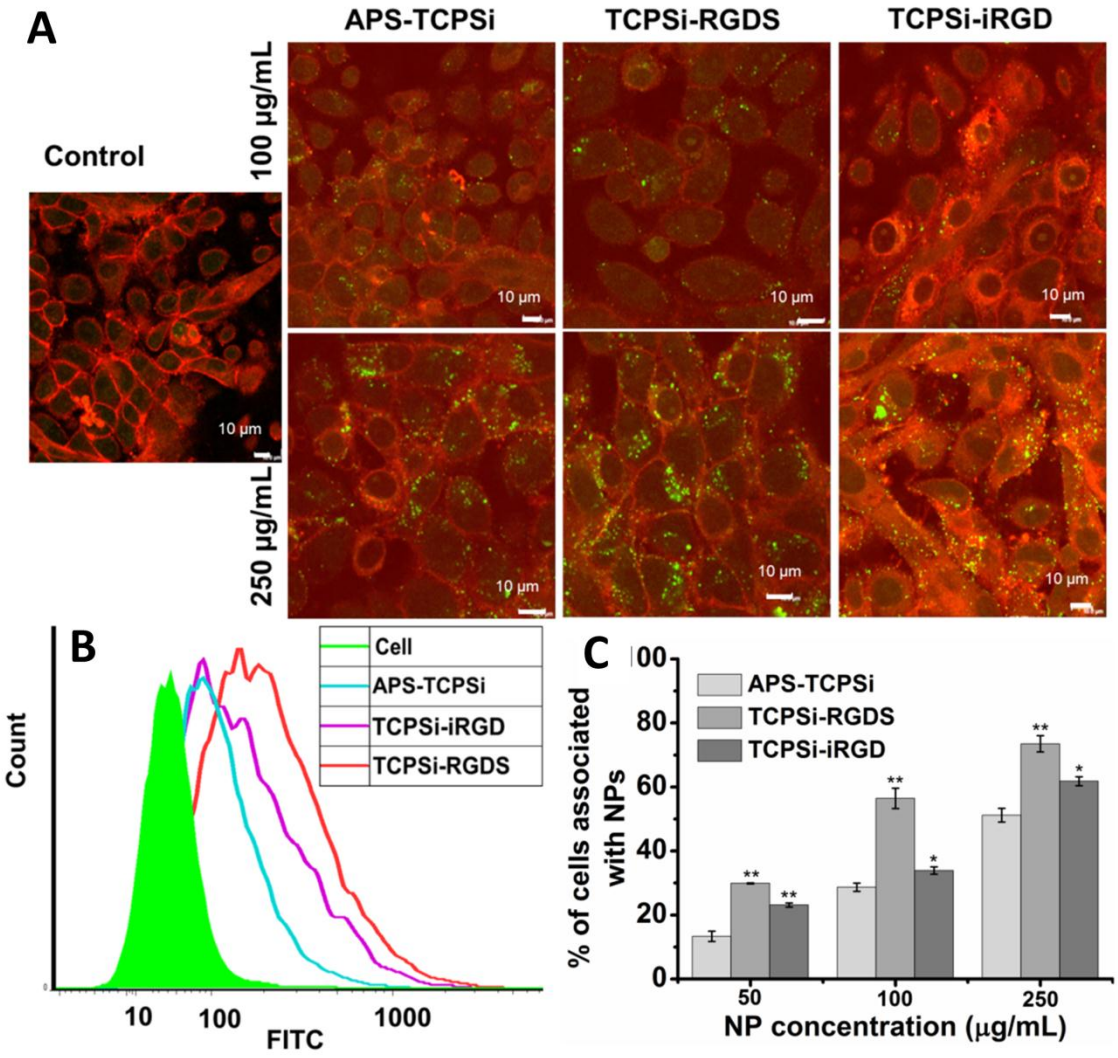

Figure 7. *Cell uptake analysis of APS-TCPSi, TCPSi-RGDS and TCPSi-iRGD incubated with EA.hy926 cells for 3 h. (A) Confocal fluorescence microscopy images of EAhy.926 cells. The NPs were covalently labeled with FITC (green) and the cell membrane was stained with CellMask (red). Scale bars are 10 µm. (B) Flow cytometry histogram graphics of the NPs at concentrations of 250 µg/mL. (C) Flow cytometry quantitative determination for the internalized NPs. Error bars represent s.d. (n ≥ 2). The level of the significant differences of the treated NPs was set at probabilities of *p < 0.05 and **p < 0.01. Copyright © (2014) Elsevier B.V. Reprinted with permission from publication (**I**).*

5.1.3 Drug loading and release

Hydrophobic drug sorafenib was used as a model drug to study the drug loading and drug dissolution profiles of the surface-modified PSi NPs. The loading degree of each NP is listed in **Table 3**. The surface modification of APS-TCPSi by RGDS and iRGD did not significantly affect the drug loading capacity of the PSi NPs.

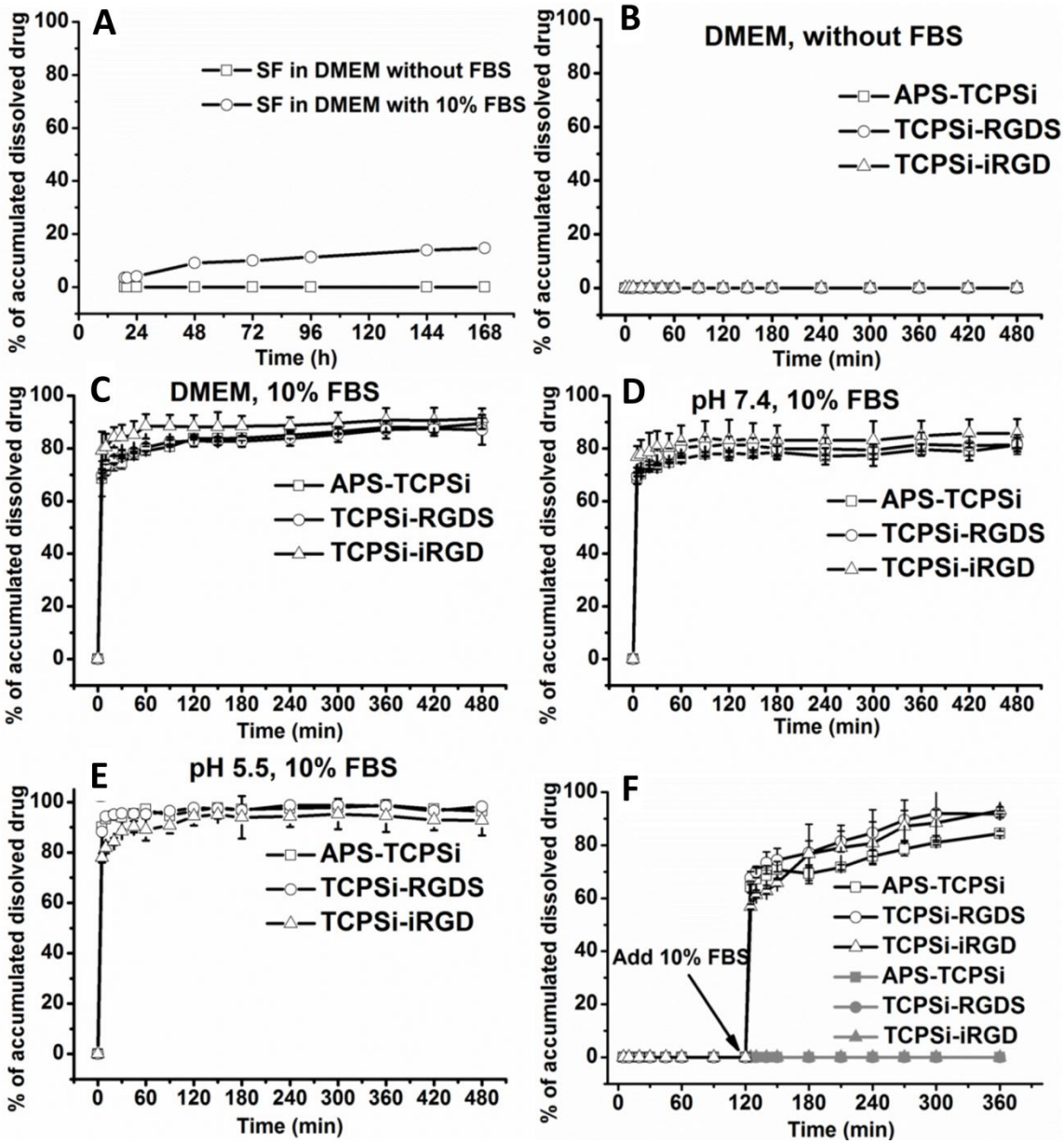

Figure 8. *Dissolution profiles of sorafenib loaded in APS-TCPSi, TCPSi-RGDS, TCPSi-iRGD in different aqueous media. Bulk sorafenib in DMEM with and without 10% FBS (A), sorafenib loaded in the NPs in DMEM without (B) and with (C) 10% FBS, in buffer solution with 10% FBS at pH 7.4 (D) and pH 5.5 (E), and in DMEM without FBS (gray symbols) or with addition of 10% FBS (empty symbols) after 120 min (F). SF denotes for sorafenib. Copyright © (2014) Elsevier B.V. Reprinted with permission from publication (**I**).*

The drug release experiments were performed in the media with and without 10% FBS (**Figure 8**). Sorafenib is a very poorly water soluble drug, and no detectable sorafenib was observed when dissolved in the medium without FBS up to 1 week (168 h). About 14% (ca. 0.5 μg/mL) of free sorafenib was gradually dissolved in the medium contained 10% FBS during 1 week (**Figure 8A**). Sorafenib was also not dissolved from the NPs in the DMEM without FBS (**Figure 8B**). However, a fast release of sorafenib was observed from

the samples of the drug loaded in any of the three NPs in the media containing 10% FBS. About 69%, 70% and 79% of sorafenib was dissolved in DMEM with 10% FBS from APS-TCPSi, TCPSi-RGDS, and TCPSi-iRGD NPs, respectively, in the first 5 min (**Figure 8C**). The enhanced drug dissolution profiles were observed in the release media with 10% FBS at pH-values of 7.4 and 5.5 (**Figure 8D**, **E**). The effect of the FBS in terms of the release of sorafenib from the PSi NPs was further confirmed by adding 10% of FBS to the dissolution media 2 h later (**Figure 8F**). About 64%, 67% and 56% of sorafenib was dissolved in 5 min from the APS-TCPSi, TCPSi-RGDS, and TCPSi-iRGD NPs, respectively. By loading poorly-water soluble drugs to the PSi NPs, the drug dissolution rate was dramatically enhanced. The surface modification of the APS-TCPSi with either RGDS or iRGD did not comprise the drug release profiles of sorafenib.

5.2 Multifunctional PSi NPs for cancer theranostics (II)

Surface modification of the NPs with homing peptides can be used for cancer diagnostics.[202] The accessibility to follow the fate of the developed nanovectors is also important in nanomedical research. A dual-labeled multifunctional system using carboxylic acid terminated PSi (UnTHCPSi) NPs was prepared for cancer theranostics. The radiolabeling of the NPs with ^{111}In was used to monitor the biodistribution of the NPs using live SPECT/CT imaging. Alexa Fluor® 488 was covalently attached to the NPs for long-term biodistribution studies. The targeting peptide iRGD was introduced to the surface of the NPs via SPAAC to form a dual-labeled targeting peptide-functionalized theranostic PSi-based nanovector.[236, 269]

5.2.1 Nanotheranostic PSi NPs preparation

UnTHCPSi NPs were conjugated with Alexa Fluor® 488 and a SPAAC click moiety DBCO-PEG_4-amine was introduced to the surface of the NPs using the NHS/EDC coupling reaction. Sequentially, azide-functionalized 1,4,7,10-tetraazacyclododecane-N,N',N'',N'''-tetraacetic acid (DOTA) and the targeting peptide iRGD was attached to the NPs using the SPAAC click reaction (**Scheme 2**). For the ^{111}In-radiolabeled multifunctional NPs, the iRGD conjugation was done after the ^{111}In-labeling. For simplicity, below the dual-labled UnTHCPSi NPs without/with iRGD are designated as UnTHCPSi-DOTA and UnTHCPSi-iRGD, respectively.

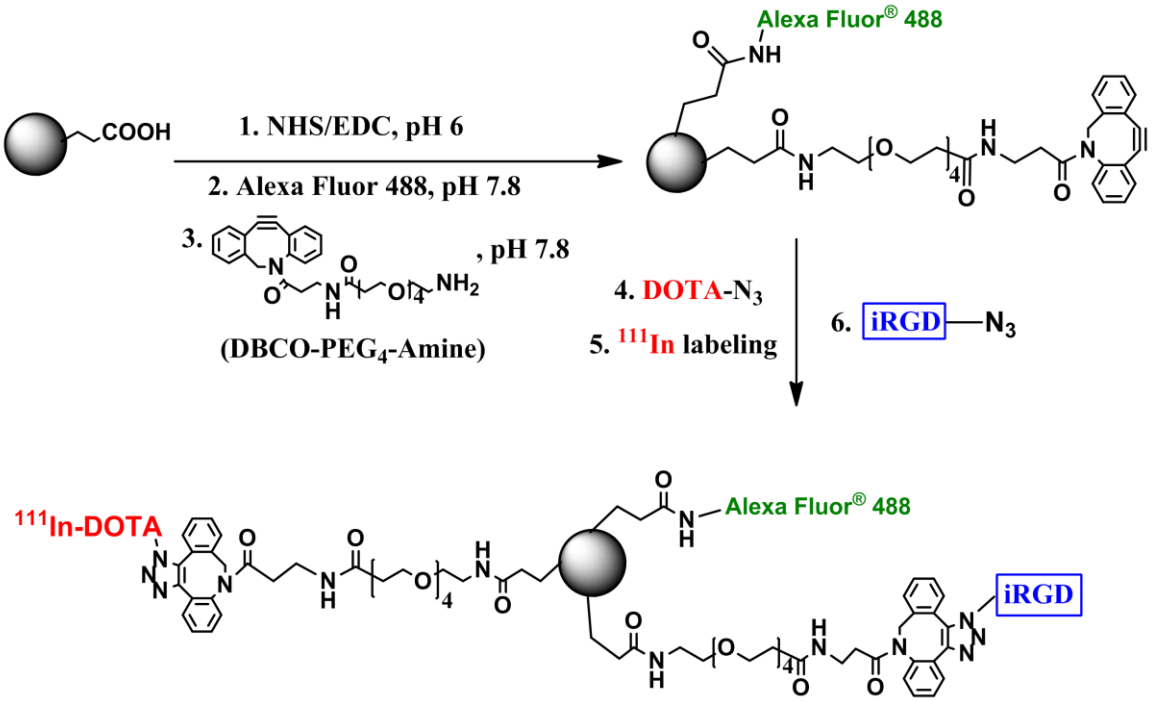

Scheme 2. *Preparation of the multifunctional PSi theranostic nanovector. Reaction 1, NHS/EDC activates the carboxylic acid group on the UnTHCPSi NPs. Reactions 2 and 3, Alexa Fluor® 488 and DBCO-PEG$_4$-amine are conjugated to the activated UnTHCPSi NPs, respectively. Reactions 4 and 6, DOTA and iRGD are conjugated to the NPs via SPAAC. In the case of the radiolabeling study, ^{111}In-labeling was performed before the iRGD conjugation (reaction 5). Copyright © (2015) ElsevierB.V. Reprinted with permission from publication (**II**).*

5.2.2 *In vivo* SPECT/CT imaging and biodistribution studies

Prostate cancer xenografted mice were used to study the *in vivo* biodistribution of the dual-labeled PSi NPs with/without iRGD modification. SPECT/CT was applied to evaluate the radiolabeling stability as well as to access the biodistribution of the radiolabeled NPs. After intravenous administration, both the NPs with/without iRGD modification were mainly accumulated in the liver and spleen, with no visible uptake of the NPs in the tumor by the SPECT/CT images (**Figure 9A**). During the first hour, minor radioactive signal was observed in the kidney for UnTHCPSi-DOTA NPs, followed by an increase in the radioactivity in the bladder. At 26 h time point, the radioactivity in the kidney was more evident for UnTHCPSi-DOTA NPs. This indicates the detachment of a small amount of ^{111}In from the UnTHCPSi-DOTA NPs. For UnTHCPSi-iRGD NPs, a minor radioactive trace was observed in the bladder from the SPECT/CT imaging of the treated mice during the first hour, but no visible radioactivity in the bladder or in the kidney was observed at 26 h time point. This indicates that, except the minor impurity of the residual ^{111}In left in the radio-labeled UnTHCPSi-iRGD sample, the ^{111}In labeling in UnTHCPSi-iRGD NPs was more stable than in bare UnTHCPSi. In the case of intratumorally administered NPs, the radioactivity of both NPs was mainly found at the injection site in the tumor, as shown by the SPECT/CT images (**Figure 9B**). There was no significant change on the biodistribution of radioactivity in SPECT/CT imaging between 1

h and 26 h, which indicated that both the NPs were retained in the tumor after intratumoral administration.

After 26 h of SPECT/CT imaging, the tumor samples were collected for quantitative γ-counting analysis to determine the tumor accumulation of the NPs. Intravenously administrated iRGD-modified NPs achieved higher tumor specific accumulation compared to the NPs without iRGD modification, as judged from the tumor-to-muscle ratio of the radioactivity (**Figure 9C**). NPs surface modified by iRGD can increase the tumor accumulation of the nanocarriers.[241, 245] In this study, after iRGD surface conjugation to the NPs, a higher tumor accumulation of the PSi NPs was achieved. Intratumoral administration of the nanocarriers can achieve a higher tumor-to-tissue ratio of the administered composites. In previous report, the elimination of the nanocarriers from the tumor is relatively fast and dependent on the properties of the nanocarriers in the case of intratumoral administration.[270] In this study, 15.5 ± 2.0 ID% and 27.3 ± 9.3 ID% were remained in the tumor 27 h post injection (p.i.) for UnTHCPSi-DOTA and UnTHCPSi-iRGD, respectively (**Figure 9D**). The iRGD surface modification rendered higher tumor retention of the NPs, but the difference was not statistically significant. Therefore, it is possible that the tumor retention of the NPs was slowed down due to the targeting peptide iRGD modification and increased interaction of PSi-iRGD NPs with the tumor cells.

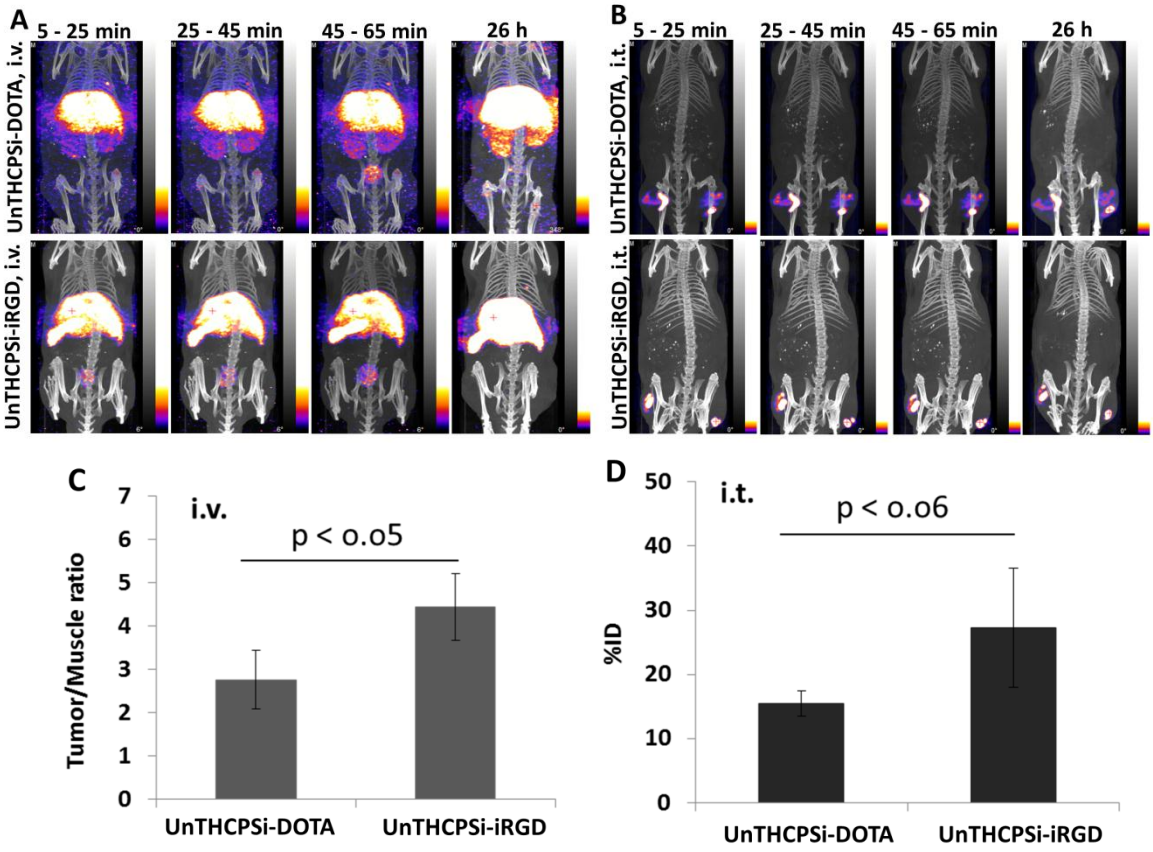

Figure 9. *In vivo biodistribution and tumor accumulation studies after intravenous (A and C) and intratumoral (B and D) administration. (A) and (B) are Nano-SPECT/CT fused images of the whole body mouse. The images were taken in a dynamic mode during 1 h at 5 min post-injection (p.i.) and at 26 h p.i. (C) and (D) are the quantitative γ-counting analyses of the radioactivity in the tumor 27 h p.i.. Copyright © (2015) ElsevierB.V. Reprinted with permission from publication (**II**).*

5.2.3 *Ex vivo* histological analysis

The long-term tissue biodistribution of the NPs can be assessed by immunofluorescence staining of the tumor samples (**Figure 10**).

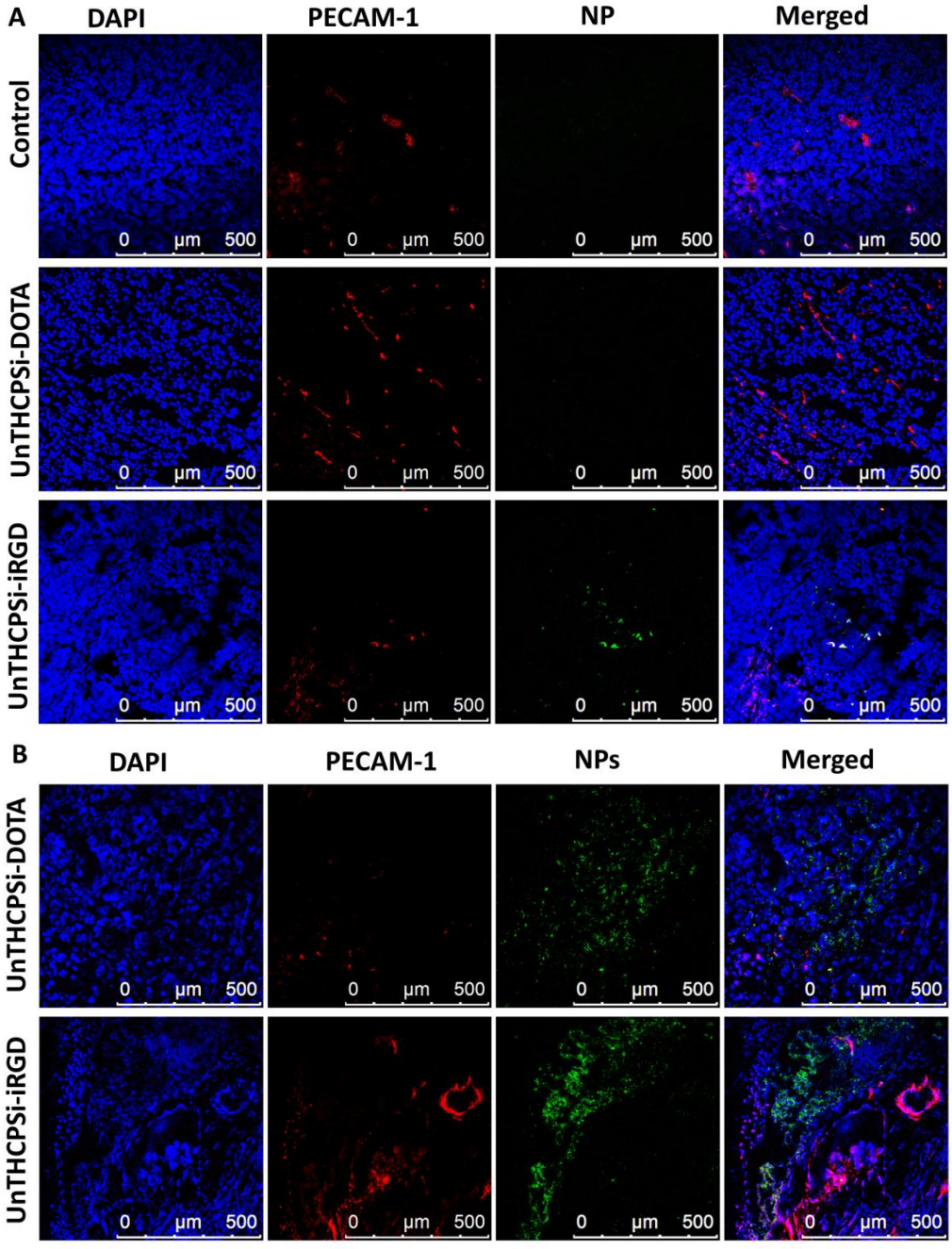

Figure 10. *Confocal images of the immunofluorescently stained tumor sections in mice after intravenous (A) and intratumoral (B) administration of the NPs. The images were taken from the middle of the tumor sections. The nuclei were stained with DAPI (blue). CD31 was visualized using antibodies pseudocolored in red. The NPs labeled with Alexa Fluor® 488 are shown in green. The merged images are presented in the last column (Scale bar: 500 µm). Copyright © (2015) ElsevierB.V. Reprinted with permission from publication (**II**).*

Anti-CD31 antibody was used to visualize the blood vasculature of the tumor. By intravenous administration, more UnTHCPSi-iRGD NPs accumulated into the tumor section than UnTHCPSi-DOTA NPs, corroborating the idea that iRGD aided to promote the NPs deep penetration into the tumor stroma (**Figure 10A**).244 In the case of NPs intratumoral administration, both UnTHCPSi-DOTA and UnTHCPSi-iRGD NPs presented a concentrated mass on the injection site of the tumor section, which was in agreement with the SPECT/CT images, where the injected NPs were accumulated in the tumor (**Figure 10B**).

5.2.4 Anticancer effect of the drug loaded in the multifunctional PSi NPs

The inhibition of the tumor growth was used to assess the antitumor effect of the drug loaded in the prepared PSi nanovectors. **Figure 11** shows the tumor growth curve presented as the ratio of the tumor size after the treatment compared to the initial tumor size before the treatment. By using two intravenous doses (24 h apart, each treatment corresponding to dose of 3 mg/kg of sorafenib), the sorafenib loaded in both the NPs suppressed similarly the tumor growth as the free sorafenib in DMSO-plasma solution (**Figure 11A**). This was probably due to the enhanced dissolution rate, and thus, the results of a fast release of sorafenib in the blood after administration by loading sorafenib into the UnTHCPSi-DOTA and UnTHCPSi-iRGD NPs.

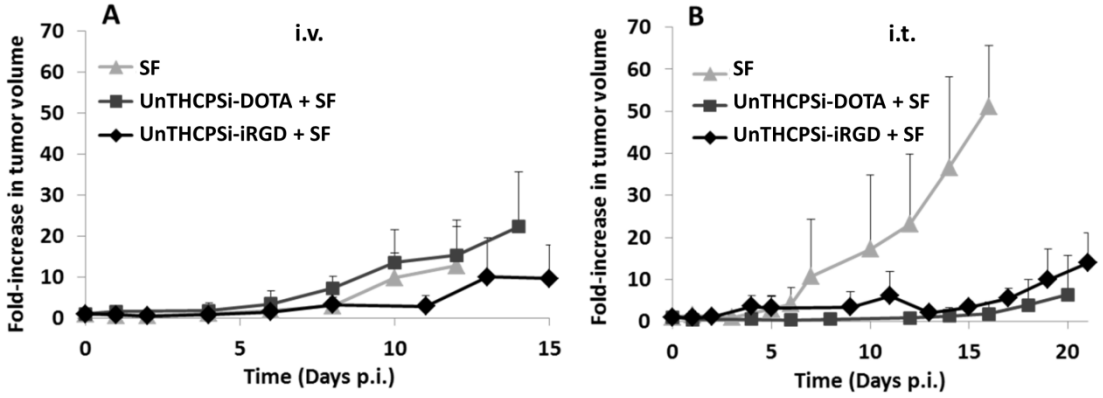

Figure 11. *Inhibition of the tumor growth of PC3-MM2 xenografts in male nude mice by the treatment of sorafenib-loaded multifunctional PSi NPs. The data is represented as mean ± s.d. (n = 4–6). The statistical differences are UnTHCPSi-iRGD + SF vs. UnTHCPSiPSi-DOTA + SF vs. SF, p = 0.3238 (intravenous administration route, Kruskall-Wallis test) and p = 0.0107 (intratumoral administration route, Kruskall-Wallis test). (i.v., intravenous; i.t., intratumoral; SF: sorafenib; p.i., post-injection). Copyright © (2015) ElsevierB.V. Reprinted with permission from publication (**II**).*

After intratumoral injection of two consecutive doses (24 h apart), sorafenib loaded in the UnTHCPSi-DOTA and UnTHCPSi-iRGD NPs presented higher inhibition effect of the tumor growth than the free sorafenib (**Figure 11B**). The tumor size of the mice increased ca. 10-fold in 20 days after the first treatment with sorafenib loaded NPs, while the tumor size increased ca. 50-fold in 16 days after the intratumoral treatment of free sorafenib solution. The fast elimination of small conventional drug molecules from the

tumor has been one of the obstacles for intratumoral administration of chemotherapeutic drugs.[222, 271] The low effect of sorafenib by intratumoral administration was likely due to the fast pumping out of the drug molecules due to the high pressure in the tumor microenvironment.[222] The PSi-based NPs were successfully retained in the tumor site with sorafenib. Due to the non-sink conditions in the tumor, the release of sorafenib was sustained from the NPs in the tumor tissue, and thus, inhibited the tumor growth.

5.3 Effect of the surface modification of the PSi NPs on the cellular uptake and protein adsorption (III)

The plasma protein association is the first biological barrier that the nanocarriers encounter after intravenous administration. Due to the high surface free energy, the plasma proteins adsorb onto the NPs and form protein corona immediately when in contact with the biological fluids.[272] The material of the nanocomposite and the physicochemical properties of the NPs, such as hydrophobicity/hydrophilicity, charge, ionization and surface roughness, can affect the protein association.[272-273] The widely studied hydrophilic PEG is one of the molecules used for the surface modification of NPs to prevent plasma protein adsorption,[247] as well as to prevent complementary C3 protein activation.[274] However, the surface modification of the NPs with PEG do not benefit towards the tumor cell uptake.[220]

In this study, targeting peptides and antifouling polymers were conjugated to PSi NPs and their effect on the cellular uptake and protein adsorption were evaluated. The THCPSi NPs are hydrophobic PSi NPs and have good stability in physiological conditions,[5] thus alkyne-terminated THCPSi (THCPSi-alkyne) NPs were surface modified using click chemistry to incorporate bioactive molecules to the PSi NP's surface. The targeting peptides (RGDS and iRGD) and antifouling polymers (poly(glutamic acid), PGA, MW 7k Da); dextran with MW of 6 kDa and 40 kDa) were chosen to be conjugated to the THCPSi-alkyne NPs using CuAAC.

5.3.1 Surface modification of THCPSi-alkyne NPs

The surface modification of the THCPSi-alkyne NPs by RGDS, iRGD, PGA, dextran 6 kDa and 40 kDa was achieved by CuAAC (**Scheme 3**) at room temperature in mild conditions, as described in the experimental part. The reaction was monitored by FTIR and the conjugation ratio was determined by TG analysis (**Table 4**). The size and zeta-potential of the NPs were determined by dynamic light scattering, as listed in **Table 4**. The size of the surface modified NPs increased gradually in consistence with the MW of the conjugated biomolecules. The zeta-potential of the NPs modified by RGDS, iRGD and PGA remained negative, because of the neutral charge of the RGDS and iRGD and negative charge of PGA in Milli-Q water. The dextran 6 kDa and 40 kDa surface modification of the THCPSi-alkyne NPs presented positive zeta-potential values.

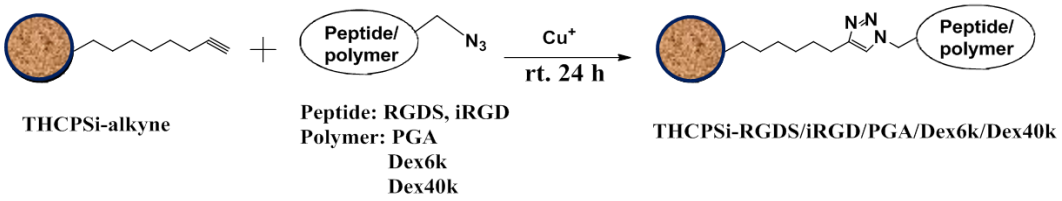

Scheme 3. *Chemical surface modification of THCPSi-alkyne by the peptides RGDS and iRGD, and the polymers PGA and dextran 6 kDa and 40kDa. Copyright © (2015) American Chemical Society. Reprinted with permission from publication* ***(III)****.*

Table 4. *The hydrodymanic size, PDI, zeta-potential and the conjugation ratio of the surface functionalized THCPSi-alkyne NPs. Copyright © (2015) American Chemical Society. Reprinted with permission from publication* ***(III)****.*

NP	Size (nm)	PDI	Zeta-potential (mV)	Conjugation ratio[a]
THCPSi-alkyne	176.3 ± 2.6	0.09 ± 0.01	–20.4 ± 0.5	–
THCPSi-RGDS	181.6 ± 2.2	0.07 ± 0.01	–22.1 ± 1.0	2.35 ± 1.70
THCPSi-iRGD	186.7 ± 1.1	0.06 ± 0.02	–24.2 ± 0.5	5.83 ± 2.48
THCPSi-PGA	180.9 ± 1.1	0.06 ± 0.02	–31.6± 0.2	N.D.[b]
THCPSi-Dex6k	200.5 ± 0.1	0.06 ± 0.02	+22.8 ± 0.3	2.62 ± 0.81
THCPSi-Dex40k	221.9 ± 1.9	0.08 ± 0.01	+14.4 ± 0.6	4.93 ± 1.41

[a]Conjugation ratio presented as the mass percentage of the conjugated biomolecules to the whole modified NPs.
[b]N.D. = No Data. TG analysis was inconclusive as the conjugated PGA did not decompose under the experimental conditions used.

5.3.2 The cellular uptake of the modified PSi NPs

Efficient cellular uptake is an important step for the drug carriers which need to deliver the drug into the cytosol. Previous work reported that THCPSi NPs display low cell uptake by Caco-2 cell monolayers and RAW264.7 macrophage cells [160]. Here, the cellular uptake of the surface modified NPs was evaluated in hybrid endothelial EAhy.926 and brain cancer U87 MG cells (**Figure 12**). The surface modification by both targeting peptides (RGDS and iRGD) and polymers (PGA, dextran 6k and 40k) increased the cellular uptake of the NPs in the EAhy.926 and U87 MG cells. For EAhy.926 cells, the order for the cellular uptake efficacy was as following: THCPSi-RGDS ~ THCPSi-iRGD > THCPSi-Dex40k > THCPSi-Dex6k > THCPSi-PGA > THCPSi-alkyne. In U87 MG cells, the cellular uptake efficacy was in the following order: THCPSi-PGA > THCPSi-RGDS ~ THCPSi-iRGD>THCPSi-Dex40k > THCPSi-Dex6k > THCPSi-alkyne. The targeting peptides RGDS and iRGD can specifically interact with the cell membrane's receptor integrin αvβ3 and increase the uptake of the conjugated cargo by integrin-expressing tumor cells.[275] It

has been reported that dextran modified microparticles increased the hydrophilicity as well as also increased the particle–cell interactions, and thus, enhanced the cellular uptake of the particles.[276] PGA incorporated NPs can undergo γ-glutamyl transpeptidase receptor mediated cell uptake, and thus, enhance the cancer cell uptake.[277]

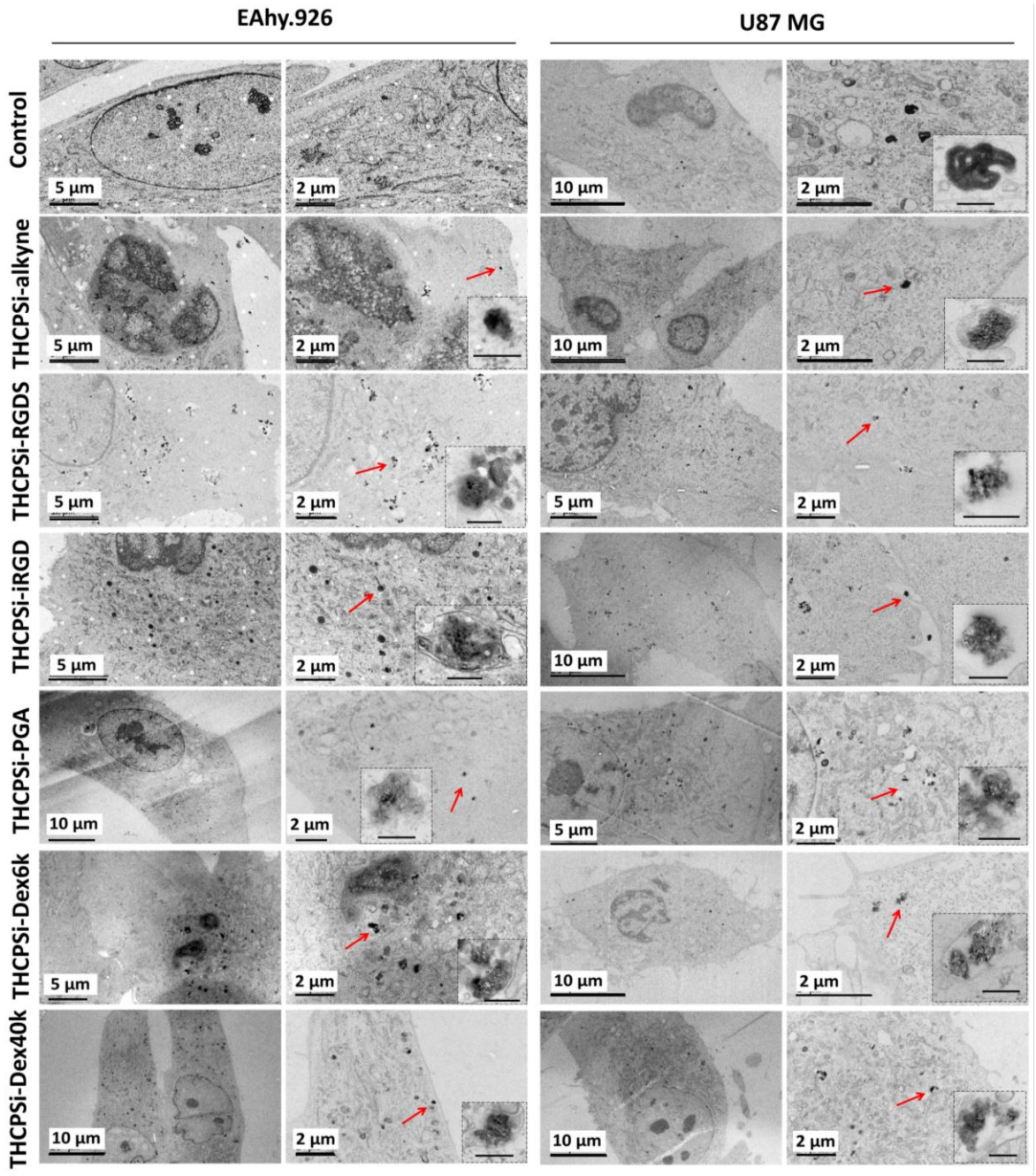

Figure 12. *TEM images of the intracellular distribution of the THCPSi-alkyne THCPSi-RGDS, THCPSi-iRGD, THCPSi-PGA, THCPSi-Dex6k and THCPSi-Dex40k NPs in EA.hy926 and U87 MG cells. Inset scale bars are 200 nm and the arrows indicate the sample of each type of THCPSi NPs. Copyright © (2015) American Chemical Society. Reprinted with permission from publication* ***(III)****.*

5.3.3 Plasma protein adsorption onto the PSi NPs

The surface modification of the NPs by hydrophilic peptides and polymers can reduce the plasma protein association.[24, 202] The plasma protein adsorption to the surface modified NPs was analyzed by SDS-PAGE and identified by MS (**Figure 13**). Unmodified THCPSi-alkyne (**Figure 13**, lane B) showed the highest tendency for protein adsorption. The THCPSi-Dex40k (**Figure 13**, lane G) displayed the least protein adsorption compared to all the other NPs, especially the protein in the high MW range 70–200 kDa. THCPSi-Dex6k (**Figure 13**, lane C) had more serum albumin adsorption compared to THCPSi-Dex40k. THCPSi-PGA (**Figure 13**, lane F) had more protein adsorption than THCPSi-Dex6k, but less than THCPSi-RGDS (**Figure 13**, lane D) or THCPSi-iRGD (**Figure 13**, lane E). The complement 3 (C3) protein is the major plasma protein involved in the inert immune recognition of exons in the plasma by macrophages.[278] In this study, only both the peptide-modified NPs activated the C3 protein by adsorption of C3 protein and converting to C3a/b form. The activation of C3 protein will accelerate the MPS uptake. However, in a recent publication, monocytes were shown to be able to uptake and deliver the RGD-modified SWNT to the tumor intersitium.[279] In the MW range of 35–70 kDa of the adsorbed protein, the two dextran-modified NPs presented similar protein adsorption profiles, while the other four NPs had similar protein adsorption profiles. There was no adsorption of fibrinogen γ chain, and less adsorption of immunoglobulin G (IgG) heavy chain, fibrinogen γ chain, clusterin, and apolipoprotein E proteins to the both dextran modified NPs. The fibrinogen proteins and immunoglobulins, and complement proteins, are the major proteins that can induce the immune system phagocytosis.[217] The protein clusterin is involved in cell apoptosis, complement mediated cell lysis and membrane recycling,[280] and also inhibits the complement activity.[281] Apolipoprotein E is a group of apolipoproteins that are involved in the hepatocytic elimination of certain type of NPs.[282] For the plasma proteins with MW below 35 kDa, all the NPs presented a similar protein association profile.

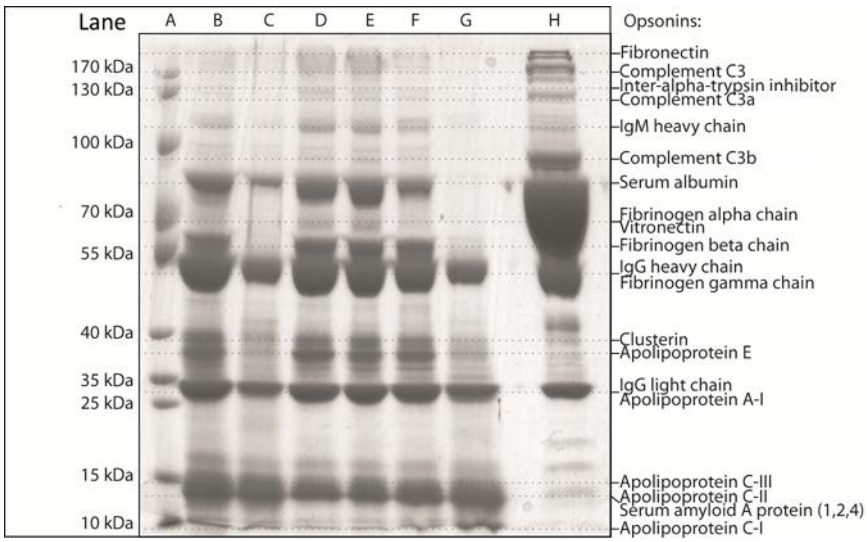

Figure 13. *SDS-PAGE analysis of the protein adsorption characteristics of the NPs. Lane A, the MW marker; Lane B, THCPSi-alkyne; Lane C, THCPSi-Dex6k; Lane D, THCPSi-RGDS; Lane E, THCPSi-iRGD; Lane F, THCPSi-PGA; Lane G, THCPSi-Dex40k; and Lane H, the pure human plasma. Copyright © (2015) American Chemical Society. Reprinted with permission from publication **(III)**.*

The surface "steric repulsion" by hydrophilic polymers has been shown to prevent the plasma protein interaction.[283] The surface modification of the NPs with different moieties, as compared to the same bare THCPSi-alkyne NPs, showed that the surface biofunctionalization affected the plasma protein association profiles.

5.4 Targeting peptides conjugated to oligonucleotide (IV)

Four peptides (iRGD, H-RN, C16Y and ATW) were chosen to study the reaction of peptide-conjugation with ASIL-6 by CuAAC. iRGD presented specific affinity to the cells overexpressing αvβ3 and αvβ5 integrins.[244] H-RN is an 11-amino acid peptide derived from the hepatocyte growth factor kringle 1 domain, which can inhibit the angiogenesis *in vitro* and *in vivo*.[284] Peptide C16Y can interact with αvβ3 and α5β1 integrins, which are presented in angiogenic cells and tumor cells.[285] ATW peptide can selectively bind to vascular endothelial growth factor-2 (VEGFR-2).[286] ASIL-6 conjugated with targeting peptides could be more efficiently delivered into the inflammatory angiogenic tissue to down-regulate the expression of IL-6 and further reduce the inflammation.

The click moiety azide was functionalized to the N-terminal of iRGD and C-terminal of all the other peptides. Alkyne moiety was induced to either 3'- or 5'- end of the ASIL-6 sequence. Both the peptides and oligonucleotides were separately synthesized through the standard protocol and purified by HPLC and further verified by MS (**Tables 5** and **6**). The peptide-oligonucleotide conjugation was performed in water/formamide solution using CuAAC (**Scheme** 4). The reverse-phase HPLC profiles of the (3')ASIL-6-iRGD conjugate showed 2 min retention time shorter than the initial (3')ASIL-6-alkyne, which might be due to the hydrophilicity of iRGD. The ASIL-6-iRGD conjugate became more hydrophilic than ASIL-alkyne. The conjugate was further confirmed by MS. Furthermore, (5')ASIL-6-alkyne and 5'-end fluorescent (6-FAM) labeled ASIL-6-alkyne (alkyne group at 3'-end) were successfully conjugated with iRGD in the same reaction manner (**Table 6**). The successful fluorescent labeling and iRGD conjugation can be very useful for further imaging and biosensor studies. These results demonstrate that CuAAC is robust to conjugate iRGD to ASIL-6 at both 3' and 5' termini, while other biofunctional molecules or labeling reagents can be introduced to the other terminal of the oligonucleotide sequence, which is very flexible way to tailor the properties of ASIL-6.

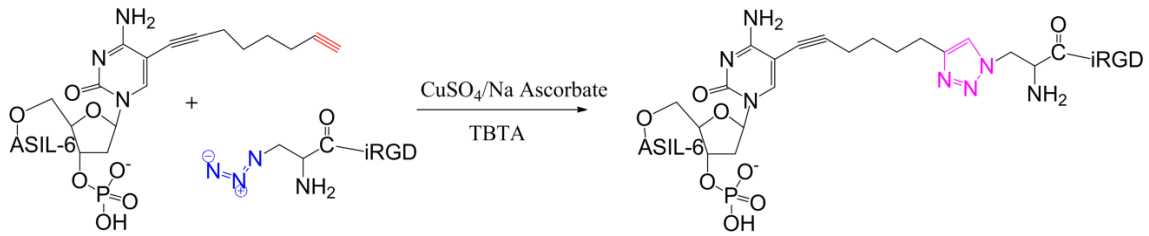

Scheme 4. *The conjugation of ASIL-6 –alkyne with azide functionalized peptides by CuAAC. Copper (II) was reduced to copper (I) by sodium ascorbate and tris(benzyltriazolylmethyl)amine (TBTA) used as copper (I)-stabilizer. Copyright © (2014) Bentham Science. Reprinted with permission from publication (**IV**).*

Table 5. *MS characterization of azide-modified peptides. Copyright © (2014) Bentham Science. Reprinted with permission from publication (**IV**).*

Peptide	The unmodified sequence of peptide	MW (Da)		Purity (%)
		Calculated	Experimental	
Linear iRGD-azide	CRGDRGPDC	1089.1	1089.4	95%
iRGD-azide	CRGDRGPDC (C1-C9)	1087.1	1087.4	98%
H-RN-azide	RNPRGEEGGPW	1365.4	1365.7	92%
C16Y-azide	DFKLFAVYIKYR	1673.9	1673.8	91%
ATW-azide	ATWLPPR	951.0	951.5	92%

Table 6. *MS characterization of alkyne functionalized ASIL-6, and the peptides conjugates. Copyright © (2014) Bentham Science. Reprinted with permission from publication (**IV**).*

Sample	MW (Da)		Purity (%)
	Calculated	Experimental	
ASIL-6-alkyne (3’ or 5’)	5034	5033	93%
5’-FAM-ASIL-6-alkyne (3’)	5571	5570	95%
ASIL-6-iRGD (3’ or 5’)	6121	6119	96%
5’-FAM-ASIL-6-iRGD (3’)	6658	6656	96%
ASIL-6-H-RN (5’)	6396	6397	91%

In addition to the iRGD, three other azide-functionalized peptides were also performed the conjugation to (3’)ASIL-6-alkyne using CuAAC. Peptide H-RN was successfully conjugated to ASIL-6 (**Table 6**), while C16Y and ATW peptides were not reacting with (3’)ASIL-6-alkyne. It is not fully understood yet why the CuAAC reaction worked with iRGD and H-RN but not with C16Y or ATW in terms of conjugation to ASIL-6. By checking the molecular structure of these four peptides, the side chains buried in iRGD and H-RN were relatively more hydrophilic than those buried in C16Y and ATW. The hydrophobicity of the side chain might play a crucial role in oligonucleotide-peptide solution-phase conjugation. The chemical structure of the side chains should be carefully considered when a functional peptide was chosen to chemically react to an oligonucleotide.

5.5 Dual-drug delivery by PSi NPs (V)

The chemotherapeutic drug methotrexate (MTX) is a folic acid analogue.[287] It induces cell death by inhibiting the activity of dihydrofolate reductase (DHFR) enzyme in the cytosol of the cells.[230] MTX has specific affinity to the folate receptor (FR) and enters into the cells through FR-mediated cellular uptake pathway.[288] FR has been over-expressed by many human malignancies.[289] However, MTX had low cellular uptake by FR deficient cells.[15] By chemical conjugation of MTX to the cationic carriers, an increase in the cellular uptake of MTX can be achieved.[232, 290-291] In this study, MTX was conjugated to amine-terminated APS-TCPSi NPs to form MTX-TCPSi NPs. In addition, the MTX-TCPSi NPs can be used to enhance the dissolution rate of poorly-water soluble drugs.

Therefore, antiangiogenic drug sorafenib was also used as a model compound physically loaded to the MTX-TCPSi conjugates. The covalent attachment of MTX and the simultaneous loading of sorafenib to MTX-TCPSi NPs, and their effect on the dissolution profiles of MTX and sorafenib, as well as the anti-proliferation and cell apoptosis of MTX-TCPSi were all evaluated here.

5.5.1 MTX-TCPSi conjugation and characterization

MTX was conjugated to the PSi NPs through the carboxylic acid group of MTX and the amine groups from the APS-TCPSi NPs to form an amide bond using the NHS/EDC coupling reaction (**Scheme 5**). The molecular structure of MTX is presented in **Scheme 5B**. The reaction was monitored by FTIR and the quantitative conjugation ratio was determined by elemental analysis. About 8.4 ± 1.6 % (molar ratio) of the amine group from APS-TCPSi was reacted with MTX, which equaled to the mass ratio of 5 μg of MTX to 1 mg of NPs. In a previous study, it has been demonstrated that the aminosilane surface moiety of APS-TCPSi can be detached by hydrolysis from the NPs surface in an aqueous buffer.[8] The released compound from MTX-TCPSi was analyzed by HPLC and MS. There was no free MTX released from the MTX-PSi NPs. Instead,; the detected compound was the protonated molecule ($[M+H]^+$, m/z 556.2) with a Mw 555.2 g/mol, which matched to the MTX with a fragment of 3-aminopropylesilicic acid (**Scheme 5D**). This result confirmed the release of MTX by detachment of (3-aminopropyl)trihydroxylsilane (**Scheme 5C**) from the MTX-TCPSi NPs, and then dehydrolyzed to the molecule presented in **Scheme 5D**.

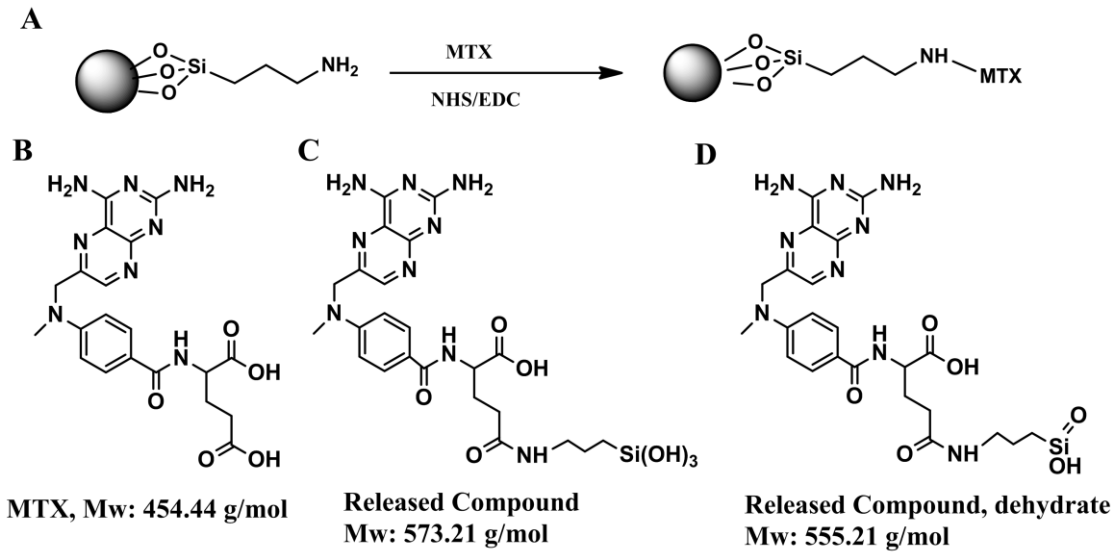

Scheme 5. *(A) MTX-conjugated to APS-TCPSi by EDC/NHS coupling reaction to form MTX-TCPSi NPs. (B) Molecular structure of MTX. (C) Released fragment from MTX-PSi NPs. (D) Dehydrate form containing MTX determined by MS. Copyright © (2015) ElsevierB.V. Reprinted with permission from publication (**V**).*

5.5.2 Evaluation of the drug release and cell apoptosis of MTX-PSi NPs

MTX inhibits the DHFR enzyme to stop the tetrahydrofolate synthesis, and thus, can cause cell death.[287] It has been reported that the effect of MTX-dendrimer conjugate inhibition of the DHFR was comparatively less active than that of the free MTX, which resulted in the conclusion that only one MTX molecule on each dendrimer could bind to the DHFR enzyme.[292] An *in vivo* study showed that MTX conjugated to a carrier via a biocleavable ester linker reached significantly higher anticancer effect than when conjugated to the non-cleavable amide bond.[78] Thus, the release of MTX from the conjugated cargos is a significant step to reach the pharmacological effect of MTX.

Here, the release profiles of MTX and sorafenib was studied by HPLC (**Figure 14**A–C). MTX showed sustained released from the MTX-TCPSi NPs. A faster release profile was obtained at pH 7.4 than at pH 5.5, which was due to the faster hydrolyzation of the surface silane moiety at higher pH-values.[8] The MTX release profiles of MTX-TCPSi NPs in buffer without FBS (**Figure 14B**) and from MTX-TCPSi loaded with sorafenib in buffer with FBS (**Figure 14C**) were similar to the release profiles of MTX-TCPSi in buffer with 10% FBS (**Figure 14A**). This showed that the cleavage of the saline moiety from the TCPSi NP surface was not affected by the serum protein or by the loading of sorafenib. Furthermore, after the loading of sorafenib to MTX-TCPSi NPs for combination therapy, the dissolution profiles of sorafenib (**Figure 14D–E**) were enhanced as a same result of the loading into the PSi NPs.

Moreover, MTX is known to induce cell death by disturbing the DNA synthesis. Thus, the programmed cell death by MTX-TCPSi conjugation was confirmed by DNA fragmentation assay accessed by 7-amino-actinomycin D (7-AAD) staining and flow cytometry analysis (**Figure 14F–G**). The low FR-expressed cell line EA.hy926 and over-expressing FR cell line U87 MG were used in this study. In both the cell lines, the MTX-TCPSi caused higher DNA fragmentation at higher concentrations, while the APS-TCPSi NPs did not induce severe DNA fragmentation. These results demonstrated that MTX-PSi NPs were uptaken by both the cells and the biological activity of the released MTX was maintained.

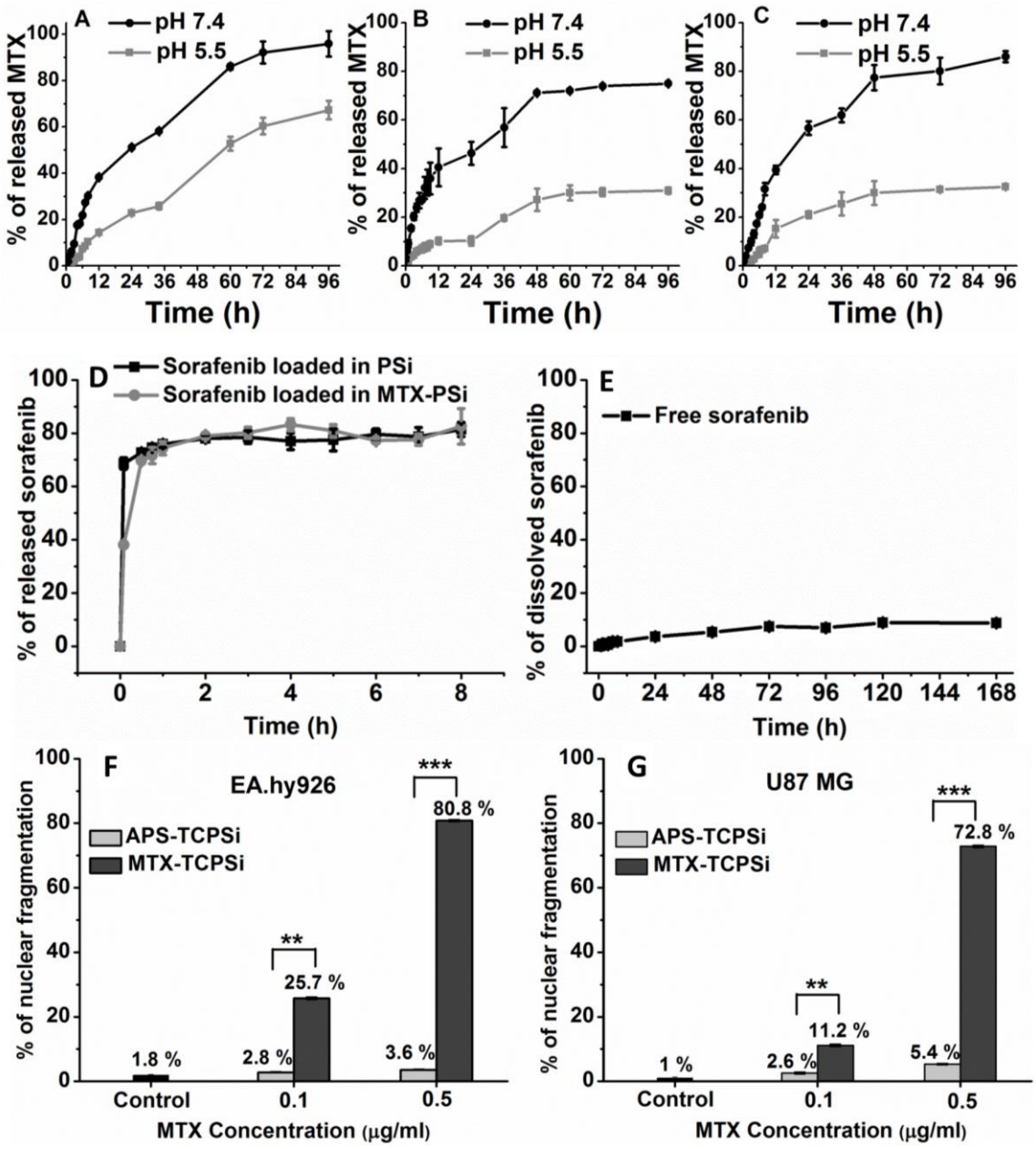

Figure 14. *MTX release from MTX-TCPSi in buffer containing 10% FBS (A), in buffer without FBS (B), and MTX released from sorafenib-loaded MTX-TCPSi NPs in buffer containing 10% FBS (C). SF dissolution from APS-TCPSi and MTX-TCPSi NPs in buffer (pH 7.4) containing 10% FBS (D), and free sorafenib dissolution profiles in buffer (pH 7.4) containing 10% FBS (E). MTX–PSi NPs induced programmed cell apoptosis in EA.hy926 (F) and U87 MG cells (G.). Copyright © (2015) ElsevierB.V. Reprinted with permission from publication (**V**).*

6. Conclusions

Chemical modifications can modulate the surface properties of NPs, which in turn can play an important role on the NPs used for biomedical applications due to the interactions of the NPs with the biological systems. Also, chemical conjugation used to prepare drug conjugates can bring new features to the drug molecules to achieve an efficient delivery.

The surface modification of APS-TCPSi NPs with targeting peptides (RGDS and iRGD) was achieved by the highly selective and robust reaction of SPAAC click chemistry. The surface modification of the PSi NPs enhanced the cellular uptake in the hybrid endothelial cells. The drug loading capacity and the enhancement of the dissolution rate of sorafenib drug by the PSi NPs were not affected by the surface modifications performed on the NPs.

Fluorescent- and radio-labeled, targeting peptide functionalized PSi NPs were prepared from UnTHCPSi NPs. The stability and accessibility of the radio-labeling of PSi NPs via DOTA-mediated chelating were verified by SPECT/CT imaging. The iRGD modification of the dual-labeled NPs improved the tumor accumulation as shown by the radioactivity counting measurements, and enhanced the NP tumor penetration as demonstrated by the *ex vivo* immunofluorescent imaging after intravenous administration. However, both non-targeted and iRGD-targeted PSi NPs were rapidly cleared from the blood stream and accumulated in the liver and spleen. By local intratumoral delivery, both the NPs were retained at the injection site for extended periods of time. H&E staining results showed a good biocompatibility of the prepared multifunctional PSi NPs.

Furthermore, the alkyne-terminated THCPSi NPs were modified with targeting peptides and anti-fouling polymers via CuAAC, and the effect on the cellular uptake and protein association were evaluated. Both the targeting peptides and anti-fouling polymers modified THCPSi-alkyne NPs enhanced the cellular uptake compared to the unmodified THCPSi-alkyne NPs. In addition, the uptake efficiency of the NPs by cancer cells was surface moiety-dependent. The associated proteins to the modified NPs were also varied due to the different surface moieties. Overall, dextran of 40 kDa with the highest MW modified THCPSi-akyne NPs presented the lowest protein adsorption tendency.

Targeting peptides iRGD and H-RN were successfully conjugated to ASIL-6 through solution-phase CuAAC reaction for angiogenic anti-inflammation therapy. Moreover, dual drug delivery was achieved by chemically conjugating MTX to cationic charged APS-TCPSi NPs and physically loading a poorly-water soluble drug, sorafenib. The dissolution rate of antiangiogenic drug sorafenib was enhanced, while the release of MTX from the APS-TCPSi NPs was sustained. The antiproliferation effect and the pharmacological activity of the conjugated MTX to low FR-expressing cells were improved.

The enhancement of the dissolution rate of poorly-water soluble drugs is an advantage of the porous structure presented by PSi nanomaterials. This dissertation developed successfully biofunctionalization methods to increase the cell–NP interactions, labeling of the NPs for tracking and imaging, drug-conjugates synthesis, and evaluated the behavior of the modified PSi NPs for potential cancer drug delivery applications. On the other hand, the ideal cancer drug delivery formulation would enhance the accumulation of the delivered cargo to the targeted tumor sites and control the drug release to reach the maximum therapeutic effect to inhibit the tumor growth with the lowest side effect. There is more work need to be done to develop the PSi based nano-drug delivery system to meet the ideal criteria for clinical applications.

Overall, the chemical modification and labeling methodologies of PSi NPs via click chemistry have been developed and their biological interactions in terms of potential

cancer therapy have been assessed in this dissertation. The surface chemical modification approaches are versatile for preparing advanced multifunctional nanomaterials for medical applications.

References

1. Hanahan, D.; Weinberg, R. A., The hallmarks of cancer. *Cell* **2000,** *100*, 57-70.
2. Hanahan, D.; Weinberg, R. A., Hallmarks of cancer: the next generation. *Cell* **2011,** *144*, 646-74.
3. Wang, R. B.; Billone, P. S.; Mullett, W. M., Nanomedicine in action: an overview of cancer nanomedicine on the market and in clinical trials. *J Nanomater* **2013,** *2013*, 629681.
4. Couvreur, P., Nanoparticles in drug delivery: past, present and future. *Adv Drug Deliv Rev* **2013,** *65*, 21-3.
5. Santos, H. A.; Bimbo, L. M.; Lehto, V. P.; Airaksinen, A. J.; Salonen, J.; Hirvonen, J., Multifunctional porous silicon for therapeutic drug delivery and imaging. *Curr Drug Discov Technol* **2011,** *8*, 228-49.
6. Jarvis, K. L.; Barnes, T. J.; Prestidge, C. A., Surface chemistry of porous silicon and implications for drug encapsulation and delivery applications. *Adv Colloid Interface Sci* **2012,** *175*, 25-38.
7. Mann, A. P.; Tanaka, T.; Somasunderam, A.; Liu, X.; Gorenstein, D. G.; Ferrari, M., E-selectin-targeted porous silicon particle for nanoparticle delivery to the bone marrow. *Adv Mater* **2011,** *23*, H278-82.
8. Makila, E.; Bimbo, L. M.; Kaasalainen, M.; Herranz, B.; Airaksinen, A. J.; Heinonen, M.; Kukk, E.; Hirvonen, J.; Santos, H. A.; Salonen, J., Amine modification of thermally carbonized porous silicon with silane coupling chemistry. *Langmuir* **2012,** *28*, 14045-54.
9. Polanski, M.; Anderson, N. L., A list of candidate cancer biomarkers for targeted proteomics. *Biomark Insights* **2007,** *1*, 1-48.
10. Ruoslahti, E., Peptides as targeting elements and tissue penetration devices for nanoparticles. *Adv Mater* **2012,** *24*, 3747-56.
11. Ruoslahti, E.; Bhatia, S. N.; Sailor, M. J., Targeting of drugs and nanoparticles to tumors. *The Journal of cell biology* **2010,** *188*, 759-68.
12. Ruoslahti, E., Specialization of tumour vasculature. *Nature reviews. Cancer* **2002,** *2*, 83-90.
13. Cal, P. M.; Frade, R. F.; Chudasama, V.; Cordeiro, C.; Caddick, S.; Gois, P. M., Targeting cancer cells with folic acid-iminoboronate fluorescent conjugates. *Chem Commun* **2014,** *50*, 5261-3.
14. Raha, S.; Paunesku, T.; Woloschak, G., Peptide-mediated cancer targeting of nanoconjugates. *Wiley interdisciplinary reviews. Nanomedicine and nanobiotechnology* **2011,** *3*, 269-81.
15. Tokarova, V.; Pittermannova, A.; Kral, V.; Rezacova, P.; Stepanek, F., Feasibility and constraints of particle targeting using the antigen-antibody interaction. *Nanoscale* **2013,** *5*, 11490-8.
16. Rosenholm, J. M.; Peuhu, E.; Bate-Eya, L. T.; Eriksson, J. E.; Sahlgren, C.; Linden, M., Cancer-cell-specific induction of apoptosis using mesoporous silica nanoparticles as drug-delivery vectors. *Small* **2010,** *6*, 1234-41.
17. Wu, C.; Han, D.; Chen, T.; Peng, L.; Zhu, G.; You, M.; Qiu, L.; Sefah, K.; Zhang, X. B.; Tan, W., Building a multifunctional aptamer-based DNA nanoassembly for targeted cancer therapy. *J Am Chem Soc* **2013,** *11*, 18644-50.
18. El-Sagheer, A. H.; Brown, T., Click chemistry with DNA. *Chem Soc Rev* **2010,** *39*, 1388-405.

19. Lallana, E.; Sousa-Herves, A.; Fernandez-Trillo, F.; Riguera, R.; Fernandez-Megia, E., Click chemistry for drug delivery nanosystems. *Pharm Res* **2012,** *29*, 1-34.
20. Rostovtsev, V. V.; Green, L. G.; Fokin, V. V.; Sharpless, K. B., A stepwise huisgen cycloaddition process: copper(I)-catalyzed regioselective "ligation" of azides and terminal alkynes. *Angewandte Chemie International Edition* **2002,** *41*, 2596-9.
21. Wittig, G.; Krebs, A., Zur existenz niedergliedriger cycloalkine, I. *Chemische Berichte* **1961,** *94*, 3260-75.
22. Tenzer, S.; Docter, D.; Kuharev, J.; Musyanovych, A.; Fetz, V.; Hecht, R.; Schlenk, F.; Fischer, D.; Kiouptsi, K.; Reinhardt, C.; Landfester, K.; Schild, H.; Maskos, M.; Knauer, S. K.; Stauber, R. H., Rapid formation of plasma protein corona critically affects nanoparticle pathophysiology. *Nat Nanotechnol* **2013,** *8*, 772-81.
23. Bertholon, I.; Vauthier, C.; Labarre, D., Complement activation by core-shell poly(isobutylcyanoacrylate)-polysaccharide nanoparticles: influences of surface morphology, length, and type of polysaccharide. *Pharm Res* **2006,** *23*, 1313-23.
24. Vauthier, C.; Persson, B.; Lindner, P.; Cabane, B., Protein adsorption and complement activation for di-block copolymer nanoparticles. *Biomaterials* **2011,** *32*, 1646-56.
25. http://www.cancer.org/cancer/cancercauses/index.
26. Ferlay, J.; Steliarova-Foucher, E.; Lortet-Tieulent, J.; Rosso, S.; Coebergh, J. W. W.; Comber, H.; Forman, D.; Bray, F., Cancer incidence and mortality patterns in Europe: Estimates for 40 countries in 2012. *European Journal of Cancer* **2013,** *49*, 1374-403.
27. Edwards, B. K.; Noone, A.-M.; Mariotto, A. B.; Simard, E. P.; Boscoe, F. P.; Henley, S. J.; Jemal, A.; Cho, H.; Anderson, R. N.; Kohler, B. A.; Eheman, C. R.; Ward, E. M., Annual report to the nation on the status of cancer, 1975-2010, featuring prevalence of comorbidity and impact on survival among persons with lung, colorectal, breast, or prostate cancer. *Cancer* **2014,** *120*, 1290-314.
28. Cheng, N.; Chytil, A.; Shyr, Y.; Joly, A.; Moses, H. L., Transforming growth factor-beta signaling-deficient fibroblasts enhance hepatocyte growth factor signaling in mammary carcinoma cells to promote scattering and invasion. *Mol Cancer Res* **2008,** *6*, 1521-33.
29. Sherr, C. J.; McCormick, F., The RB and p53 pathways in cancer. *Cancer cell* **2002,** *2*, 103-12.
30. Adams, J. M.; Cory, S., The Bcl-2 apoptotic switch in cancer development and therapy. *Oncogene* **2007,** *26*, 1324-37.
31. Blasco, M. A., Telomeres and human disease: ageing, cancer and beyond. *Nat Rev Genet* **2005,** *6*, 611-22.
32. Hanahan, D.; Folkman, J., Patterns and emerging mechanisms of the angiogenic switch during tumorigenesis. *Cell* **1996,** *86*, 353-64.
33. Sporn, M. B., The war on cancer. *The Lancet* **1996,** *347*, 1377-81.
34. Jones, P. A.; Baylin, S. B., The epigenomics of cancer. *Cell* **2007,** *128*, 683-92.
35. DeNardo, D. G.; Andreu, P.; Coussens, L. M., Interactions between lymphocytes and myeloid cells regulate pro- versus anti-tumor immunity. *Cancer Metastasis Rev* **2010,** *29*, 309-16.
36. Jones, R. G.; Thompson, C. B., Tumor suppressors and cell metabolism: a recipe for cancer growth. *Genes Dev* **2009,** *23*, 537-48.
37. Teng, M. W.; Swann, J. B.; Koebel, C. M.; Schreiber, R. D.; Smyth, M. J., Immune-mediated dormancy: an equilibrium with cancer. *J Leukoc Biol* **2008,** *84*, 988-93.
38. Roth, W.; Weller, M., Chemotherapy and immunotherapy of malignant glioma: molecular mechanisms and clinical perspectives. *Cell Mol Life Sci* **1999,** *56*, 481-506.

39. Morgan, K., Radiotherapy-induced skin reactions: prevention and cure. *Br J Nurs* **2014,** *23*, S24-S32.
40. Ciardiello, F.; Caputo, R.; Bianco, R.; Damiano, V.; Fontanini, G.; Cuccato, S.; De Placido, S.; Bianco, A. R.; Tortora, G., Inhibition of growth factor production and angiogenesis in human cancer cells by ZD1839 (Iressa), a selective epidermal growth factor receptor tyrosine kinase inhibitor. *Clinical cancer research : an official journal of the American Association for Cancer Research* **2001,** *7*, 1459-65.
41. Goel, G.; Sun, W., Cancer immunotherapy in clinical practice -- the past, present, and future. *Chin J Cancer* **2014,** *33*, 445-57.
42. Ellis, L.; Atadja, P. W.; Johnstone, R. W., Epigenetics in cancer: targeting chromatin modifications. *Molecular cancer therapeutics* **2009,** *8*, 1409-20.
43. Jain, R. K., Normalization of tumor vasculature: an emerging concept in antiangiogenic therapy. *Science* **2005,** *307*, 58-62.
44. Kerbel, R. S., Antiangiogenic therapy: a universal chemosensitization strategy for cancer? *Science* **2006,** *312*, 1171-5.
45. Rosen, L., Antiangiogenic strategies and agents in clinical trials. *Oncologist* **2000,** *1*, 20-7.
46. Al-Husein, B.; Abdalla, M.; Trepte, M.; Deremer, D. L.; Somanath, P. R., Antiangiogenic therapy for cancer: an update. *Pharmacotherapy* **2012,** *32*, 1095-111.
47. Cancer multidrug resistance. *Nat Biotech*.
48. Creixell, M.; Peppas, N. A., Co-delivery of siRNA and therapeutic agents using nanocarriers to overcome cancer resistance. *Nano Today* **2012,** *7*, 367-79.
49. Ohyanagi, F.; Yanagitani, N.; Kudo, K.; Kawano, Y.; Sakatani, T.; Tanimoto, A.; Nishizawa, H.; Horiike, A.; Hagiwara, S.; Horai, T.; Nishio, M., Phase II study of docetaxel-plus-bevacizumab combination therapy in patients previously treated for aAdvanced non-squamous non-small cell lung cancer. *Anticancer Res* **2014,** *34*, 5153-8.
50. Xie, J.; Lee, S.; Chen, X., Nanoparticle-based theranostic agents. *Adv Drug Deliver Rev* **2010,** *62*, 1064-79.
51. Skubitz, K. M., Phase II trial of pegylated-liposomal doxorubicin (Doxil) in mesothelioma. *Cancer Invest* **2002,** *20*, 693-9.
52. Lyass, O.; Uziely, B.; Ben-Yosef, R.; Tzemach, D.; Heshing, N. I.; Lotem, M.; Brufman, G.; Gabizon, A., Correlation of toxicity with pharmacokinetics of pegylated liposomal doxorubicin (Doxil) in metastatic breast carcinoma. *Cancer* **2000,** *89*, 1037-47.
53. Gabizon, A. A., Pegylated liposomal doxorubicin: metamorphosis of an old drug into a new form of chemotherapy. *Cancer Invest* **2001,** *19*, 424-36.
54. Waterhouse, D. N.; Tardi, P. G.; Mayer, L. D.; Bally, M. B., A comparison of liposomal formulations of doxorubicin with drug administered in free form: changing toxicity profiles. *Drug Saf* **2001,** *24*, 903-20.
55. Harris, L.; Batist, G.; Belt, R.; Rovira, D.; Navari, R.; Azarnia, N.; Welles, L.; Winer, E., Liposome-encapsulated doxorubicin compared with conventional doxorubicin in a randomized multicenter trial as first-line therapy of metastatic breast carcinoma. *Cancer* **2002,** *94*, 25-36.
56. Forssen, E. A., The design and development of DaunoXome® for solid tumor targeting in vivo. *Adv Drug Deliver Rev* **1997,** *24*, 133-50.
57. Allen, T. M.; Martin, F. J., Advantages of liposomal delivery systems for anthracyclines. *Seminars in Oncology* **2004,** *31, Supplement 13*, 5-15.

58. Guarneri, V.; Dieci, M. V.; Conte, P., Enhancing intracellular taxane delivery: current role and perspectives of nanoparticle albumin-bound paclitaxel in the treatment of advanced breast cancer. *Expert Opin Pharmacother* **2012,** *13*, 395-406.
59. Hawkins, M. J.; Soon-Shiong, P.; Desai, N., Protein nanoparticles as drug carriers in clinical medicine. *Adv Drug Deliv Rev* **2008,** *60*, 876-85.
60. Chawla, S. P.; Chua, V. S.; Fernandez, L.; Quon, D.; Saralou, A.; Blackwelder, W. C.; Hall, F. L.; Gordon, E. M., Phase I/II and phase II studies of targeted gene delivery in vivo: intravenous Rexin-G for chemotherapy-resistant sarcoma and osteosarcoma. *Mol Ther* **2009,** *17*, 1651-7.
61. Avramis, V. I.; Tiwari, P. N., Asparaginase (native ASNase or pegylated ASNase) in the treatment of acute lymphoblastic leukemia. *International journal of nanomedicine* **2006,** *1*, 241-54.
62. Gaynon, P. S., Childhood acute lymphoblastic leukaemia and relapse. *British Journal of Haematology* **2005,** *131*, 579-87.
63. Lenz, H. J., Management and preparedness for infusion and hypersensitivity reactions. *Oncologist* **2007,** *12*, 601-9.
64. Wang, Y.-X. J., Superparamagnetic iron oxide based MRI contrast agents: current status of clinical application. *Quantitative Imaging in Medicine and Surgery* **2011,** *1*, 35-40.
65. Gao, Y.; Xie, J.; Chen, H.; Gu, S.; Zhao, R.; Shao, J.; Jia, L., Nanotechnology-based intelligent drug design for cancer metastasis treatment. *Biotechnol Adv* **2014,** *32*, 761-77.
66. das Neves, J.; Amiji, M. M.; Bahia, M. F.; Sarmento, B., Nanotechnology-based systems for the treatment and prevention of HIV/AIDS. *Adv Drug Deliver Rev* **2010,** *62*, 458-77.
67. Luk, B. T.; Zhang, L., Current advances in polymer-based nanotheranostics for cancer treatment and diagnosis. *ACS Appl Mater Interfaces* **2014,** *22*, 22.
68. Allen, T. M.; Cullis, P. R., Liposomal drug delivery systems: from concept to clinical applications. *Adv Drug Deliver Rev* **2013,** *65*, 36-48.
69. Decker, C.; Schubert, H.; May, S.; Fahr, A., Pharmacokinetics of temoporfin-loaded liposome formulations: correlation of liposome and temoporfin blood concentration. *J Control Release* **2013,** *166*, 277-85.
70. Liu, Y.; Ran, R.; Chen, J.; Kuang, Q.; Tang, J.; Mei, L.; Zhang, Q.; Gao, H.; Zhang, Z.; He, Q., Paclitaxel loaded liposomes decorated with a multifunctional tandem peptide for glioma targeting. *Biomaterials* **2014,** *35*, 4835-47.
71. Bibi, S.; Lattmann, E.; Mohammed, A. R.; Perrie, Y., Trigger release liposome systems: local and remote controlled delivery? *J Microencapsul* **2012,** *29*, 262-76.
72. Mitchell, N.; Kalber, T. L.; Cooper, M. S.; Sunassee, K.; Chalker, S. L.; Shaw, K. P.; Ordidge, K. L.; Badar, A.; Janes, S. M.; Blower, P. J.; Lythgoe, M. F.; Hailes, H. C.; Tabor, A. B., Incorporation of paramagnetic, fluorescent and PET/SPECT contrast agents into liposomes for multimodal imaging. *Biomaterials* **2013,** *34*, 1179-92.
73. Kore, G.; Kolate, A.; Nej, A.; Misra, A., Polymeric micelle as multifunctional pharmaceutical carriers. *J Nanosci Nanotechnol* **2014,** *14*, 288-307.
74. Sabbatini, P.; Aghajanian, C.; Dizon, D.; Anderson, S.; Dupont, J.; Brown, J. V.; Peters, W. A.; Jacobs, A.; Mehdi, A.; Rivkin, S.; Eisenfeld, A. J.; Spriggs, D., Phase II study of CT-2103 in patients with recurrent epithelial ovarian, fallopian tube, or primary peritoneal carcinoma. *Journal of clinical oncology : official journal of the American Society of Clinical Oncology* **2004,** *22*, 4523-31.

75. Singer, J. W.; Shaffer, S.; Baker, B.; Bernareggi, A.; Stromatt, S.; Nienstedt, D.; Besman, M., Paclitaxel poliglumex (XYOTAX; CT-2103): an intracellularly targeted taxane. *Anticancer Drugs* **2005,** *16*, 243-54.
76. Wang, K.; Zhang, X.; Liu, Y.; Liu, C.; Jiang, B.; Jiang, Y., Tumor penetrability and anti-angiogenesis using iRGD-mediated delivery of doxorubicin-polymer conjugates. *Biomaterials* **2014,** *35*, 8735-47.
77. Huang, B.; Otis, J.; Joice, M.; Kotlyar, A.; Thomas, T. P., PSMA-targeted stably linked "dendrimer-glutamate urea-methotrexate" as a prostate cancer therapeutic. *Biomacromolecules* **2014,** *15*, 915-23.
78. Das, M.; Datir, S. R.; Singh, R. P.; Jain, S., Augmented anticancer activity of a targeted, intracellularly activatable, theranostic nanomedicine based on fluorescent and radiolabeled, methotrexate-folic acid-multiwalled carbon nanotube conjugate. *Mol Pharm* **2013**, 10, 2537-57.
79. Schreier, S.; Malheiros, S. V. P.; de Paula, E., Surface active drugs: self-association and interaction with membranes and surfactants. Physicochemical and biological aspects. *Biochimica et Biophysica Acta (BBA) - Biomembranes* **2000,** *1508*, 210-34.
80. Yang, J.; Yao, M. H.; Wen, L.; Song, J. T.; Zhang, M. Z.; Zhao, Y. D.; Liu, B., Multifunctional quantum dot-polypeptide hybrid nanogel for targeted imaging and drug delivery. *Nanoscale* **2014,** *6*, 11282-92.
81. Wang, C.; Mallela, J.; Garapati, U. S.; Ravi, S.; Chinnasamy, V.; Girard, Y.; Howell, M.; Mohapatra, S., A chitosan-modified graphene nanogel for noninvasive controlled drug release. *Nanomedicine-Uk* **2013,** *9*, 903-11.
82. Zan, M.; Li, J.; Luo, S.; Ge, Z., Dual pH-triggered multistage drug delivery systems based on host-guest interaction-associated polymeric nanogels. *Chem Commun* **2014,** *50*, 7824-7.
83. He, H.; Cattran, A. W.; Nguyen, T.; Nieminen, A. L.; Xu, P., Triple-responsive expansile nanogel for tumor and mitochondria targeted photosensitizer delivery. *Biomaterials* **2014,** *35*, 9546-53.
84. Salva, R.; Le Meins, J. F.; Sandre, O.; Brulet, A.; Schmutz, M.; Guenoun, P.; Lecommandoux, S., Polymersome shape transformation at the nanoscale. *Acs Nano* **2013,** *7*, 9298-311.
85. Bei, D.; Meng, J.; Youan, B.-B. C., Engineering nanomedicines for improved melanoma therapy: progress and promises. *Nanomedicine-Uk* **2010,** *5*, 1385-1399.
86. Astruc, D.; Boisselier, E.; Ornelas, C., Dendrimers designed for functions: from physical, photophysical, and supramolecular properties to applications in sensing, catalysis, molecular electronics, photonics, and nanomedicine. *Chem Rev* **2010,** *110*, 1857-959.
87. Huang, B.; Kukowska-Latallo, J. F.; Tang, S.; Zong, H.; Johnson, K. B.; Desai, A.; Gordon, C. L.; Leroueil, P. R.; Baker, J. R., Jr., The facile synthesis of multifunctional PAMAM dendrimer conjugates through copper-free click chemistry. *Bioorg Med Chem Lett* **2012,** *22*, 3152-6.
88. Sunoqrot, S.; Bugno, J.; Lantvit, D.; Burdette, J. E.; Hong, S., Prolonged blood circulation and enhanced tumor accumulation of folate-targeted dendrimer-polymer hybrid nanoparticles. *J Control Release* **2014,** *191*, 115-22.
89. McNerny, D. Q.; Kukowska-Latallo, J. F.; Mullen, D. G.; Wallace, J. M.; Desai, A. M.; Shukla, R.; Huang, B.; Banaszak Holl, M. M.; Baker, J. R., Jr., RGD dendron bodies; synthetic avidity agents with defined and potentially interchangeable effector sites that can substitute for antibodies. *Bioconjug Chem* **2009,** *20*, 1853-9.

90. Biricova, V.; Laznickova, A.; Laznicek, M.; Polasek, M.; Hermann, P., Radiolabeling of PAMAM dendrimers conjugated to a pyridine-N-oxide DOTA analog with ^{111}In: optimization of reaction conditions and biodistribution. *J Pharm Biomed Anal* **2011,** *56*, 505-12.
91. Lesniak, W. G.; Mishra, M. K.; Jyoti, A.; Balakrishnan, B.; Zhang, F.; Nance, E.; Romero, R.; Kannan, S.; Kannan, R. M., Biodistribution of fluorescently labeled PAMAM dendrimers in neonatal rabbits: effect of neuroinflammation. *Mol Pharm* **2013,** *10*, 4560-71.
92. Zong, H.; Thomas, T. P.; Lee, K. H.; Desai, A. M.; Li, M. H.; Kotlyar, A.; Zhang, Y.; Leroueil, P. R.; Gam, J. J.; Banaszak Holl, M. M.; Baker, J. R., Jr., Bifunctional PAMAM dendrimer conjugates of folic acid and methotrexate with defined ratio. *Biomacromolecules* **2012,** *13*, 982-91.
93. Lohcharoenkal, W.; Wang, L.; Chen, Y. C.; Rojanasakul, Y., Protein nanoparticles as drug delivery carriers for cancer therapy. *Biomed Res Int* **2014,** 2014, *180549*.
94. Heddle, J. G., Protein cages, rings and tubes: useful components of future nanodevices? *Nanotechnol Sci Appl* **2008,** *1*, 67-78.
95. Kratz, F.; Roth, T.; Fichiner, I.; Schumacher, P.; Fiebig, H. H.; Unger, C., *In vitro* and *in vivo* efficacy of acid-sensitive transferrin and albumin doxorubicin conjugates in a human xenograft panel and in the MDA-MB-435 mamma carcinoma model. *J Drug Target* **2000,** *8*, 305-18.
96. Jahanshahi, M.; Sanati, M. H.; Babaei, Z., Optimization of parameters for the fabrication of gelatin nanoparticles by the Taguchi robust design method. *Journal of Applied Statistics* **2008,** *35*, 1345-53.
97. Urry, D. W., Physical chemistry of biological free energy transduction as demonstrated by elastic protein-based polymers†. *The Journal of Physical Chemistry B* **1997,** *101*, 11007-28.
98. Ezpeleta, I.; Irache, J. M.; Stainmesse, S.; Chabenat, C.; Gueguen, J.; Popineau, Y.; Orecchioni, A.-M., Gliadin nanoparticles for the controlled release of all-trans-retinoic acid. *Int J Pharmaceut* **1996,** *131*, 191-200.
99. Zhang, Q.; Jiang, Q.; Li, N.; Dai, L.; Liu, Q.; Song, L.; Wang, J.; Li, Y.; Tian, J.; Ding, B.; Du, Y., DNA origami as an in vivo drug delivery vehicle for cancer therapy. *Acs Nano* **2014,** *8*, 6633-43.
100. Chao, J.; Liu, H.; Su, S.; Wang, L.; Huang, W.; Fan, C., Structural DNA nanotechnology for intelligent drug delivery. *Small* **2014**, *10*, 4625-35.
101. Hamner, K. L.; Alexander, C. M.; Coopersmith, K.; Reishofer, D.; Provenza, C.; Maye, M. M., Using temperature-sensitive smart polymers to regulate DNA-mediated nanoassembly and encoded nanocarrier drug release. *Acs Nano* **2013,** *7*, 7011-20.
102. Monserud, J. H.; Schwartz, D. K., Mechanisms of surface-mediated DNA hybridization. *Acs Nano* **2014,** *8*, 4488-99.
103. Chou, L. Y.; Zagorovsky, K.; Chan, W. C., DNA assembly of nanoparticle superstructures for controlled biological delivery and elimination. *Nat Nanotechnol* **2014,** *9*, 148-55.
104. Venancio-Marques, A.; Bergen, A.; Rossi-Gendron, C.; Rudiuk, S.; Baigl, D., Photosensitive polyamines for high-performance photocontrol of DNA higher-order structure. *Acs Nano* **2014,** *8*, 3654-63.
105. Roh, Y. H.; Lee, J. B.; Shopsowitz, K. E.; Dreaden, E. C.; Morton, S. W.; Poon, Z.; Hong, J.; Yamin, I.; Bonner, D. K.; Hammond, P. T., Layer-by-layer assembled anti-sense DNA microsponge particles for efficient delivery of cancer therapeutics. *Acs Nano* **2014**, 8, 9767-80.

106. Zhang, Z.; Wang, J.; Chen, C., Near-infrared light-mediated nanoplatforms for cancer thermo-chemotherapy and optical imaging. *Adv Mater* **2013,** *25*, 3869-80.
107. Xia, Y.; Li, W.; Cobley, C. M.; Chen, J.; Xia, X.; Zhang, Q.; Yang, M.; Cho, E. C.; Brown, P. K., Gold Nanocages: from synthesis to theranostic applications. *Accounts Chem Res* **2011,** *44*, 914-24.
108. O'Connell, M. J.; Bachilo, S. M.; Huffman, C. B.; Moore, V. C.; Strano, M. S.; Haroz, E. H.; Rialon, K. L.; Boul, P. J.; Noon, W. H.; Kittrell, C.; Ma, J.; Hauge, R. H.; Weisman, R. B.; Smalley, R. E., Band gap fluorescence from individual single-walled carbon nanotubes. *Science* **2002,** *297*, 593-6.
109. Gao, L.; Nie, L.; Wang, T.; Qin, Y.; Guo, Z.; Yang, D.; Yan, X., Carbon nanotube delivery of the GFP gene into mammalian cells. *ChemBioChem* **2006,** *7*, 239-42.
110. Cherukuri, P.; Bachilo, S. M.; Litovsky, S. H.; Weisman, R. B., Near-infrared fluorescence microscopy of single-walled carbon nanotubes in phagocytic cells. *J Am Chem Soc* **2004,** *126*, 15638-9.
111. Wang, Y. X., Superparamagnetic iron oxide based MRI contrast agents: current status of clinical application. *Quant Imaging Med Surg* **2011,** *1*, 35-40.
112. Huang, Q.; Bao, C.; Lin, Y.; Chen, J.; Liu, Z.; Zhu, L., Disulfide-phenylazide: a reductively cleavable photoreactive linker for facile modification of nanoparticle surfaces. *J Mater Chem B* **2013,** *1*, 1125-32.
113. Shirazi, A. N.; Paquin, K. L.; Howlett, N. G.; Mandal, D.; Parang, K., Cyclic peptide-capped gold nanoparticles for enhanced siRNA delivery. *Molecules* **2014,** *19*, 13319-31.
114. Barhoumi, A.; Wang, W.; Zurakowski, D.; Langer, R. S.; Kohane, D. S., Photothermally targeted thermosensitive polymer-masked nanoparticles. *Nano Lett* **2014,** *14*, 3697-701.
115. Melancon, M. P.; Zhou, M.; Zhang, R.; Xiong, C.; Allen, P.; Wen, X.; Huang, Q.; Wallace, M.; Myers, J. N.; Stafford, R. J.; Liang, D.; Ellington, A. D.; Li, C., Selective uptake and imaging of aptamer- and antibody-conjugated hollow nanospheres targeted to epidermal growth factor receptors overexpressed in head and neck cancer. *Acs Nano* **2014,** *8*, 4530-8.
116. Kumar, A.; Huo, S.; Zhang, X.; Liu, J.; Tan, A.; Li, S.; Jin, S.; Xue, X.; Zhao, Y.; Ji, T.; Han, L.; Liu, H.; Zhang, J.; Zou, G.; Wang, T.; Tang, S.; Liang, X. J., Neuropilin-1-targeted gold nanoparticles enhance therapeutic efficacy of platinum(IV) drug for prostate cancer treatment. *Acs Nano* **2014,** *8*, 4205-20.
117. Liu, Z.; Sun, X.; Nakayama-Ratchford, N.; Dai, H., Supramolecular chemistry on water-soluble carbon nanotubes for drug loading and delivery. *Acs Nano* **2007,** *1*, 50-56.
118. Vallet-Regi, M.; Colilla, M.; Gonzalez, B., Medical applications of organic-inorganic hybrid materials within the field of silica-based bioceramics. *Chem Soc Rev* **2011,** *40*, 596-607.
119. Vallet-Regi, M.; Balas, F.; Arcos, D., Mesoporous materials for drug delivery. *Angew Chem Int Ed Engl* **2007,** *46*, 7548-58.
120. http://www.news.cornell.edu/stories/2011/01/cornell-dots-get-first-trial-humans.
121. Yang, Y.; Li, J., Lipid, protein and poly(NIPAM) coated mesoporous silica nanoparticles for biomedical applications. *Adv Colloid Interface Sci* **2014,** *207*, 155-63.
122. Sun, J. T.; Piao, J. G.; Wang, L. H.; Javed, M.; Hong, C. Y.; Pan, C. Y., One-pot synthesis of redox-responsive polymers-coated mesoporous silica nanoparticles and their controlled drug release. *Macromol Rapid Commun* **2013,** *34*, 1387-94.

123. Jambhrunkar, S.; Qu, Z.; Popat, A.; Yang, J.; Noonan, O.; Acauan, L.; Ahmad Nor, Y.; Yu, C.; Karmakar, S., Effect of surface functionality of silica nanoparticles on cellular uptake and cytotoxicity. *Mol Pharm* **2014,** *11*, 3642-55.
124. Pan, L.; Liu, J.; He, Q.; Shi, J., MSN-mediated sequential vascular-to-cell nuclear-targeted drug delivery for efficient tumor regression. *Adv Mater* **2014,** *26*, 6742-8.
125. Chen, Y.; Chen, H.; Shi, J., In vivo bio-safety evaluations and diagnostic/therapeutic applications of chemically designed mesoporous silica nanoparticles. *Adv Mater* **2013,** *25*, 3144-76.
126. Wu, Y.; Shi, M.; Zhao, L.; Feng, W.; Li, F.; Huang, C., Visible-light-excited and europium-emissive nanoparticles for highly-luminescent bioimaging in vivo. *Biomaterials* **2014,** *35*, 5830-9.
127. Granitzer, P.; Rumpf, K., Magnetic nanoparticles embedded in a silicon matrix. *Materials* **2011,** *4*, 908-928.
128. Nam, J.; Won, N.; Bang, J.; Jin, H.; Park, J.; Jung, S.; Park, Y.; Kim, S., Surface engineering of inorganic nanoparticles for imaging and therapy. *Adv Drug Deliv Rev* **2013,** *65*, 622-48.
129. Chen, H.; Sulejmanovic, D.; Moore, T.; Colvin, D. C.; Qi, B.; Mefford, O. T.; Gore, J. C.; Alexis, F.; Hwu, S. J.; Anker, J. N., Iron-loaded magnetic nanocapsules for pH-triggered drug release and MRI imaging. *Chem Mater* **2014,** *26*, 2105-12.
130. Wang, D.; Fei, B.; Halig, L. V.; Qin, X.; Hu, Z.; Xu, H.; Wang, Y. A.; Chen, Z.; Kim, S.; Shin, D. M.; Chen, Z. G., Targeted iron-oxide nanoparticle for photodynamic therapy and imaging of head and neck cancer. *Acs Nano* **2014,** *8*, 6620-32.
131. Ketkar-Atre, A.; Struys, T.; Dresselaers, T.; Hodenius, M.; Mannaerts, I.; Ni, Y.; Lambrichts, I.; Van Grunsven, L. A.; De Cuyper, M.; Himmelreich, U., *In vivo* hepatocyte MR imaging using lactose functionalized magnetoliposomes. *Biomaterials* **2014,** *35*, 1015-24.
132. Uhlir, A. J., Electrolytic shaping of germanium and silicon. *Bell System Technical Journal* **1956,** *35*, 15.
133. Cullis, A. G.; Canham, L. T., Visible light emission due to quantum size effects in highly porous crystalline silicon. *Nature* **1991,** *353*, 335-8.
134. Canham, L. T., Bioactive silicon structure fabrication through nanoetching techniques. *Adv Mater* **1995,** *7*, 1033-7.
135. Maniya, N. H.; Patel, S. R.; Murthy, Z. V. P., Electrochemical preparation of microstructured porous silicon layers for drug delivery applications. *Superlattices and Microstructures* **2013,** *55*, 144-50.
136. Canham, L. T.; Saunders, S. J.; Heeley, P. B.; Keir, A. M.; Cox, T. I., Rapid chemography of porous silicon undergoing hydrolysis. *Adv Mater* **1994,** *6*, 865-8.
137. Anglin, E. J.; Cheng, L.; Freeman, W. R.; Sailor, M. J., Porous silicon in drug delivery devices and materials. *Adv Drug Deliv Rev* **2008,** *60*, 1266-77.
138. Gardelis, S.; Hamilton, B., The effect of surface modification on the luminescence of porous silicon. *J Appl Phys* **1994,** *76*, 5327-33.
139. Hadj Zoubir, N.; Vergnat, M.; Delatour, T.; Burneau, A.; de Donato, P., Interpretation of the luminescence quenching in chemically etched porous silicon by the desorption of SiH3 species. *Applied Physics Letters* **1994,** *65*, 82-4.
140. Salonen, J.; Lehto, V.-P.; Laine, E., Thermal oxidation of free-standing porous silicon films. *Applied Physics Letters* **1997,** *70*, 637-9.
141. Salonen, J.; Lehto, V. P.; Laine, E., The room temperature oxidation of porous silicon. *Appl Surf Sci* **1997,** *120*, 191-8.

142. Salonen, J.; Lehto, V. P.; Björkqvist, M.; Laine, E.; Niinistö, L., Studies of thermally-carbonized porous silicon surfaces. *physica status solidi (a)* **2000,** *182*, 123-6.
143. Salonen, J.; Laine, E.; Niinistö, L., Thermal carbonization of porous silicon surface by acetylene. *J Appl Phys* **2002,** *91*, 456-61.
144. Salonen, J.; Björkqvist, M.; Laine, E.; Niinistö, L., Stabilization of porous silicon surface by thermal decomposition of acetylene. *Appl Surf Sci* **2004,** *225*, 389-94.
145. Boukherroub, R.; Wojtyk, J. T. C.; Wayner, D. D. M.; Lockwood, D. J., Thermal hydrosilylation of undecylenic acid with porous silicon. *Journal of the Electrochemical Society* **2002,** *149*, H59-H63.
146. Geobaldo, F.; Rivolo, P.; Ugliengo, P.; Garrone, E., A new route to the surface functionalisation of porous silicon. *Sensors and Actuators B: Chemical* **2004,** *100*, 29-32.
147. Salonen, J.; Laine, E.; Niinistö, L., Thermal analysis of hydrosilylation of 1-dodecene on porous silicon surface. *physica status solidi (a)* **2003,** *197*, 246-50.
148. Bateman, J. E.; Eagling, R. D.; Worrall, D. R.; Horrocks, B. R.; Houlton, A., Alkylation of porous silicon by direct reaction with alkenes and alkynes. *Angewandte Chemie International Edition* **1998,** *37*, 2683-5.
149. Boukherroub, R.; Morin, S.; Wayner, D. D. M.; Bensebaa, F.; Sproule, G. I.; Baribeau, J. M.; Lockwood, D. J., Ideal passivation of luminescent porous silicon by thermal, noncatalytic reaction with alkenes and aldehydes. *Chem Mater* **2001,** *13*, 2002-11.
150. Stewart, M. P.; Buriak, J. M., Photopatterned hydrosilylation on porous silicon. *Angewandte Chemie International Edition* **1998,** *37*, 3257-60.
151. Björkqvist, M.; Salonen, J.; Laine, E.; Niinistö, L., Comparison of stabilizing treatments on porous silicon for sensor applications. *physica status solidi (a)* **2003,** *197*, 374-7.
152. Ciampi, S.; Bocking, T.; Kilian, K. A.; Harper, J. B.; Gooding, J. J., Click chemistry in mesoporous materials: functionalization of porous silicon rugate filters. *Langmuir* **2008,** *24*, 5888-92.
153. Guan, B.; Ciampi, S.; Le Saux, G.; Gaus, K.; Reece, P. J.; Gooding, J. J., Different functionalization of the internal and external surfaces in mesoporous materials for biosensing applications using "click" chemistry. *Langmuir* **2011,** *27*, 328-34.
154. Flavel, B. S.; Jasieniak, M.; Velleman, L.; Ciampi, S.; Luais, E.; Peterson, J. R.; Griesser, H. J.; Shapter, J. G.; Gooding, J. J., Grafting of poly(ethylene glycol) on click chemistry modified Si(100) surfaces. *Langmuir* **2013,** *29*, 8355-62.
155. Stewart, M. P.; Robins, E. G.; Geders, T. W.; Allen, M. J.; Cheul Choi, H.; Buriak, J. M., Three methods for stabilization and functionalization of porous silicon surfaces via hydrosilylation and alectrografting reactions. *physica status solidi (a)* **2000,** *182*, 109-115.
156. Bao, Z.; Weatherspoon, M. R.; Shian, S.; Cai, Y.; Graham, P. D.; Allan, S. M.; Ahmad, G.; Dickerson, M. B.; Church, B. C.; Kang, Z.; Abernathy Iii, H. W.; Summers, C. J.; Liu, M.; Sandhage, K. H., Chemical reduction of three-dimensional silica micro-assemblies into microporous silicon replicas. *Nature* **2007,** *446*, 172-175.
157. Wang, J.-F.; Wang, K.-X.; Du, F.-H.; Guo, X.-X.; Jiang, Y.-M.; Chen, J.-S., Amorphous silicon with high specific surface area prepared by a sodiothermic reduction method for supercapacitors. *Chem Commun* **2013,** *49*, 5007-9.
158. Magasinski, A.; Dixon, P.; Hertzberg, B.; Kvit, A.; Ayala, J.; Yushin, G., High-performance lithium-ion anodes using a hierarchical bottom-up approach. *Nat Mater* **2010,** *9*, 353-8.

159. Dai, F.; Zai, J.; Yi, R.; Gordin, M. L.; Sohn, H.; Chen, S.; Wang, D., Bottom-up synthesis of high surface area mesoporous crystalline silicon and evaluation of its hydrogen evolution performance. *Nature communications* **2014,** *5*, 3605.
160. Bimbo, L. M.; Sarparanta, M.; Santos, H. A.; Airaksinen, A. J.; Makila, E.; Laaksonen, T.; Peltonen, L.; Lehto, V. P.; Hirvonen, J.; Salonen, J., Biocompatibility of thermally hydrocarbonized porous silicon nanoparticles and their biodistribution in rats. *Acs Nano* **2010,** *4*, 3023-32.
161. Shahbazi, M. A.; Hamidi, M.; Makila, E. M.; Zhang, H.; Almeida, P. V.; Kaasalainen, M.; Salonen, J. J.; Hirvonen, J. T.; Santos, H. A., The mechanisms of surface chemistry effects of mesoporous silicon nanoparticles on immunotoxicity and biocompatibility. *Biomaterials* **2013,** *34*, 7776-89.
162. Tolli, M. A.; Ferreira, M. P.; Kinnunen, S. M.; Rysa, J.; Makila, E. M.; Szabo, Z.; Serpi, R. E.; Ohukainen, P. J.; Valimaki, M. J.; Correia, A. M.; Salonen, J. J.; Hirvonen, J. T.; Ruskoaho, H. J.; Santos, H. A., In vivo biocompatibility of porous silicon biomaterials for drug delivery to the heart. *Biomaterials* **2014,** *35*, 8394-405.
163. Shen, J.; Xu, R.; Mai, J.; Kim, H. C.; Guo, X.; Qin, G.; Yang, Y.; Wolfram, J.; Mu, C.; Xia, X.; Gu, J.; Liu, X.; Mao, Z. W.; Ferrari, M.; Shen, H., High capacity nanoporous silicon carrier for systemic delivery of gene silencing therapeutics. *Acs Nano* **2013,** *7*, 9867-80.
164. Jaganathan, H.; Godin, B., Biocompatibility assessment of Si-based nano- and micro-particles. *Adv Drug Deliv Rev* **2012,** *64*, 1800-19.
165. Tanaka, T.; Godin, B.; Bhavane, R.; Nieves-Alicea, R.; Gu, J.; Liu, X.; Chiappini, C.; Fakhoury, J. R.; Amra, S.; Ewing, A.; Li, Q.; Fidler, I. J.; Ferrari, M., *In vivo* evaluation of safety of nanoporous silicon carriers following single and multiple dose intravenous administrations in mice. *Int J Pharm* **2010,** *402*, 190-7.
166. Low, S. P.; Voelcker, N. H.; Canham, L. T.; Williams, K. A., The biocompatibility of porous silicon in tissues of the eye. *Biomaterials* **2009,** *30*, 2873-80.
167. Cheng, L.; Anglin, E.; Cunin, F.; Kim, D.; Sailor, M. J.; Falkenstein, I.; Tammewar, A.; Freeman, W. R., Intravitreal properties of porous silicon photonic crystals: a potential self-reporting intraocular drug-delivery vehicle. *Br J Ophthalmol* **2008,** *92*, 705-11.
168. Nieto, A.; Hou, H.; Sailor, M. J.; Freeman, W. R.; Cheng, L., Ocular silicon distribution and clearance following intravitreal injection of porous silicon microparticles. *Experimental eye research* **2013,** *116*, 161-8.
169. Jugdaohsingh, R.; Anderson, S. H.; Tucker, K. L.; Elliott, H.; Kiel, D. P.; Thompson, R. P.; Powell, J. J., Dietary silicon intake and absorption. *Am J Clin Nutr* **2002,** *75*, 887-93.
170. Salonen, J.; Kaukonen, A. M.; Hirvonen, J.; Lehto, V. P., Mesoporous silicon in drug delivery applications. *J Pharm Sci* **2008,** *97*, 632-53.
171. Kayahan, E., The role of surface oxidation on luminescence degradation of porous silicon. *Appl Surf Sci* **2011,** *257*, 4311-6.
172. Godin, B.; Gu, J.; Serda, R. E.; Bhavane, R.; Tasciotti, E.; Chiappini, C.; Liu, X.; Tanaka, T.; Decuzzi, P.; Ferrari, M., Tailoring the degradation kinetics of mesoporous silicon structures through PEGylation. *J Biomed Mater Res A* **2010,** *94*, 1236-43.
173. Park, J. H.; Gu, L.; von Maltzahn, G.; Ruoslahti, E.; Bhatia, S. N.; Sailor, M. J., Biodegradable luminescent porous silicon nanoparticles for in vivo applications. *Nat Mater* **2009,** *8*, 331-6.
174. Salonen, J.; Laitinen, L.; Kaukonen, A. M.; Tuura, J.; Bjorkqvist, M.; Heikkila, T.; Vaha-Heikkila, K.; Hirvonen, J.; Lehto, V. P., Mesoporous silicon microparticles for

oral drug delivery: loading and release of five model drugs. *J Control Release* **2005,** *108*, 362-74.
175. Wu, E. C.; Andrew, J. S.; Buyanin, A.; Kinsella, J. M.; Sailor, M. J., Suitability of porous silicon microparticles for the long-term delivery of redox-active therapeutics. *Chem Commun* **2011,** *47*, 5699-701.
176. Secret, E.; Maynadier, M.; Gallud, A.; Gary-Bobo, M.; Chaix, A.; Belamie, E.; Maillard, P.; Sailor, M. J.; Garcia, M.; Durand, J. O.; Cunin, F., Anionic porphyrin-grafted porous silicon nanoparticles for photodynamic therapy. *Chem Commun* **2013,** *49*, 4202-4.
177. Kilpeläinen, M.; Riikonen, J.; Vlasova, M. A.; Huotari, A.; Lehto, V. P.; Salonen, J.; Herzig, K. H.; Järvinen, K., In vivo delivery of a peptide, ghrelin antagonist, with mesoporous silicon microparticles. *J Control Release* **2009,** *137*, 166-70.
178. Kovalainen, M.; Monkare, J.; Kaasalainen, M.; Riikonen, J.; Lehto, V. P.; Salonen, J.; Herzig, K. H.; Jarvinen, K., Development of porous silicon nanocarriers for parenteral peptide delivery. *Mol Pharm* **2013,** *10*, 353-9.
179. Huotari, A.; Xu, W.; Monkare, J.; Kovalainen, M.; Herzig, K. H.; Lehto, V. P.; Jarvinen, K., Effect of surface chemistry of porous silicon microparticles on glucagon-like peptide-1 (GLP-1) loading, release and biological activity. *Int J Pharm* **2013,** *454*, 67-73.
180. Bimbo, L. M.; Makila, E.; Laaksonen, T.; Lehto, V. P.; Salonen, J.; Hirvonen, J.; Santos, H. A., Drug permeation across intestinal epithelial cells using porous silicon nanoparticles. *Biomaterials* **2011,** *32*, 2625-33.
181. Liu, D.; Bimbo, L. M.; Makila, E.; Villanova, F.; Kaasalainen, M.; Herranz-Blanco, B.; Caramella, C. M.; Lehto, V. P.; Salonen, J.; Herzig, K. H.; Hirvonen, J.; Santos, H. A., Co-delivery of a hydrophobic small molecule and a hydrophilic peptide by porous silicon nanoparticles. *J Control Release* **2013,** *170*, 268-78.
182. Zhang, H.; Liu, D.; Shahbazi, M. A.; Makila, E.; Herranz-Blanco, B.; Salonen, J.; Hirvonen, J.; Santos, H. A., Fabrication of a multifunctional nano-in-micro drug delivery platform by microfluidic templated encapsulation of porous silicon in polymer matrix. *Adv Mater* **2014,** *26*, 4497-503.
183. Riikonen, J.; Makila, E.; Salonen, J.; Lehto, V. P., Determination of the physical state of drug molecules in mesoporous silicon with different surface chemistries. *Langmuir* **2009,** *25*, 6137-42.
184. Bimbo, L. M.; Denisova, O. V.; Makila, E.; Kaasalainen, M.; De Brabander, J. K.; Hirvonen, J.; Salonen, J.; Kakkola, L.; Kainov, D.; Santos, H. A., Inhibition of influenza a virus infection in vitro by saliphenylhalamide-loaded porous silicon nanoparticles. *Acs Nano* **2013,** *7*, 6884-93.
185. Tahvanainen, M.; Rotko, T.; Makila, E.; Santos, H. A.; Neves, D.; Laaksonen, T.; Kallonen, A.; Hamalainen, K.; Peura, M.; Serimaa, R.; Salonen, J.; Hirvonen, J.; Peltonen, L., Tablet preformulations of indomethacin-loaded mesoporous silicon microparticles. *Int J Pharm* **2012,** *422*, 125-31.
186. Wang, F.; Hui, H.; Barnes, T. J.; Barnett, C.; Prestidge, C. A., Oxidized mesoporous silicon microparticles for improved oral delivery of poorly soluble drugs. *Mol Pharm* **2010,** *7*, 227-36.
187. Kovalainen, M.; Monkare, J.; Makila, E.; Salonen, J.; Lehto, V. P.; Herzig, K. H.; Jarvinen, K., Mesoporous silicon (PSi) for sustained peptide delivery: effect of psi microparticle surface chemistry on peptide YY3-36 release. *Pharm Res* **2012,** *29*, 837-46.

188. Araujo, F.; Shrestha, N.; Shahbazi, M. A.; Fonte, P.; Makila, E. M.; Salonen, J. J.; Hirvonen, J. T.; Granja, P. L.; Santos, H. A.; Sarmento, B., The impact of nanoparticles on the mucosal translocation and transport of GLP-1 across the intestinal epithelium. *Biomaterials* **2014,** *35*, 9199-207.
189. Jarvis, K. L.; Barnes, T. J.; Prestidge, C. A., Thermal oxidation for controlling protein interactions with porous silicon. *Langmuir* **2010,** *26*, 14316-22.
190. Foraker, A.; Walczak, R.; Cohen, M.; Boiarski, T.; Grove, C.; Swaan, P., Microfabricated porous silicon particles enhance paracellular delivery of insulin across intestinal Caco-2 cell monolayers. *Pharm Res-Dordr* **2003,** *20*, 110-6.
191. Shrestha, N.; Shahbazi, M. A.; Araujo, F.; Zhang, H.; Makila, E. M.; Kauppila, J.; Sarmento, B.; Salonen, J. J.; Hirvonen, J. T.; Santos, H. A., Chitosan-modified porous silicon microparticles for enhanced permeability of insulin across intestinal cell monolayers. *Biomaterials* **2014,** *17*, 00517-1.
192. Cross, D.; Burmester, J. K., Gene therapy for cancer treatment: past, present and future. *Clin Med Res* **2006,** *4*, 218-27.
193. Meng, H.; Mai, W. X.; Zhang, H.; Xue, M.; Xia, T.; Lin, S.; Wang, X.; Zhao, Y.; Ji, Z.; Zink, J. I.; Nel, A. E., Codelivery of an optimal drug/siRNA combination using mesoporous silica nanoparticles to overcome drug resistance in breast cancer in vitro and in vivo. *Acs Nano* **2013,** *7*, 994-1005.
194. Tanaka, T.; Mangala, L. S.; Vivas-Mejia, P. E.; Nieves-Alicea, R.; Mann, A. P.; Mora, E.; Han, H. D.; Shahzad, M. M.; Liu, X.; Bhavane, R.; Gu, J.; Fakhoury, J. R.; Chiappini, C.; Lu, C.; Matsuo, K.; Godin, B.; Stone, R. L.; Nick, A. M.; Lopez-Berestein, G.; Sood, A. K.; Ferrari, M., Sustained small interfering RNA delivery by mesoporous silicon particles. *Cancer Res* **2010,** *70*, 3687-96.
195. Shen, H.; Rodriguez-Aguayo, C.; Xu, R.; Gonzalez-Villasana, V.; Mai, J.; Huang, Y.; Zhang, G.; Guo, X.; Bai, L.; Qin, G.; Deng, X.; Li, Q.; Erm, D. R.; Aslan, B.; Liu, X.; Sakamoto, J.; Chavez-Reyes, A.; Han, H. D.; Sood, A. K.; Ferrari, M.; Lopez-Berestein, G., Enhancing chemotherapy response with sustained EphA2 silencing using multistage vector delivery. *Clinical cancer research : an official journal of the American Association for Cancer Research* **2013,** *19*, 1806-15.
196. Goh, A. S.; Chung, A. Y.; Lo, R. H.; Lau, T. N.; Yu, S. W.; Chng, M.; Satchithanantham, S.; Loong, S. L.; Ng, D. C.; Lim, B. C.; Connor, S.; Chow, P. K., A novel approach to brachytherapy in hepatocellular carcinoma using a phosphorous^{32} (^{32}P) brachytherapy delivery device--a first-in-man study. *Int J Radiat Oncol Biol Phys* **2007,** *67*, 786-92.
197. Santos, H. A.; Hirvonen, J., Nanostructured porous silicon materials: potential candidates for improving drug delivery. Nanomedicine (Lond). 2012, *7*,1281-4.
198. Xu, R.; Huang, Y.; Mai, J.; Zhang, G.; Guo, X.; Xia, X.; Koay, E. J.; Qin, G.; Erm, D. R.; Li, Q.; Liu, X.; Ferrari, M.; Shen, H., Multistage vectored siRNA targeting ataxia-telangiectasia mutated for breast cancer therapy. *Small* **2013,** *9*, 1799-808.
199. Mai, J.; Huang, Y.; Mu, C.; Zhang, G.; Xu, R.; Guo, X.; Xia, X.; Volk, D. E.; Lokesh, G. L.; Thiviyanathan, V.; Gorenstein, D. G.; Liu, X.; Ferrari, M.; Shen, H., Bone marrow endothelium-targeted therapeutics for metastatic breast cancer. *J Control Release* **2014,** *187*, 22-9.
200. Zhang, M.; Xu, R.; Xia, X.; Yang, Y.; Gu, J.; Qin, G.; Liu, X.; Ferrari, M.; Shen, H., Polycation-functionalized nanoporous silicon particles for gene silencing on breast cancer cells. *Biomaterials* **2014,** *35*, 423-31.

201. Gu, L.; Hall, D. J.; Qin, Z.; Anglin, E.; Joo, J.; Mooney, D. J.; Howell, S. B.; Sailor, M. J., *In vivo* time-gated fluorescence imaging with biodegradable luminescent porous silicon nanoparticles. *Nature communications* **2013,** *4*, 2326.
202. Kinnari, P. J.; Hyvonen, M. L.; Makila, E. M.; Kaasalainen, M. H.; Rivinoja, A.; Salonen, J. J.; Hirvonen, J. T.; Laakkonen, P. M.; Santos, H. A., Tumour homing peptide-functionalized porous silicon nanovectors for cancer therapy. *Biomaterials* **2013,** *34*, 9134-41.
203. Tasciotti, E.; Liu, X.; Bhavane, R.; Plant, K.; Leonard, A. D.; Price, B. K.; Cheng, M. M.; Decuzzi, P.; Tour, J. M.; Robertson, F.; Ferrari, M., Mesoporous silicon particles as a multistage delivery system for imaging and therapeutic applications. Nat Nanotechnol. 2008, *3*, 151-7.
204. Sarparanta, M.; Makila, E.; Heikkila, T.; Salonen, J.; Kukk, E.; Lehto, V. P.; Santos, H. A.; Hirvonen, J.; Airaksinen, A. J., ^{18}F-labeled modified porous silicon particles for investigation of drug delivery carrier distribution *in vivo* with positron emission tomography. *Mol Pharm* **2011,** *8*, 1799-806.
205. Sarparanta, M.; Bimbo, L. M.; Rytkonen, J.; Makila, E.; Laaksonen, T. J.; Laaksonen, P.; Nyman, M.; Salonen, J.; Linder, M. B.; Hirvonen, J.; Santos, H. A.; Airaksinen, A. J., Intravenous delivery of hydrophobin-functionalized porous silicon nanoparticles: stability, plasma protein adsorption and biodistribution. *Mol Pharm* **2012,** *9*, 654-63.
206. Heinrich, J. L.; Curtis, C. L.; Credo, G. M.; Sailor, M. J.; Kavanagh, K. L., Luminescent colloidal silicon suspensions from porous silicon. *Science* **1992,** *255*, 66-8.
207. Tilley, R. D.; Yamamoto, K., The microemulsion synthesis of hydrophobic and hydrophilic silicon nanocrystals. *Adv Mater* **2006,** *18*, 2053-6.
208. Jurbergs, D.; Rogojina, E.; Mangolini, L.; Kortshagen, U., Silicon nanocrystals with ensemble quantum yields exceeding 60%. *Applied Physics Letters* **2006,** *88*, 233116.
209. Bouccara, S.; Fragola, A.; Giovanelli, E.; Sitbon, G.; Lequeux, N.; Pons, T.; Loriette, V., Time-gated cell imaging using long lifetime near-infrared-emitting quantum dots for autofluorescence rejection. *J Biomed Opt* **2014,** *19*, 051208.
210. Ananta, J. S.; Godin, B.; Sethi, R.; Moriggi, L.; Liu, X.; Serda, R. E.; Krishnamurthy, R.; Muthupillai, R.; Bolskar, R. D.; Helm, L.; Ferrari, M.; Wilson, L. J.; Decuzzi, P., Geometrical confinement of gadolinium-based contrast agents in nanoporous particles enhances T1 contrast. *Nat Nanotechnol* **2010,** *5*, 815-21.
211. Kinsella, J. M.; Ananda, S.; Andrew, J. S.; Grondek, J. F.; Chien, M.-P.; Scadeng, M.; Gianneschi, N. C.; Ruoslahti, E.; Sailor, M. J., Enhanced magnetic resonance contrast of Fe3O4 nanoparticles trapped in a porous silicon nanoparticle host. *Adv Mater* **2011,** *23*, H248-H253.
212. José Alonso, M., Nanomedicines for overcoming biological barriers. *Biomedicine & Pharmacotherapy* **2004,** *58*, 168-72.
213. http://www.cancer.org/treatment/treatmentsandsideeffects/guidetocancerdrugs/methotrexate.
214. http://www.cancer.gov/cancertopics/druginfo/fda-sorafenib-tosylate.
215. Pang, K. S., Modeling of intestinal drug absorption: roles of transporters and metabolic enzymes. *Drug Metabolism and Disposition* **2003,** *31*, 1507-19.
216. Yang, Y.; Wang, S.; Wang, Y.; Wang, X.; Wang, Q.; Chen, M., Advances in self-assembled chitosan nanomaterials for drug delivery. Biotechnol Adv. 2014, 32, 1301-16.

217. Liu, D.; Liu, F.; Song, Y. K., Recognition and clearance of liposomes containing phosphatidylserine are mediated by serum opsonin. *Biochimica et biophysica acta* **1995,** *12*, 140-6.
218. Clark, J. W.; Eder, J. P.; Ryan, D.; Lathia, C.; Lenz, H. J., Safety and pharmacokinetics of the dual action Raf kinase and vascular endothelial growth factor receptor inhibitor, BAY 43-9006, in patients with advanced, refractory solid tumors. *Clin Cancer Res* **2005,** *11*, 5472-80.
219. Sadauskas, E.; Wallin, H.; Stoltenberg, M.; Vogel, U.; Doering, P.; Larsen, A.; Danscher, G., Kupffer cells are central in the removal of nanoparticles from the organism. *Part Fibre Toxicol* **2007,** *4*, 10.
220. Pozzi, D.; Colapicchioni, V.; Caracciolo, G.; Piovesana, S.; Capriotti, A. L.; Palchetti, S.; De Grossi, S.; Riccioli, A.; Amenitsch, H.; Lagana, A., Effect of polyethyleneglycol (PEG) chain length on the bio-nano-interactions between PEGylated lipid nanoparticles and biological fluids: from nanostructure to uptake in cancer cells. *Nanoscale* **2014,** *6*, 2782-92.
221. Saggar, J. K.; Yu, M.; Tan, Q.; Tannock, I. F., The tumor microenvironment and strategies to improve drug distribution. *Front Oncol* **2013,** *3* 154.
222. Nichols, J. W.; Bae, Y. H., EPR: Evidence and fallacy. *J Control Release*. 2014, *190*, 451-64.
223. Nie, S., Understanding and overcoming major barriers in cancer nanomedicine. *Nanomedicine (Lond)*. 2010, *54*, 523-8.
224. Torchilin, V., Tumor delivery of macromolecular drugs based on the EPR effect. *Adv Drug Deliv Rev* **2011,** *63*, 131-5.
225. Zeng, B. J.; Chuan, Y. P.; O'Sullivan, B.; Caminschi, I.; Lahoud, M. H.; Thomas, R.; Middelberg, A. P., Receptor-specific delivery of protein antigen to dendritic cells by a nanoemulsion formed using top-down non-covalent click self-assembly. *Small* **2013,** *9*, 3736-42.
226. Zhu, J.; Zheng, L.; Wen, S.; Tang, Y.; Shen, M.; Zhang, G.; Shi, X., Targeted cancer theranostics using alpha-tocopheryl succinate-conjugated multifunctional dendrimer-entrapped gold nanoparticles. *Biomaterials* **2014,** *35*, 7635-46.
227. http://www.cancer.org/treatment/treatmentsandsideeffects/guidetocancerdrugs/doxorubicin.
228. http://www.cancer.org/treatment/treatmentsandsideeffects/guidetocancerdrugs/cisplatin.
229. http://www.cancerresearchuk.org/about-cancer/cancers-in-general/treatment/cancer-drugs/paclitaxel.
230. Neradil, J.; Pavlasova, G.; Veselska, R., New mechanisms for an old drug; DHFR- and non-DHFR-mediated effects of methotrexate in cancer cells. *Klin Onkol* **2012,** *25*, 2S87-92.
231. Ma, D.; Zhang, H. B.; Chen, Y. Y.; Lin, J. T.; Zhang, L. M., New cyclodextrin derivative containing poly(L-lysine) dendrons for gene and drug co-delivery. *J Colloid Interface Sci* **2013,** *405*, 305-11.
232. Chen, J.; Huang, L.; Lai, H.; Lu, C.; Fang, M.; Zhang, Q.; Luo, X., Methotrexate-loaded PEGylated chitosan nanoparticles: synthesis, characterization, and *in vitro* and *in vivo* antitumoral activity. *Mol Pharm* **2014,** *11*, 2213-23.
233. Ryser, H. J.; Shen, W. C., Conjugation of methotrexate to poly (L-lysine) as a potential way to overcome drug resistance. *Cancer* **1980,** *45*, 1207-11.
234. Silpe, J. E.; Sumit, M.; Thomas, T. P.; Huang, B.; Kotlyar, A.; van Dongen, M. A.; Banaszak Holl, M. M.; Orr, B. G.; Choi, S. K., Avidity modulation of folate-targeted

multivalent dendrimers for evaluating biophysical models of cancer targeting nanoparticles. *ACS Chem Biol* **2013,** *8*, 2063-71.
235. Weis, S. M.; Cheresh, D. A., αV integrins in angiogenesis and cancer. *Cold Spring Harb Perspect Med* **2011,** *1*, a006478.
236. Shen, J.; Meng, Q.; Sui, H.; Yin, Q.; Zhang, Z.; Yu, H.; Li, Y., iRGD conjugated TPGS mediates codelivery of paclitaxel and survivin shRNA for the reversal of lung cancer resistance. *Mol Pharm* **2013,** *11*, 2579-91.
237. Backer, M. V.; Aloise, R.; Przekop, K.; Stoletov, K.; Backer, J. M., Molecular vehicles for targeted drug delivery. *Bioconjug Chem* **2002,** *13*, 462-7.
238. Ganapathy, V.; Ge, R.; Grazioli, A.; Xie, W.; Banach-Petrosky, W.; Kang, Y.; Lonning, S.; McPherson, J.; Yingling, J. M.; Biswas, S.; Mundy, G. R.; Reiss, M., Targeting the transforming growth factor-beta pathway inhibits human basal-like breast cancer metastasis. *Mol Cancer* **2010,** *9*, 122.
239. Varkouhi, A. K.; Scholte, M.; Storm, G.; Haisma, H. J., Endosomal escape pathways for delivery of biologicals. *J Control Release* **2011,** *151*, 220-8.
240. Gu, L.; Ruff, L. E.; Qin, Z.; Corr, M.; Hedrick, S. M.; Sailor, M. J., Multivalent porous silicon nanoparticles enhance the immune activation potency of agonistic CD40 antibody. *Adv Mater* **2012,** *24*, 3981-7.
241. Sugahara, K. N.; Teesalu, T.; Karmali, P. P.; Kotamraju, V. R.; Agemy, L.; Greenwald, D. R.; Ruoslahti, E., Coadministration of a tumor-penetrating peptide enhances the efficacy of cancer drugs. *Science* **2010,** *328*, 1031-5.
242. Guan, B.; Magenau, A.; Ciampi, S.; Gaus, K.; Reece, P. J.; Gooding, J. J., Antibody modified porous silicon microparticles for the selective capture of cells. *Bioconjug Chem* **2014,** *25*, 1282-9.
243. Pierschbacher, M. D.; Ruoslahti, E., Cell attachment activity of fibronectin can be duplicated by small synthetic fragments of the molecule. *Nature* **1984,** *309*, 30-33.
244. Sugahara, K. N.; Teesalu, T.; Karmali, P. P.; Kotamraju, V. R.; Agemy, L.; Girard, O. M.; Hanahan, D.; Mattrey, R. F.; Ruoslahti, E., Tissue-penetrating delivery of compounds and nanoparticles into tumors. *Cancer cell* **2009,** *16*, 510-20.
245. Su, S.; Wang, H.; Liu, X.; Wu, Y.; Nie, G., iRGD-coupled responsive fluorescent nanogel for targeted drug delivery. *Biomaterials* **2013,** *34*, 3523-33.
246. Al-Jamal, K. T.; Nunes, A.; Methven, L.; Ali-Boucetta, H.; Li, S.; Toma, F. M.; Herrero, M. A.; Al-Jamal, W. T.; ten Eikelder, H. M.; Foster, J.; Mather, S.; Prato, M.; Bianco, A.; Kostarelos, K., Degree of chemical functionalization of carbon nanotubes determines tissue distribution and excretion profile. *Angew Chem Int Ed Engl* **2012,** *51*, 6389-93.
247. Sacchetti, C.; Motamedchaboki, K.; Magrini, A.; Palmieri, G.; Mattei, M.; Bernardini, S.; Rosato, N.; Bottini, N.; Bottini, M., Surface polyethylene glycol conformation influences the protein corona of polyethylene glycol-modified single-walled carbon nanotubes: potential implications on biological performance. *Acs Nano* **2013,** *7*, 1974-89.
248. Kim, B. S.; Yang, W. Y.; Ryu, J. H.; Yoo, Y. S.; Lee, M., Carbohydrate-coated nanocapsules from amphiphilic rod-coil molecule: binding to bacterial type 1 pili. *Chem Commun* **2005,** *21*, 2035-7.
249. Egli, S.; Nussbaumer, M. G.; Balasubramanian, V.; Chami, M.; Bruns, N.; Palivan, C.; Meier, W., Biocompatible functionalization of polymersome surfaces: a new approach to surface immobilization and cell targeting using polymersomes. *J Am Chem Soc* **2011,** *133*, 4476-83.

250. Meeuwissen, S. A.; Debets, M. F.; van Hest, J. C. M., Copper-free click chemistry on polymersomes: pre- vs. post-self-assembly functionalisation. *Polym Chem-Uk* **2012,** *3*, 1783-95.
251. Cutler, C. S.; Hennkens, H. M.; Sisay, N.; Huclier-Markai, S.; Jurisson, S. S., Radiometals for combined imaging and therapy. *Chem Rev* **2013,** *113*, 858-83.
252. Huang, G.; Zhang, C.; Li, S.; Khemtong, C.; Yang, S. G.; Tian, R.; Minna, J. D.; Brown, K. C.; Gao, J., A novel strategy for surface modification of superparamagnetic iron oxide nanoparticles for lung cancer imaging. *J Mater Chem* **2009,** *19*, 6367-72.
253. Singh, Y.; Murat, P.; Defrancq, E., Recent developments in oligonucleotide conjugation. *Chem Soc Rev* **2010,** *39*, 2054-70.
254. Xi, W.; Scott, T. F.; Kloxin, C. J.; Bowman, C. N., Click chemistry in materials science. *Adv Funct Mater* **2014,** *24*, 2572-90.
255. Kolb, H. C.; Finn, M. G.; Sharpless, K. B., Click chemistry: diverse chemical function from a few good reactions. *Angew Chem Int Ed Engl* **2001,** *40*, 2004-21.
256. Sletten, E. M.; Bertozzi, C. R., From mechanism to mouse: a tale of two bioorthogonal reactions. *Acc Chem Res* **2011,** *44*, 666-76.
257. Debets, M. F.; van Berkel, S. S.; Dommerholt, J.; Dirks, A. T.; Rutjes, F. P.; van Delft, F. L., Bioconjugation with strained alkenes and alkynes. *Acc Chem Res* **2011,** *44*, 805-15.
258. Kilian, K. A.; Bocking, T.; Gaus, K.; Gooding, J. J., Introducing distinctly different chemical functionalities onto the internal and external surfaces of mesoporous materials. *Angew Chem Int Ed Engl* **2008,** *47*, 2697-9.
259. Zhu, Y.; Gupta, B.; Guan, B.; Ciampi, S.; Reece, P. J.; Gooding, J. J., Photolithographic strategy for patterning preformed, chemically modified, porous silicon photonic crystal using click chemistry. *ACS Appl Mater Interfaces* **2013,** *5*, 6514-21.
260. Secret, E.; Smith, K.; Dubljevic, V.; Moore, E.; Macardle, P.; Delalat, B.; Rogers, M. L.; Johns, T. G.; Durand, J. O.; Cunin, F.; Voelcker, N. H., Antibody-functionalized porous silicon nanoparticles for vectorization of hydrophobic drugs. *Adv Healthc Mater* **2013**, *2*, 718-27.
261. Almeida, P. V.; Shahbazi, M. A.; Makila, E.; Kaasalainen, M.; Salonen, J.; Hirvonen, J.; Santos, H. A., Amine-modified hyaluronic acid-functionalized porous silicon nanoparticles for targeting breast cancer tumors. *Nanoscale* **2014,** *6*, 10377-87.
262. Bimbo, L. M.; Makila, E.; Raula, J.; Laaksonen, T.; Laaksonen, P.; Strommer, K.; Kauppinen, E. I.; Salonen, J.; Linder, M. B.; Hirvonen, J.; Santos, H. A., Functional hydrophobin-coating of thermally hydrocarbonized porous silicon microparticles. *Biomaterials* **2011,** *32*, 9089-99.
263. Bimbo, L. M.; Sarparanta, M.; Makila, E.; Laaksonen, T.; Laaksonen, P.; Salonen, J.; Linder, M. B.; Hirvonen, J.; Airaksinen, A. J.; Santos, H. A., Cellular interactions of surface modified nanoporous silicon particles. *Nanoscale* **2012,** *4*, 3184-92.
264. Sarparanta, M. P.; Bimbo, L. M.; Makila, E. M.; Salonen, J. J.; Laaksonen, P. H.; Helariutta, A. M.; Linder, M. B.; Hirvonen, J. T.; Laaksonen, T. J.; Santos, H. A.; Airaksinen, A. J., The mucoadhesive and gastroretentive properties of hydrophobin-coated porous silicon nanoparticle oral drug delivery systems. *Biomaterials* **2012,** *33*, 3353-62.
265. Parodi, A.; Quattrocchi, N.; van de Ven, A. L.; Chiappini, C.; Evangelopoulos, M.; Martinez, J. O.; Brown, B. S.; Khaled, S. Z.; Yazdi, I. K.; Enzo, M. V.; Isenhart, L.; Ferrari, M.; Tasciotti, E., Synthetic nanoparticles functionalized with biomimetic leukocyte membranes possess cell-like functions. *Nat Nanotechnol* **2013,** *8*, 61-8.

266. Teesalu, T.; Sugahara, K. N.; Kotamraju, V. R.; Ruoslahti, E., C-end rule peptides mediate neuropilin-1-dependent cell, vascular, and tissue penetration. *Proc Natl Acad Sci U S A* **2009,** *106*, 16157-62.
267. Brunauer, S.; Emmett, P. H.; Teller, E., Adsorption of gases in multimolecular layers. *J Am Chem Soc* **1938,** *60*, 309-19.
268. Pierschbacher, M. D.; Ruoslahti, E., Variants of the cell recognition site of fibronectin that retain attachment-promoting activity. *Proc Natl Acad Sci USA* **1984,** *81*, 5985-8.
269. Tian, Y.; Li, S.; Song, J.; Ji, T.; Zhu, M.; Anderson, G. J.; Wei, J.; Nie, G., A doxorubicin delivery platform using engineered natural membrane vesicle exosomes for targeted tumor therapy. *Biomaterials* **2014,** *35*, 2383-90.
270. Lammers, T.; Peschke, P.; Kuhnlein, R.; Subr, V.; Ulbrich, K.; Huber, P.; Hennink, W.; Storm, G., Effect of intratumoral injection on the biodistribution and the therapeutic potential of HPMA copolymer-based drug delivery systems. *Neoplasia* **2006,** *8*, 788-95.
271. Han, H. D.; Byeon, Y.; Jeon, H. N.; Shin, B. C., Enhanced localization of anticancer drug in tumor tissue using polyethylenimine-conjugated cationic liposomes. *Nanoscale Res Lett* **2014,** *9*, 209.
272. Monopoli, M. P.; Aberg, C.; Salvati, A.; Dawson, K. A., Biomolecular coronas provide the biological identity of nanosized materials. *Nat Nanotechnol* **2012,** *7*, 779-86.
273. Mahon, E.; Salvati, A.; Baldelli Bombelli, F.; Lynch, I.; Dawson, K. A., Designing the nanoparticle-biomolecule interface for "targeting and therapeutic delivery". *J Control Release* **2012,** *161*, 164-74.
274. D'Addio, S. M.; Saad, W.; Ansell, S. M.; Squiers, J. J.; Adamson, D. H.; Herrera-Alonso, M.; Wohl, A. R.; Hoye, T. R.; Macosko, C. W.; Mayer, L. D.; Vauthier, C.; Prud'homme, R. K., Effects of block copolymer properties on nanocarrier protection from in vivo clearance. *J Control Release* **2012,** *162*, 208-17.
275. Peng, W.; Sung, L. A., RGD-containing ankyrin externalized onto the cell surface triggers alphaVbeta3 integrin-mediated erythrophagocytosis. *Biochem Biophys Res Commun* **2011,** *407*, 466-71.
276. Cassano, R.; Ferrarelli, T.; Schätzlein, A. G.; Uchegbu, I. F.; Trombino, S., Dextran-pegylated microparticles for enhanced cellular uptake of hydrophobic drugs. *Eur J Pharm Biopharm* **2013,** *84*, 540-8.
277. Peng, S.-F.; Tseng, M. T.; Ho, Y.-C.; Wei, M.-C.; Liao, Z.-X.; Sung, H.-W., Mechanisms of cellular uptake and intracellular trafficking with chitosan/DNA/poly(γ-glutamic acid) complexes as a gene delivery vector. *Biomaterials* **2011,** *32*, 239-48.
278. Sim, R. B.; Laich, A., Serine proteases of the complement system. *Biochem Soc Trans* **2000,** *28* (5), 545-50.
279. Smith, B. R.; Ghosn, E. E.; Rallapalli, H.; Prescher, J. A.; Larson, T.; Herzenberg, L. A.; Gambhir, S. S., Selective uptake of single-walled carbon nanotubes by circulating monocytes for enhanced tumour delivery. *Nat Nanotechnol* **2014,** *9*, 481-7.
280. Jones, S. E.; Jomary, C., Clusterin. *Int J Biochem Cell Biol* **2002,** *34*, 427-31.
281. Tschopp, J.; Chonn, A.; Hertig, S.; French, L. E., Clusterin, the human apolipoprotein and complement inhibitor, binds to complement C7, C8 beta, and the b domain of C9. *J Immunol* **1993,** *151*, 2159-65.
282. Yan, X.; Kuipers, F.; Havekes, L. M.; Havinga, R.; Dontje, B.; Poelstra, K.; Scherphof, G. L.; Kamps, J. A., The role of apolipoprotein E in the elimination of

liposomes from blood by hepatocytes in the mouse. *Biochem Biophys Res Commun* **2005,** *328*, 57-62.
283. Labarre, D.; Vauthier, C.; Chauvierre, C.; Petri, B.; Muller, R.; Chehimi, M. M., Interactions of blood proteins with poly(isobutylcyanoacrylate) nanoparticles decorated with a polysaccharidic brush. *Biomaterials* **2005,** *26*, 5075-84.
284. Xu, Y.; Zhao, H.; Zheng, Y.; Gu, Q.; Ma, J.; Xu, X., A novel antiangiogenic peptide derived from hepatocyte growth factor inhibits neovascularization in vitro and in vivo. *Mol Vis* **2010,** *16*, 1982-95.
285. Kim, H.; Csaky, K. G., Nanoparticle-integrin antagonist C16Y peptide treatment of choroidal neovascularization in rats. *J Control Release* **2010,** *142*, 286-93.
286. Binetruy-Tournaire, R.; Demangel, C.; Malavaud, B.; Vassy, R.; Rouyre, S.; Kraemer, M.; Plouet, J.; Derbin, C.; Perret, G.; Mazie, J. C., Identification of a peptide blocking vascular endothelial growth factor (VEGF)-mediated angiogenesis. *Embo J* **2000,** *19*, 1525-33.
287. Gonen, N.; Assaraf, Y. G., Antifolates in cancer therapy: structure, activity and mechanisms of drug resistance. *Drug Resist Updat* **2012,** *15*, 183-210.
288. Barton, A. K.; Antoieta, C., Receptor-mediated folate accumulation is regulated by the cellular folate content. *Proc Natl Acad Sci U S A* **1986,** *83*, 5983-7.
289. Zwicke, G. L.; Mansoori, G. A.; Jeffery, C. J., Utilizing the folate receptor for active targeting of cancer nanotherapeutics. *Nano Rev* **2012,** *3*, 18496.
290. Gurdag, S.; Khandare, J.; Stapels, S.; Matherly, L. H.; Kannan, R. M., Activity of dendrimer-methotrexate conjugates on methotrexate-sensitive and -resistant cell lines. *Bioconjug Chem* **2006,** *17*, 275-83.
291. Kaminskas, L. M.; Kelly, B. D.; McLeod, V. M.; Boyd, B. J.; Krippner, G. Y.; Williams, E. D.; Porter, C. J., Pharmacokinetics and tumor disposition of PEGylated, methotrexate conjugated poly-l-lysine dendrimers. *Mol Pharm* **2009,** *6*, 1190-204.
292. Thomas, T. P.; Huang, B.; Choi, S. K.; Silpe, J. E.; Kotlyar, A.; Desai, A. M.; Zong, H.; Gam, J.; Joice, M.; Baker, J. R., Jr., Polyvalent dendrimer-methotrexate as a folate receptor-targeted cancer therapeutic. *Mol Pharm* **2012,** *9*, 2669-76.